Linköping Studies in Science and Technology
Thesis No. 1271

Control of EGR and VGT for emission control and pumping work minimization in diesel engines

Johan Wahlström

Department of Electrical Engineering
Linköpings universitet, S–581 83 Linköping, Sweden
Linköping 2006

Control of EGR and VGT for emission control and pumping work minimization in diesel engines

johwa@isy.liu.se
http://www.fs.isy.liu.se/
Department of Electrical Engineering,
Linköpings universitet,
S–581 83 Linköping,
Sweden.

ISBN 91-85643-83-1
ISSN 0280-7971
LiU-TEK-LIC-2006:52

Abstract

Legislators steadily increase the demands on lowered emissions from heavy duty vehicles. To meet these demands it is necessary to integrate technologies like Exhaust Gas Recirculation (EGR) and Variable Geometry Turbochargers (VGT) together with advanced control systems. A control structure with PID controllers and selectors is proposed and investigated for coordinated control of EGR valve and VGT position in heavy duty diesel engines. Main control goals are to fulfill the legislated emission levels, to reduce the fuel consumption, and to fulfill safe operation of the turbocharger. These goals are achieved through regulation of normalized oxygen/fuel ratio, λ_O, and intake manifold EGR-fraction. These are chosen as main performance variables since they are strongly coupled to the emissions, compared to manifold pressure or air mass flow, which makes it easy to adjust set-points depending on e.g. measured emissions during an emission calibration process. In addition a mechanism for fuel efficient operation is incorporated in the structure, this is achieved by minimizing the pumping work.

To design a successful control structure, a mean value model of a diesel engine is developed and validated. The intended applications of the model are system analysis, simulation, and development of model-based control systems. Model equations and tuning methods for the model parameters are described for each subsystem in the model. Static and dynamic validations of the entire model show mean relative errors that are less than 12 %.

Based on a system analysis of the model, a key characteristic behind the control structure is that λ_O is controlled by the EGR-valve and EGR-fraction by the VGT-position, in order to handle a sign reversal in the system from VGT to λ_O. For efficient calibration an automatic controller tuning method is developed. The controller objectives are captured in a cost function, that is evaluated utilizing a method choosing representative transients. The performance is evaluated on the European Transient Cycle. It is demonstrated how the weights in the cost function influence behavior, and that the tuning method is important in order to improve the control performance compared to if only a standard method is used. It is also demonstrated that the controller structure performs well regarding all control objectives. In combination with its efficient tuning, the controller structure thus fulfills all requirements for successful application.

Acknowledgments

This work has been performed at the department of Electrical Engineering, division of Vehicular Systems, Linköpings universitet, Sweden. I am grateful to my professor and supervisor Lars Nielsen for letting me join this group, for all the discussions we have had, and for proofreading my work.

I would like to thank my second supervisor Lars Eriksson for many interesting discussions, for giving valuable feedback on the work, and for telling me how to improve my research. Thanks go to Erik Frisk and Jonas Biteus for all the help regarding Latex. Carolina Fröberg and Susana Högne are acknowledged for all their administrative help and the staff at Vehicular Systems for creating a nice working atmosphere.

I also thank Magnus Pettersson and Mats Jennische at Scania CV AB for the valuable meetings, for showing great interest, and for the measurement supply. Also the Swedish Energy Agency are gratefully acknowledged for their financial support.

A special thank goes to Johan Sjöberg for being a nice friend, for getting me interested in automatic control and vehicular systems during the undergraduate studies, for giving me a tip of a master's thesis project at Vehicular Systems, and for proofreading parts of my work.

Finally, I would like to express my gratitude to my parents, my sister, my brother, and Kristin for always being there and giving me support and encouragement.

Linköping, September 2006

Johan Wahlström

Contents

1

Introduction

Legislated emission limits for heavy duty trucks are constantly reduced. To fulfill the requirements, technologies like Exhaust Gas Recirculation (EGR) and Variable Geometry Turbochargers (VGT) have been introduced. The primary emission reduction mechanisms utilized to control the emissions are that NO_x can be reduced by increasing the intake manifold EGR-fraction and smoke can be reduced by increasing the air/fuel ratio (Heywood, 1988). However, the EGR fraction and air/fuel ratio depend in complicated ways on the EGR and VGT actuation. It is therefore necessary to have coordinated control of the EGR and VGT to reach the legislated emission limits in NO_x and smoke. Various approaches for coordinated control of the EGR and VGT for emission abatement have been published. Guzzella and Amstutz (1998) present a good overview of different control aspects of diesel engines with EGR and VGT, and in Nieuwstadt et al. (2000) there is a comparison of some control approaches with different selections of performance variables. Other control approaches are described in Amstutz and Re (1995); Jankovic et al. (1998); Nieuwstadt et al. (1998); Stefanopoulou et al. (2000); Amman et al. (2003); Jung (2003); Rückert et al. (2004); Rajamani (2005).

This thesis develops and investigates a structure for coordinated EGR and VGT control, which provides a convenient way to handle emission requirements and at the same time optimizes the engine efficiency. Formulating the emission control strategy in terms of performance variables that have a direct relation to the NO_x and smoke emissions gives a structure with natural separation, where a controls engineer can focus on the control loop performance while the calibration engineer can fine tune the controller set-points to fulfill the emission limits.

Exhaust gases, present in the intake, also contain oxygen which makes it more

suitable to define and use the oxygen/fuel ratio instead of the traditional air/fuel ratio. The main motive for this is that it is the oxygen contents that is crucial for smoke generation. The exact definition of the normalized oxygen/fuel ratio λ_O is given by Eq. (2.14) in Chap. 2. Besides λ_O it is natural to use EGR-fraction as the other main performance variable.

Fuel consumption is a prioritized area for diesel engines in general and for heavy duty diesel engines in particular. To facilitate improved fuel economy the proposed control structure also has a mechanism for optimizing the fuel consumption by minimizing the pumping work. In diesel engines large λ_O is allowed which leads to an extra degree of freedom when λ_O is greater than its set-point. This extra degree of freedom can be used to minimize the pumping work. Choosing λ_O and EGR-fraction as the main performance variables gives information about when it is allowed to minimize the pumping and this is more straightforward compared to control of manifold pressure and air mass flow. This is due to that it is the value of λ_O that decides when it is allowed to minimize the pumping work.

1.1 Proposed control approach

This thesis proposes a control structure for coordinated control of EGR-fraction and oxygen/fuel ratio λ_O, which is a novel choice of performance variables. Previous related work, as cited above, cover other control approaches with different performance variables in the loop. The most common choice of performance variables in the papers above are compressor air mass flow and intake manifold pressure, see e.g. Jung (2003). Other choices are intake manifold pressure and EGR-fraction (Nieuwstadt et al., 2000), exhaust manifold pressure and compressor air mass flow (Jankovic et al., 1998), intake manifold pressure and EGR flow (Rückert et al., 2004), intake manifold pressure and cylinder air mass flow (Amman et al., 2003), or turbine and EGR flow (Rajamani, 2005).

There are two main advantages with the choice of EGR-fraction and oxygen/fuel ratio λ_O as performance variables. The first advantage is as mentioned above that these variables are strongly connected to the emissions, compared to e.g. manifold pressure and air mass flow. The second advantage, which follows from the first one, is that a natural separation within the engine control system is obtained. The performance variables are handled in a fast inner loop, whereas trade-offs between e.g. emissions and response time for different operating conditions are made in an outer loop. This fits well with industrial practice where the dynamic response of the inner loop controller can be designed by an engine control group, and by that giving a well defined interface to for example the calibration engineers responsible for the outer loops giving the reference values for EGR-fraction and λ_O. This means that it is easy to adjust set-points for different operating conditions, different hardware configurations, and different legislative requirements depending on the measured emissions during the emission calibration process. The idea with two loops is depicted in Fig. 1.1. It is also easy to choose proper actions in the outer loop, if the set-points for EGR-fraction or oxygen/fuel ratio λ_O are not achieved, by

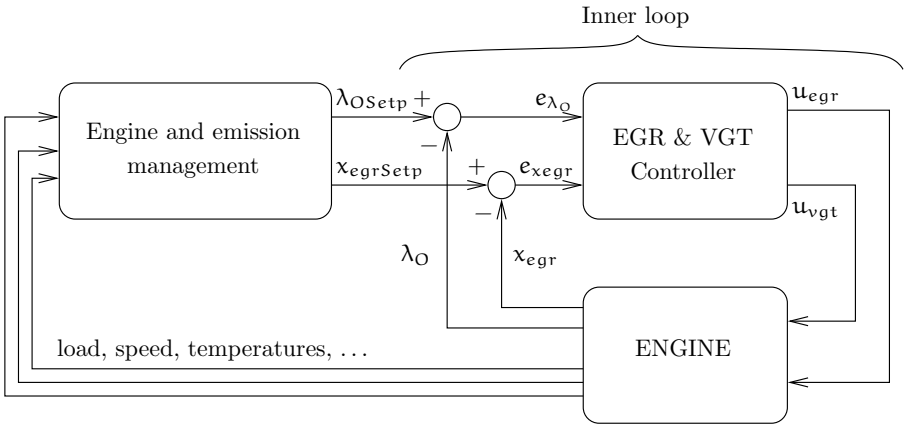

Figure 1.1 *A cascade control structure, with an inner loop where EGR and VGT actuators are controlled using the main performance variables EGR fraction* x_{egr} *and oxygen/fuel ratio* λ_O*. This sketch is a simplified illustration of the main idea that will be completed in Sec. 4.2 to also include fuel control and turbo protection.*

changing other actuations like the fuel injection timing. Neither EGR-fraction nor λ_O are normally measured and have to be estimated using observers. The observer design is important, but it is not the focus in this thesis. Examples of observer designs for thermodynamic states and gas compositions can be found in Nieuwstadt et al. (2000); Kolmanovsky et al. (2000); Andersson and Eriksson (2004); Rajamani (2005); Swartling (2005); Jerhammar and Höckerdal (2006).

A third advantage with using λ_O and EGR-fraction as performance variables is that it provides direct information about when it is allowed to minimize the pumping work. As explained above, this is due to that it is the value of λ_O that decides when it is allowed to minimize the pumping work. With this structure the emission levels are maintained due to the set-point selection and the decoupling achieved by the control loops.

In addition to control of EGR-fraction and λ_O it is also necessary to have load control, since the driver's demand must be actuated. This is achieved through basic fuel control using feedforward. Furthermore it is also important to monitor and control the turbocharger speed since aggressive transients can cause damage through over-speeding.

1.2 Control objectives

The primary performance variables to be controlled are engine torque M_e, normalized oxygen/fuel ratio λ_O, intake manifold EGR-fraction x_{egr} and turbocharger

speed n_t. The goal is to follow a driving cycle while maintaining low emissions, low fuel consumption, and suitable turbocharger speeds, which together with the discussion above gives the following control objectives for the performance variables.

1. λ_O should be greater than a soft limit, a set-point λ_{OSetp}, which enables a trade off between emission, fuel consumption, and response time.

2. λ_O is not allowed to go below a hard minimum limit λ_{Omin}, otherwise there will be too much smoke. λ_{Omin} is always smaller than λ_{OSetp}.

3. The EGR-fraction x_{egr} should follow its set-point $x_{egrSetp}$. There will be more NO_x if the EGR-fraction is too low and there will be more smoke if the EGR-fraction is too high.

4. The engine torque should follow the set-point from the driver's demand.

5. The turbocharger speed is not allowed to exceed a maximum limit, otherwise the turbocharger can be damaged.

6. Minimize the pumping loss M_p in stationary points in order to decrease the fuel consumption.

The aim is now to develop a control structure that achieves all these control objectives.

1.3 Outline

The outline of the thesis is as follows. Chap. 2 describes a mean value diesel engine model which is focused on gas flows. The engine model is used to evaluate system properties and control strategies through simulation. Model equations and tuning methods for the model parameters are described for each subsystem in the model and a dynamic validation of the complete model is performed. A system analysis of the model is performed in Chap. 3 by simulating step responses over the entire operating region. Based on this system analysis and the control objectives in Sec. 1.2 a controller structure, that minimizes the pumping work in steady-state, is proposed in Chap. 4. For successful application of the control structure, an automatic tuning method for the controller parameters is developed together with a method for selecting challenging transients in a driving cycle. The tuning method is based on optimization of a cost function, that reflects the control objectives. Finally, conclusions are drawn in Chap. 5.

1.4 List of publications

This thesis is based on the following publications:

- Wahlström, J., Eriksson, L., Nielsen, L., and Pettersson, M. (2005). PID controllers and their tuning for EGR and VGT control in Diesel engines. In *Preprints of the 16th IFAC World Congress*, Prague, Czech Republic.
- Wahlström, J. and Eriksson, L. (2006). Modeling of a Diesel engine with VGT and EGR including oxygen mass fraction. Technical report, Vehicular Systems, Department of Electrical Engineering, Linköping University.
- Wahlström, J., Eriksson, L., Nielsen, L., and Jennische, M. An EGR and VGT control structure for emission control and pumping work minimization in Diesel engines. Submitted to Control Engineering Practice.

2

Mean value modeling of a diesel engine

When developing and validating a controller, it is desirable to have a model that describes the system dynamics and the nonlinear effects. Therefore, the objective of this chapter is to construct a mean value diesel engine model with VGT and EGR. The model should be able to describe stationary operations and dynamics that are important for gas flow control. The intended usage of the model are system analysis, simulation and development of model-based control systems. In order to decrease the amount of tuning parameters, flows and efficiencies are modeled based upon physical relationships and parametric models instead of look-up tables. The model is implemented in MATLAB/SIMULINK using a component library.

The structure of the model is described in Sec. 2.1. Sec. 2.2 describes the model equations for the intake and exhaust manifold. The cylinder flows, cylinder temperature, and cylinder torque are modeled in Sec. 2.3. In Sec. 2.4 a model of the EGR-valve is proposed and in Sec. 2.5 model equations for the turbocharger are described. The intercooler and EGR-cooler are modeled in Sec. 2.6. A summary of the model assumptions and the model equations is given in Sec. 2.7. Tuning and validation of the model are performed in Sec. 2.8.

2.1 Model structure

The structure of the model can be seen in Fig. 2.1. To be able to implement a model-based controller in a control system the model must be small. Therefore the model has only seven states: intake and exhaust manifold pressures (p_{im} and p_{em}), oxygen mass fraction in the intake and exhaust manifold (X_{Oim} and X_{Oem}), turbocharger speed (ω_t), and two states describing the actuator dynamics for the

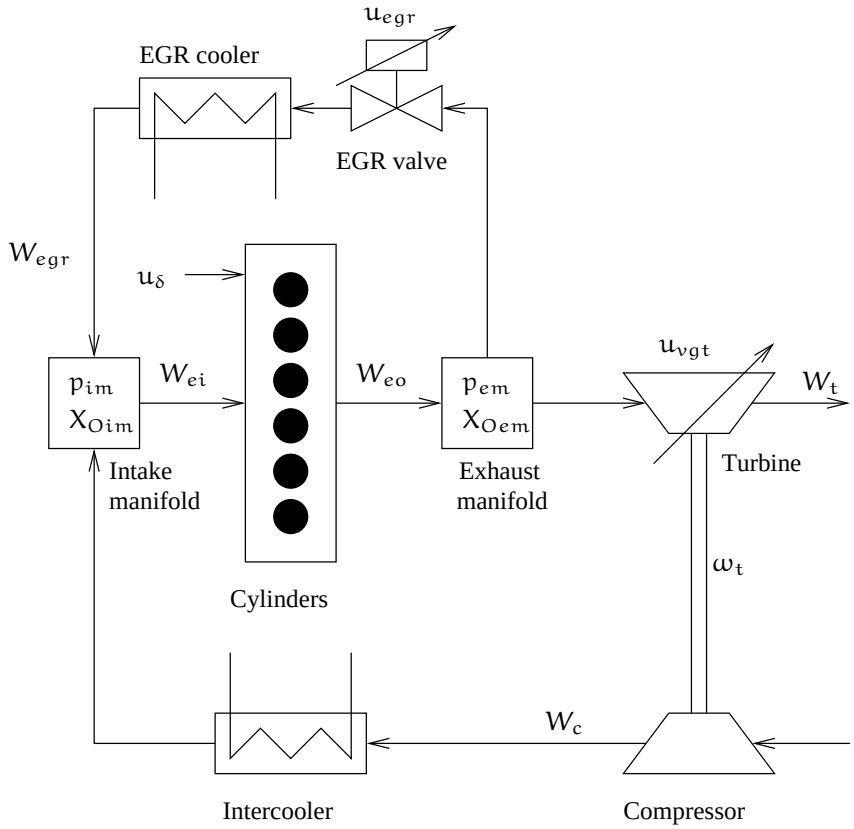

Figure 2.1 *A model structure of the diesel engine. It has three control inputs and five main states related to the engine (p_{im}, p_{em}, X_{Oim}, X_{Oem}, and ω_t). In addition, there are two states for actuator dynamics ($\tilde{u}_{egr}$ and $\tilde{u}_{vgt}$).*

two control signals ($\tilde{u}_{egr}$ and $\tilde{u}_{vgt}$). These states are collected in a state vector x

$$x = (p_{im} \quad p_{em} \quad X_{Oim} \quad X_{Oem} \quad \omega_t \quad \tilde{u}_{egr} \quad \tilde{u}_{vgt})^T \tag{2.1}$$

Descriptions of the nomenclature, the variables and the indices can be found in Appendix A.

The modeling effort is focused on the gas flows, and it is important that the model can be utilized both for different vehicles and for engine testing, calibration, and certification in an engine test cell. In many of these situations the engine operation is defined by the rotational speed n_e, for example given as an input from a drivecycle, and therefore it is natural to parameterize the model using engine

Table 2.1 *Measured variables during stationary measurements.*

Variable	Description	Unit
M_e	Engine torque	Nm
n_e	Rotational engine speed	rpm
n_t	Rotational turbine speed	rpm
p_{amb}	Ambient pressure	Pa
p_{em}	Exhaust manifold pressure	Pa
p_{im}	Intake manifold pressure	Pa
T_{amb}	Ambient temperature	K
T_c	Temperature after compressor	K
T_{em}	Exhaust manifold temperature	K
T_{im}	Intake manifold temperature	K
T_t	Temperature after turbine	K
u_{egr}	EGR control signal. 0 - closed, 100 - open	%
u_{vgt}	VGT control signal. 0 - closed, 100 - open	%
u_δ	Injected amount of fuel	mg/cycle
W_c	Compressor mass flow	kg/s
x_{egr}	EGR fraction	–

speed. The resulting model is thus expressed in state space form as

$$\dot{x} = f(x, u, n_e) \tag{2.2}$$

where the engine speed n_e is considered as an input to the model, and u is the control input vector

$$u = (u_\delta \quad u_{egr} \quad u_{vgt})^T \tag{2.3}$$

which contains mass of injected fuel u_δ, EGR-valve position u_{egr}, and VGT actuator position u_{vgt}. The EGR-valve is closed when $u_{egr} = 0\,\%$ and open when $u_{egr} = 100\,\%$. The VGT is closed when $u_{vgt} = 0\,\%$ and open when $u_{vgt} = 100\,\%$.

2.1.1 Measurements

To tune and validate the model, stationary and dynamic measurements have been performed in an engine laboratory at Scania CV AB, and these are described below.

Stationary measurements

The stationary data consists of measurements at stationary conditions in 82 operating points, that are scattered over a large operating region covering different loads, speeds, VGT- and EGR-positions. These 82 operating points also include the European Stationary Cycle (ESC). The variables that were measured during stationary measurements can be seen in Tab. 2.1. The EGR fraction is calculated by measuring the carbon dioxide concentration in the intake and exhaust manifolds.

Table 2.2 *Measured variables during dynamic measurements.*

Variable	Description	Unit
M_e	Engine torque	Nm
n_e	Rotational engine speed	rpm
n_t	Rotational turbine speed	rpm
p_{em}	Exhaust manifold pressure	Pa
p_{im}	Intake manifold pressure	Pa
u_{egr}	EGR control signal. 0 - closed, 100 - open	%
u_{vgt}	VGT control signal. 0 - closed, 100 - open	%
u_δ	Injected amount of fuel	mg/cycle
W_c	Compressor mass flow	kg/s

Dynamic measurements

The dynamic data consists of measurements at dynamic conditions with steps in VGT control signal, EGR control signal, and fuel injection in several different operating points. The measurements are sampled with a frequency of 1 Hz, except for the steps in fuel injection where the measurements are sampled with a frequency of 10 Hz. These measurements are used in Sec. 2.8 for tuning of dynamic models and validation of the total engine model. The variables that were measured during dynamic measurements can be seen in Tab. 2.2.

2.1.2 Parameter estimation

Parameters in static models are estimated automatically using least squares optimization and data from stationary measurements. Parameters in dynamic models (volumes and an inertia) are estimated by adjusting these parameters manually until simulations of the complete model follow the dynamic responses in the dynamic measurements.

2.1.3 Relative error

Relative errors are calculated and used to evaluate the tuning and the validation of the model. Relative errors for stationary measurements between a measured variable $y_{meas,stat}$ and a modeled variable $y_{mod,stat}$ are calculated as

$$\text{stationary relative error}(i) = \frac{y_{meas,stat}(i) - y_{mod,stat}(i)}{\frac{1}{N}\sum_{i=1}^{N} y_{meas,stat}(i)} \tag{2.4}$$

where i is an operating point. Relative errors for dynamic measurements between a measured variable $y_{meas,dyn}$ and a modeled variable $y_{mod,dyn}$ are calculated as

$$\text{dynamic relative error}(j) = \frac{y_{meas,dyn}(j) - y_{mod,dyn}(j)}{\frac{1}{N}\sum_{i=1}^{N} y_{meas,stat}(i)} \tag{2.5}$$

where j is a time sample. In order to make a fair comparison between these relative errors, both the stationary and the dynamic relative error have the same stationary measurement in the denominator and the mean value of this stationary measurement is calculated in order to avoid large relative errors when $y_{meas,stat}$ is small.

2.2 Manifolds

The intake and exhaust manifolds are modeled as dynamic systems with two states each, pressure and oxygen mass fraction. The standard isothermal model (Heywood, 1988), that is based upon mass conservation, the ideal gas law, and that the manifold temperature is constant or varies slowly, has the differential equations for the manifold pressures

$$\begin{aligned} \frac{d}{dt} p_{im} &= \frac{R_a T_{im}}{V_{im}} (W_c + W_{egr} - W_{ei}) \\ \frac{d}{dt} p_{em} &= \frac{R_e T_{em}}{V_{em}} (W_{eo} - W_t - W_{egr}) \end{aligned} \tag{2.6}$$

There are two sets of thermodynamic properties: air has the ideal gas constant R_a and the specific heat capacity ratio γ_a, and exhaust gas has the ideal gas constant R_e and the specific heat capacity ratio γ_e. The intake manifold temperature T_{im} is assumed to be constant and equal to the cooling temperature in the intercooler, the exhaust manifold temperature T_{em} will be described in Sec. 2.3.2, and V_{im} and V_{em} are the manifold volumes. The mass flows W_c, W_{egr}, W_{ei}, W_{eo}, and W_t will be described in Sec. 2.3 to 2.5.

The EGR fraction in the intake manifold is calculated as

$$x_{egr} = \frac{W_{egr}}{W_c + W_{egr}} \tag{2.7}$$

Note that the EGR gas also contains oxygen that affects the oxygen fuel ratio in the cylinder. This effect is considered by modeling the oxygen concentrations X_{Oim} and X_{Oem} in the control volumes. These concentrations are defined as (Vigild, 2001)

$$X_{Oim} = \frac{m_{Oim}}{m_{totim}}, \quad X_{Oem} = \frac{m_{Oem}}{m_{totem}} \tag{2.8}$$

where m_{Oim} and m_{Oem} are the oxygen masses, and m_{totim} and m_{totem} are the total masses in the intake and exhaust manifolds. Differentiating X_{Oim} and X_{Oem} and using mass conservation (Vigild, 2001) give the following differential equations

$$\begin{aligned} \frac{d}{dt} X_{Oim} &= \frac{R_a T_{im}}{p_{im} V_{im}} ((X_{Oem} - X_{Oim}) W_{egr} + (X_{Oc} - X_{Oim}) W_c) \\ \frac{d}{dt} X_{Oem} &= \frac{R_e T_{em}}{p_{em} V_{em}} (X_{Oe} - X_{Oem}) W_{eo} \end{aligned} \tag{2.9}$$

where X_{Oc} is the constant oxygen concentration in air passing the compressor, i.e. $X_{Oc} = 23.14\%$, and X_{Oe} is the oxygen concentration in the exhaust gases out from the engine cylinders, X_{Oe} will be described in Sec. 2.3.1.

Tuning parameters

- V_{im} and V_{em}: manifold volumes.

Tuning method

The tuning parameters V_{im} and V_{em} are obtained by adjusting these parameters manually until simulations of the complete model follow the dynamic responses in the dynamic measurements, see Sec. 2.8.1.

2.3 Cylinder

Three sub-models describe the behavior of the cylinder, these are:

- A mass flow model that models the flows through the cylinder, the oxygen to fuel ratio, and the oxygen concentration out from the cylinder.
- A model of the cylinder out temperature.
- A cylinder torque model.

2.3.1 Cylinder flow

The total mass flow W_{ei} into the cylinders is modeled using the volumetric efficiency η_{vol} (Heywood, 1988)

$$W_{ei} = \frac{\eta_{vol}\, p_{im}\, n_e\, V_d}{120\, R_a\, T_{im}} \tag{2.10}$$

where p_{im} and T_{im} are the pressure and temperature in the intake manifold, n_e is the engine speed and V_d is the displaced volume. The volumetric efficiency is in its turn modeled as

$$\eta_{vol} = c_{vol1}\sqrt{p_{im}} + c_{vol2}\sqrt{n_e} + c_{vol3} \tag{2.11}$$

The fuel mass flow W_f into the cylinders is controlled by u_δ, which gives the injected mass of fuel in mg per cycle and cylinder

$$W_f = \frac{10^{-6}}{120}\, u_\delta\, n_e\, n_{cyl} \tag{2.12}$$

where n_{cyl} is the number of cylinders. The mass flow W_{eo} out from the cylinder is given by the mass balance as

$$W_{eo} = W_f + W_{ei} \tag{2.13}$$

The oxygen to fuel ratio λ_O in the cylinder is defined as

$$\lambda_O = \frac{W_{ei}\, X_{Oim}}{W_f\, (O/F)_s} \tag{2.14}$$

where $(O/F)_s$ is the stoichiometric relation between oxygen and fuel masses.

During the combustion, the oxygen is burned in the presence of fuel. In diesel engines $\lambda_O > 1$ to avoid smoke. Therefore, it is assumed that $\lambda_O > 1$ and the oxygen concentration out from the cylinder can then be calculated as the unburned oxygen fraction

$$X_{Oe} = \frac{W_{ei}\, X_{Oim} - W_f\, (O/F)_s}{W_{eo}} \tag{2.15}$$

Tuning parameters

- c_{vol1}, c_{vol2}, c_{vol3}: volumetric efficiency constants

Tuning method

The tuning parameters c_{vol1}, c_{vol2}, and c_{vol3} are obtained by solving a linear least-squares problem that minimizes $(W_{ei} - W_{ei,meas})^2$ with c_{vol1}, c_{vol2}, and c_{vol3} as the optimization variables. The variable W_{ei} is the model in Eq. (2.10) and (2.11) and $W_{ei,meas}$ is estimated from stationary measurements as $W_{ei,meas} = W_c/(1-x_{egr})$. Stationary measurements are used as inputs to the model during the tuning and the result can be seen in Fig. 2.2, which compares W_{ei} and $W_{ei,meas}$.

2.3.2 Cylinder out temperature

The cylinder out temperature T_e is modeled in the same way as in Skogtjärn (2002). This approach is based upon ideal gas Seliger cycle calculations that give the cylinder out temperature

$$T_e = \eta_{sc}\, \Pi_e^{1-1/\gamma_a}\, r_c^{1-\gamma_a}\, x_p^{1/\gamma_a - 1} \left(q_{in} \left(\frac{1 - x_{cv}}{c_{pa}} + \frac{x_{cv}}{c_{va}} \right) + T_1\, r_c^{\gamma_a - 1} \right) \tag{2.16}$$

where η_{sc} is a compensation factor for non ideal cycles and x_{cv} the ratio of fuel consumed during constant volume combustion. The rest of the fuel $(1-x_{cv})$ is used during constant pressure combustion. Further, this model consists of the pressure quotient over the cylinder

$$\Pi_e = \frac{p_{em}}{p_{im}} \tag{2.17}$$

the pressure quotient between point 3 (after combustion) and point 2 (before combustion) in the Seliger cycle

$$x_p = \frac{p_3}{p_2} = 1 + \frac{q_{in}\, x_{cv}}{c_{va}\, T_1\, r_c^{\gamma_a - 1}} \tag{2.18}$$

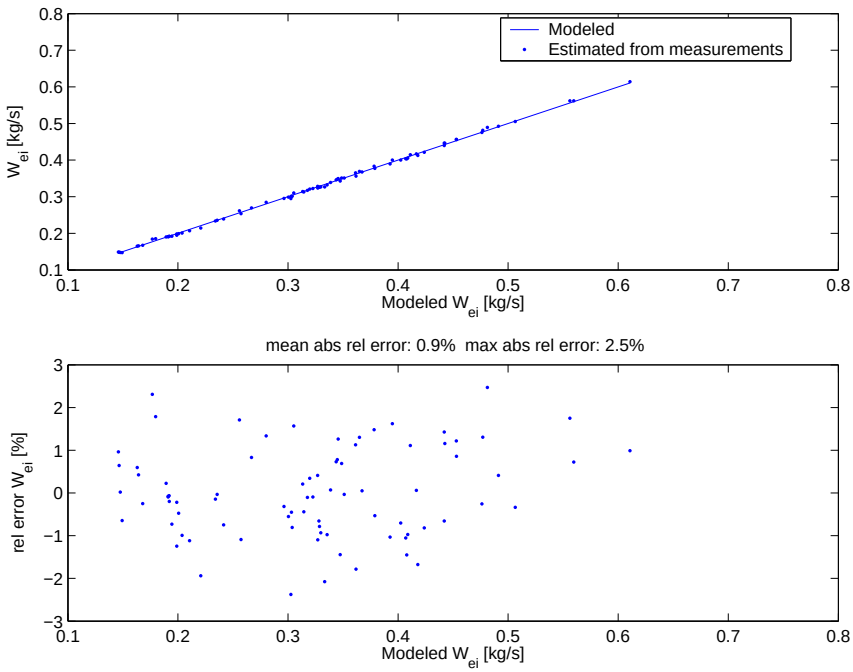

Figure 2.2 **Top:** *Comparison of modeled mass flow* W_{ei} *into the cylinders and estimated* W_{ei} *from measurements.* **Bottom:** *Relative errors for modeled* W_{ei} *as function of modeled* W_{ei} *at steady state.*

the specific energy contents of the charge

$$q_{in} = \frac{W_f \, q_{HV}}{W_{ei} + W_f} \, (1 - x_r) \tag{2.19}$$

the temperature at inlet valve closing after intake stroke and mixing

$$T_1 = x_r \, T_e + (1 - x_r) \, T_{im} \tag{2.20}$$

the residual gas fraction

$$x_r = \frac{\Pi_e^{1/\gamma_a} \, x_p^{-1/\gamma_a}}{r_c \, x_v} \tag{2.21}$$

and the volume quotient between point 3 (after combustion) and point 2 (before combustion) in the Seliger cycle

$$x_v = \frac{v_3}{v_2} = 1 + \frac{q_{in} \, (1 - x_{cv})}{c_{pa} \left(\frac{q_{in} \, x_{cv}}{c_{va}} + T_1 \, r_c^{\gamma_a - 1} \right)} \tag{2.22}$$

Since the equations above are non-linear and depend on each other, the cylinder out temperature is calculated numerically using a fixed point iteration which starts with the initial values $x_{r,0}$ and $T_{1,0}$. Then the following equations are applied in each iteration k

$$\begin{aligned}
q_{in,k+1} &= \frac{W_f\, q_{HV}}{W_{ei} + W_f}\,(1 - x_{r,k}) \\
x_{p,k+1} &= 1 + \frac{q_{in,k+1}\, x_{cv}}{c_{va}\, T_{1,k}\, r_c^{\gamma_a - 1}} \\
x_{v,k+1} &= 1 + \frac{q_{in,k+1}\,(1 - x_{cv})}{c_{pa}\left(\frac{q_{in,k+1}\, x_{cv}}{c_{va}} + T_{1,k}\, r_c^{\gamma_a - 1}\right)} \\
x_{r,k+1} &= \frac{\Pi_e^{1/\gamma_a}\, x_{p,k+1}^{-1/\gamma_a}}{r_c\, x_{v,k+1}} \\
T_{e,k+1} &= \eta_{sc}\, \Pi_e^{1-1/\gamma_a}\, r_c^{1-\gamma_a}\, x_{p,k+1}^{1/\gamma_a - 1}\left(q_{in,k+1}\left(\frac{1 - x_{cv}}{c_{pa}} + \frac{x_{cv}}{c_{va}}\right) + T_{1,k}\, r_c^{\gamma_a - 1}\right) \\
T_{1,k+1} &= x_{r,k+1}\, T_{e,k+1} + (1 - x_{r,k+1})\, T_{im}
\end{aligned} \tag{2.23}$$

In each sample during dynamic simulation, the initial values $x_{r,0}$ and $T_{1,0}$ are set to the solutions of x_r and T_1 from the previous sample.

Exhaust manifold temperature

The cylinder out temperature model above does not describe the exhaust manifold temperature completely due to heat losses. This is illustrated in Fig. 2.3a which shows a comparison between measured and modeled exhaust manifold temperature and in this figure it is assumed that the exhaust manifold temperature is equal to the cylinder out temperature, i.e. $T_{em} = T_e$. The relative error between model and measurement seems to increase from a negative error to a positive error for increasing mass flow W_{eo} out from the cylinder. The exhaust manifold temperature is measured in the exhaust manifold, thus the heat losses to the surroundings in the exhaust pipes between the cylinder and the exhaust manifold must be taken into consideration.

This temperature drop is modeled as a function of mass flow out from the cylinder, see Model 1 in Eriksson (2002).

$$T_{em} = T_{amb} + (T_e - T_{amb})\, e^{-\frac{h_{tot}\, \pi\, d_{pipe}\, l_{pipe}\, n_{pipe}}{W_{eo}\, c_{pe}}} \tag{2.24}$$

where T_{amb} is the ambient temperature, h_{tot} the total heat transfer coefficient, d_{pipe} the pipe diameter, l_{pipe} the pipe length and n_{pipe} the number of pipes. Using this model, the mean and maximum absolute relative error is reduced, see Fig. 2.3b.

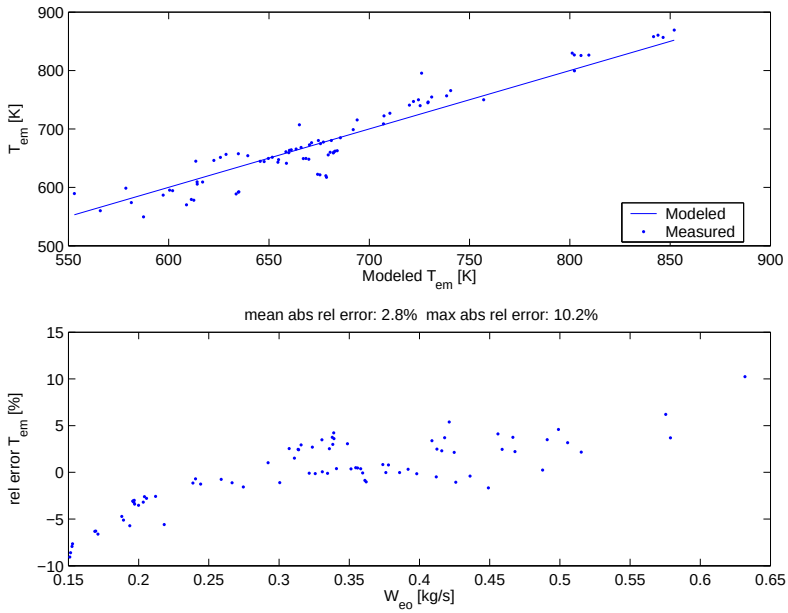

a. Without a model for heat losses in the exhaust pipes, i.e. $\mathsf{T}_{\mathrm{em}} = \mathsf{T}_{\mathrm{e}}$.

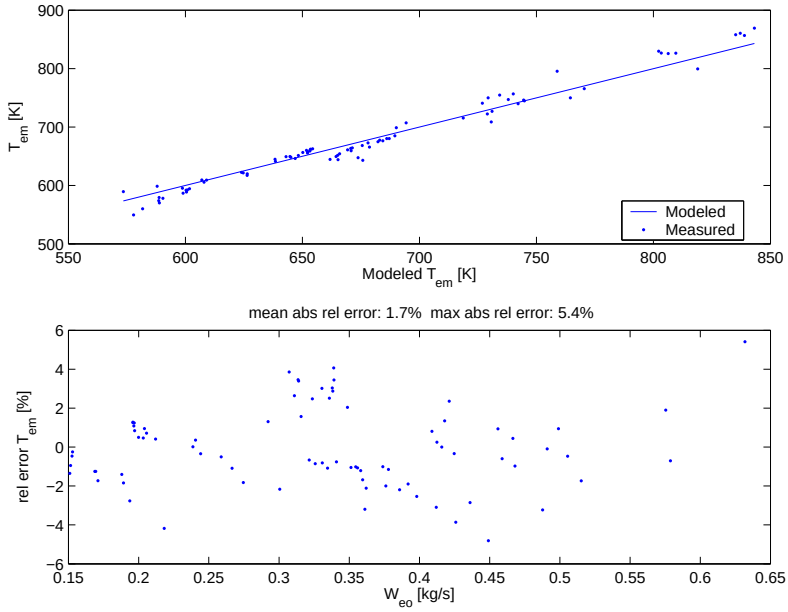

b. With model (2.24) for heat losses in the exhaust pipes.

Figure 2.3 *Modeled and measured exhaust manifold temperature* T_{em} *and relative errors for modeled* T_{em} *at steady state.*

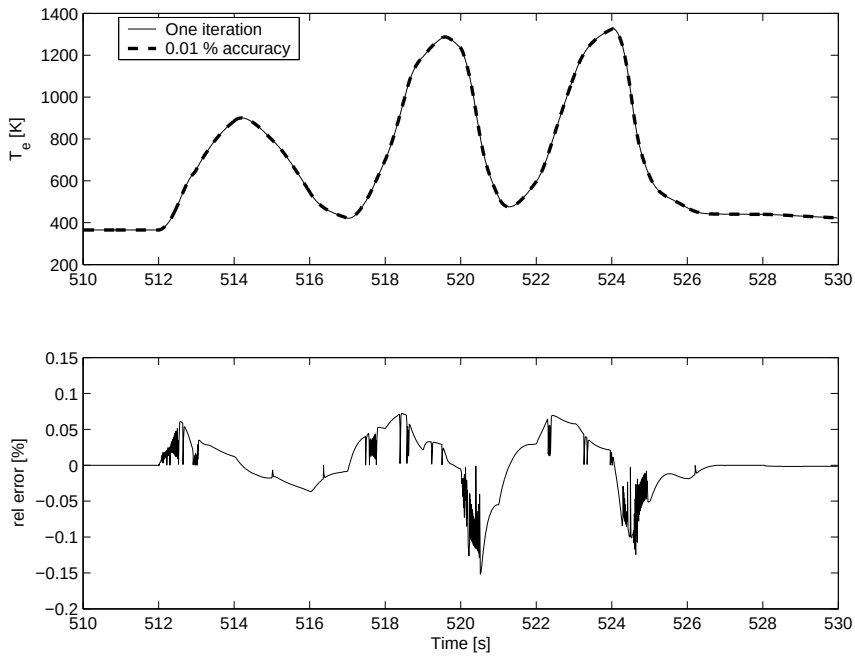

Figure 2.4 *The cylinder out temperature* T_e *is calculated by simulating the total engine model during the complete European Transient Cycle. This figure shows the part of the European Transient Cycle that consists of the maximum relative error.* **Top:** *The fixed point iteration Eq.* (2.23) *is used in two ways: by using one iteration and to get 0.01 % accuracy.* **Bottom:** *Relative errors between the solutions from one iteration and 0.01 % accuracy.*

Approximating the solution to the cylinder out temperature

As explained above, the cylinder out temperature is calculated numerically using the fixed point iteration Eq. (2.23). Fig. 2.4 shows that it is sufficient to use one iteration in this iterative process. This is shown by comparing the solution from one iteration with one that has a sufficient number of iterations to give a solution with 0.01 % accuracy. The maximum absolute relative error of the solution from one iteration (compared to the solution with 0.01 % accuracy) is 0.15 %. This error is small because the fixed point iteration Eq. (2.23) has initial values that are close to the solution. Consequently, it is sufficient to use one iteration in this model since the mean absolute relative error of the exhaust manifold temperature model (compared to the measurements in Fig. 2.3b) is 1.7 %.

Tuning parameters

- η_{sc}: compensation factor for non ideal cycles
- x_{cv}: the ratio of fuel consumed during constant volume combustion
- h_{tot}: the total heat transfer coefficient

Tuning method

The tuning parameters η_{sc}, x_{cv}, and h_{tot} are obtained by solving a non-linear least-squares problem that minimizes $(T_{em} - T_{em,meas})^2$ with η_{sc}, x_{cv}, and h_{tot} as the optimization variables. The variable T_{em} is the model in Eq. (2.23) and (2.24) with stationary measurements as inputs to the model, and $T_{em,meas}$ is a stationary measurement. The result of the tuning is shown in Fig. 2.3b.

2.3.3 Cylinder torque

The torque produced by the engine M_e is modeled using three different engine components; the gross indicated torque M_{ig}, the pumping torque M_p, and the friction torque M_{fric} (Heywood, 1988).

$$M_e = M_{ig} - M_p - M_{fric} \tag{2.25}$$

The pumping torque is modeled using the intake and exhaust manifold pressures.

$$M_p = \frac{V_d}{4\pi}(p_{em} - p_{im}) \tag{2.26}$$

The gross indicated torque is coupled to the energy that comes from the fuel

$$M_{ig} = \frac{u_\delta \, 10^{-6} \, n_{cyl} \, q_{HV} \, \eta_{ig}}{4\pi} \tag{2.27}$$

Assuming that the engine is always running at optimal injection timing, the gross indicated efficiency η_{ig} is modeled as

$$\eta_{ig} = \eta_{igch}\left(1 - \frac{1}{r_c^{\gamma_{cyl}-1}}\right) \tag{2.28}$$

where the parameter η_{igch} is estimated from measurements, r_c is the compression ratio, and γ_{cyl} is the specific heat capacity ratio for the gas in the cylinder. The friction torque is assumed to follow a polynomial function

$$M_{fric} = \frac{V_d}{4\pi} 10^5 \left(c_{fric1} \, n_{eratio}^2 + c_{fric2} \, n_{eratio} + c_{fric3}\right) \tag{2.29}$$

where

$$n_{eratio} = \frac{n_e}{1000} \tag{2.30}$$

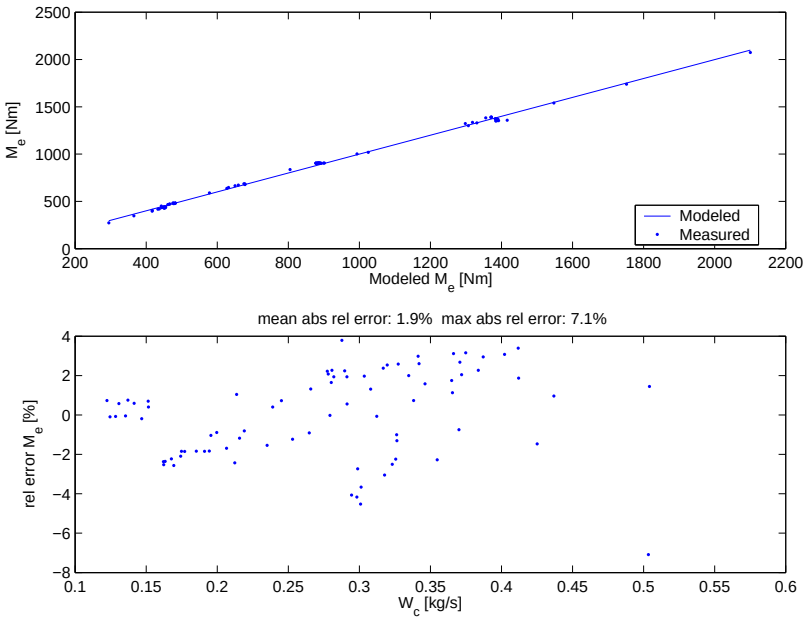

Figure 2.5 *Comparison of measurements and model for the engine torque* M_e *at steady state.* **Top:** *Modeled and measured engine torque* M_e. **Bottom:** *Relative errors for modeled* M_e.

Tuning model parameters

- η_{igch}: combustion chamber efficiency

- c_{fric1}, c_{fric2}, c_{fric3}: coefficients in the polynomial function for the friction torque

Tuning method

The tuning parameters η_{igch}, c_{fric1}, c_{fric2}, and c_{fric3} are obtained by solving a linear least-squares problem that minimizes $(M_e + M_p - M_{e,meas} - M_{p,meas})^2$ with the tuning parameters as the optimization variables. The model of $M_e + M_p$ is obtained by solving $M_e + M_p$ from Eq. (2.25) and $M_{e,meas} + M_{p,meas}$ is estimated from stationary measurements as $M_{e,meas} + M_{p,meas} = M_e + V_d(p_{em} - p_{im})/(4\pi)$. Stationary measurements are used as inputs to the model. The result of the tuning can be seen in Fig. 2.5.

2.4 EGR-valve

The mass flow through the EGR-valve is modeled as a simplification of a compressible flow restriction with variable area (Heywood, 1988) and with the assumption that there is no reverse flow when $p_{em} < p_{im}$. The motive for this assumption is to construct a simple model. The model can be extended with reverse flow, but this increases the complexity of the model since a reverse flow model requires mixing of different temperatures and oxygen fractions in the exhaust manifold and a change of the temperature and the gas constant in the EGR mass flow model. However, p_{em} is larger than p_{im} in normal operating points, consequently the assumption above will not effect the model behavior in these operating points. Furthermore, reverse flow is not measured and can therefore not be validated.

The mass flow through the restriction is

$$W_{egr} = \frac{A_{egr}\, p_{em}\, \Psi_{egr}}{\sqrt{T_{em}\, R_e}} \tag{2.31}$$

where

$$\Psi_{egr} = \sqrt{\frac{2\gamma_e}{\gamma_e - 1}\left(\Pi_{egr}^{2/\gamma_e} - \Pi_{egr}^{1+1/\gamma_e}\right)} \tag{2.32}$$

Measurement data shows that Eq. (2.32) does not give a sufficiently accurate description of the EGR flow. Pressure pulsations in the exhaust manifold or the influence of the EGR-cooler could be two different explanations for this phenomenon. In order to maintain the density influence ($p_{em}/(\sqrt{T_{em}\, R_e})$) in Eq. (2.31) and the simplicity in the model, the function Ψ_{egr} is instead modeled as a parabolic function (see Fig. 2.6 where Ψ_{egr} is plotted as function of Π_{egr}).

$$\Psi_{egr} = 1 - \left(\frac{1 - \Pi_{egr}}{1 - \Pi_{egropt}} - 1\right)^2 \tag{2.33}$$

The pressure quotient Π_{egr} over the valve is limited when the flow is choked, i.e. when sonic conditions are reached in the throat, and when $1 < p_{im}/p_{em}$, i.e. no backflow can occur.

$$\Pi_{egr} = \begin{cases} \Pi_{egropt} & \text{if } \frac{p_{im}}{p_{em}} < \Pi_{egropt} \\ \frac{p_{im}}{p_{em}} & \text{if } \Pi_{egropt} \le \frac{p_{im}}{p_{em}} \le 1 \\ 1 & \text{if } 1 < \frac{p_{im}}{p_{em}} \end{cases} \tag{2.34}$$

For a compressible flow restriction, the standard model for Π_{egropt} is

$$\Pi_{egropt} = \left(\frac{2}{\gamma_e + 1}\right)^{\frac{\gamma_e}{\gamma_e - 1}} \tag{2.35}$$

but the accuracy of the EGR flow model is improved by replacing the physical value of Π_{egropt} in Eq. (2.35) with a tuning parameter (Andersson, 2005).

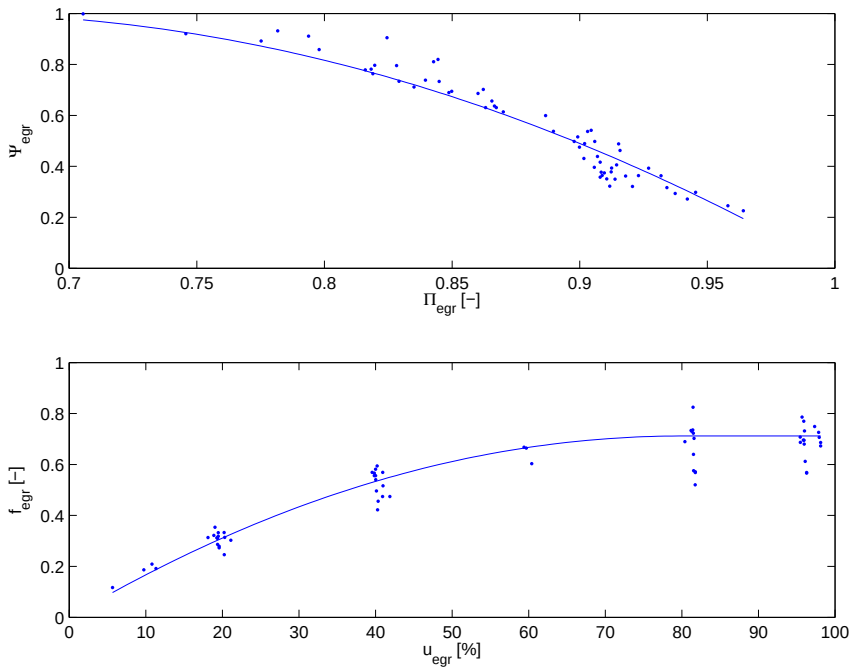

Figure 2.6 *Comparison of estimated points from measurements and two sub-models for the EGR flow W_{egr} at steady state showing how different variables in the sub-models depend on each other. Note that this is not a validation of the sub-models since the estimated points for the sub-models depend on the model tuning.* **Top:** *Ψ_{egr} as function of pressure quotient Π_{egr}. The estimated points are calculated by solving Ψ_{egr} from Eq. (2.31). The model is described by Eq. (2.33).* **Bottom:** *Effective area ratio f_{egr} as function of control signal u_{egr}. The estimated points are calculated by solving f_{egr} from Eq. (2.31). The model is described by Eq. (2.37).*

The effective area

$$A_{egr} = A_{egrmax}\, f_{egr}(\tilde{u}_{egr}) \tag{2.36}$$

is modeled as a polynomial function of the EGR valve position $\tilde{u}_{egr}$ (see Fig. 2.6 where f_{egr} is plotted as function of u_{egr})

$$f_{egr}(\tilde{u}_{egr}) = \begin{cases} c_{egr1}\,\tilde{u}_{egr}^2 + c_{egr2}\,\tilde{u}_{egr} + c_{egr3} & \text{if } \tilde{u}_{egr} \leq -\frac{c_{egr2}}{2\,c_{egr1}} \\ c_{egr3} - \frac{c_{egr2}^2}{4\,c_{egr1}} & \text{if } \tilde{u}_{egr} > -\frac{c_{egr2}}{2\,c_{egr1}} \end{cases} \tag{2.37}$$

where $\tilde{u}_{egr}$ describes the EGR actuator dynamic

$$\frac{d}{dt}\tilde{u}_{egr} = \frac{1}{\tau_{egr}}(u_{egr}(t-\tau_{degr}) - \tilde{u}_{egr}) \tag{2.38}$$

The EGR-valve is open when $\tilde{u}_{egr} = 100\%$ and closed when $\tilde{u}_{egr} = 0\%$. The values of τ_{egr} and τ_{degr} have been provided by industry.

Tuning parameters

- Π_{egropt}: optimal value of Π_{egr} for maximum value of the function Ψ_{egr} in Eq. (2.33)
- c_{egr1}, c_{egr2}, c_{egr3}: coefficients in the polynomial function for the effective area

Tuning method

The tuning parameter Π_{egropt} is obtained by solving a non-linear least-squares problem that minimizes $(W_{egr} - W_{egr,meas})^2$ with Π_{egropt} as the optimization variable. In each iteration in the non-linear least-squares solver, the values for c_{egr1}, c_{egr2}, and c_{egr3} are set to be the solution of a linear least-squares problem that minimizes $(W_{egr} - W_{egr,meas})^2$ for the current value of Π_{egropt}. The variable W_{egr} is described by the model Eq. (2.31) and $W_{egr,meas}$ is estimated from measurements as $W_{egr,meas} = W_c\, x_{egr}/(1 - x_{egr})$. Stationary measurements are used as inputs to the model. The result of the tuning is shown in Fig. 2.7.

2.5 Turbocharger

The turbocharger consist of a turbo inertia model, a turbine model, and a compressor model.

2.5.1 Turbo inertia

For the turbo speed ω_t, Newton's second law gives

$$\frac{d}{dt}\omega_t = \frac{P_t\,\eta_m - P_c}{J_t\,\omega_t} \tag{2.39}$$

where J_t is the inertia, P_t is the power delivered by the turbine, P_c is the power required to drive the compressor, and η_m is the mechanical efficiency in the turbocharger.

Tuning parameter

- J_t: turbo inertia

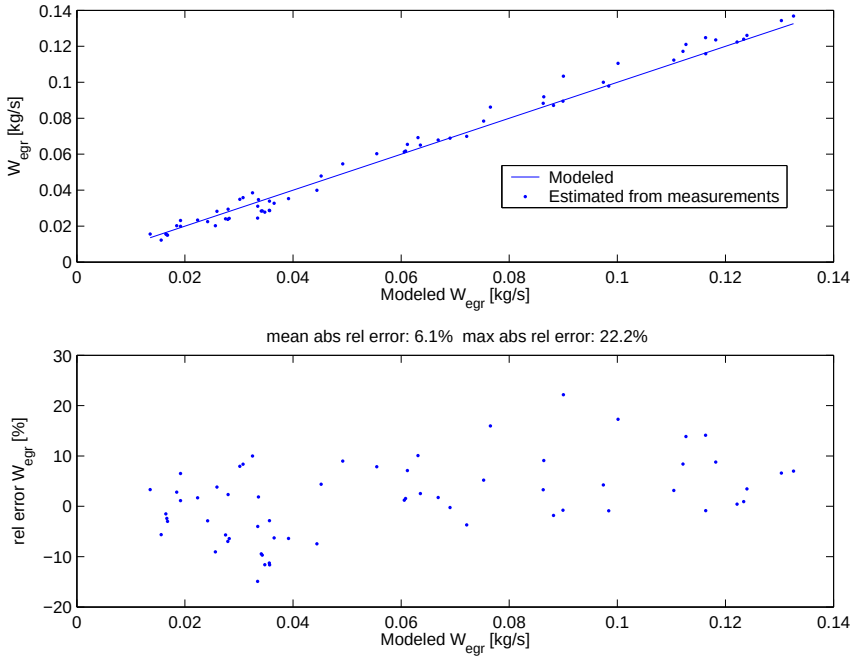

Figure 2.7 **Top:** *Comparison between modeled EGR flow* W_{egr} *and estimated* W_{egr} *from measurements at steady state.* **Bottom:** *Relative errors for* W_{egr} *at steady state.*

Tuning method

The tuning parameter J_t is obtained by adjusting this parameter manually until simulations of the complete model follow the dynamic responses in the dynamic measurements, see Sec. 2.8.1.

2.5.2 Turbine

The turbine models are the total turbine efficiency and the turbine mass flow.

Turbine efficiency

One way to model the power P_t is to use the turbine efficiency η_t, which is defined as (Heywood, 1988)

$$\eta_t = \frac{P_t}{P_{t,s}} = \frac{T_{em} - T_t}{T_{em}(1 - \Pi_t^{1-1/\gamma_e})} \tag{2.40}$$

where T_t is the temperature after the turbine, Π_t is the pressure ratio

$$\Pi_t = \frac{p_{amb}}{p_{em}} \tag{2.41}$$

and $P_{t,s}$ is the power from the isentropic process

$$P_{t,s} = W_t \, c_{pe} \, T_{em} \left(1 - \Pi_t^{1-1/\gamma_e}\right) \tag{2.42}$$

where W_t is the turbine mass flow.

However, Eq. (2.40) is not applicable due to heat losses in the turbine which cause temperature drops in the temperatures T_t and T_{em}. Consequently, there will be errors for η_t if Eq. (2.40) is used to calculate η_t from measurements. One way to overcome this is to model the temperature drops, but it is difficult to tune these models since there exists no measurements of these temperature drops. Another way to overcome this, that is frequently used in the literature, is to use another efficiency that are approximatively equal to η_t. This approximation utilizes that

$$P_t \, \eta_m = P_c \tag{2.43}$$

at steady state according to Eq. (2.39). Consequently, $P_t \approx P_c$ at steady state. Using this approximation in Eq. (2.40), another efficiency η_{tm} is obtained

$$\eta_{tm} = \frac{P_c}{P_{t,s}} = \frac{W_c \, c_{pa} (T_c - T_{amb})}{W_t \, c_{pe} \, T_{em} \left(1 - \Pi_t^{1-1/\gamma_e}\right)} \tag{2.44}$$

where T_c is the temperature after the compressor and W_c is the compressor mass flow. The temperature T_{em} in Eq. (2.44) introduces less errors compared to the temperature difference $T_{em} - T_t$ in Eq. (2.40) due to that the absolute value of T_{em} is larger than the absolute value of $T_{em} - T_t$. Consequently, Eq. (2.44) introduces less errors compared to Eq. (2.40) since Eq. (2.44) does not consist of $T_{em} - T_t$. The temperatures T_c and T_{amb} are low and they introduce less errors compared to T_{em} and T_t since the heat losses in the compressor are comparatively small. Another advantage of using Eq. (2.44) is that the individual variables P_t and η_m in Eq. (2.39) do not have to be modeled. Instead, the product $P_t \, \eta_m$ is modeled using Eq. (2.43) and (2.44)

$$P_t \, \eta_m = P_c = \eta_{tm} \, P_{t,s} = \eta_{tm} \, W_t \, c_{pe} \, T_{em} \left(1 - \Pi_t^{1-1/\gamma_e}\right) \tag{2.45}$$

Measurements show that η_{tm} depends on the blade speed ratio (BSR) as a parabolic function (Watson and Janota, 1982), see Fig. 2.8 where η_{tm} is plotted as function of BSR.

$$\eta_{tm} = \eta_{tm,max} - c_m (BSR - BSR_{opt})^2 \tag{2.46}$$

The blade speed ratio is the quotient of the turbine blade tip speed and the speed which a gas reaches when expanded isentropically at the given pressure ratio Π_t

$$BSR = \frac{R_t \, \omega_t}{\sqrt{2 \, c_{pe} \, T_{em} \left(1 - \Pi_t^{1-1/\gamma_e}\right)}} \tag{2.47}$$

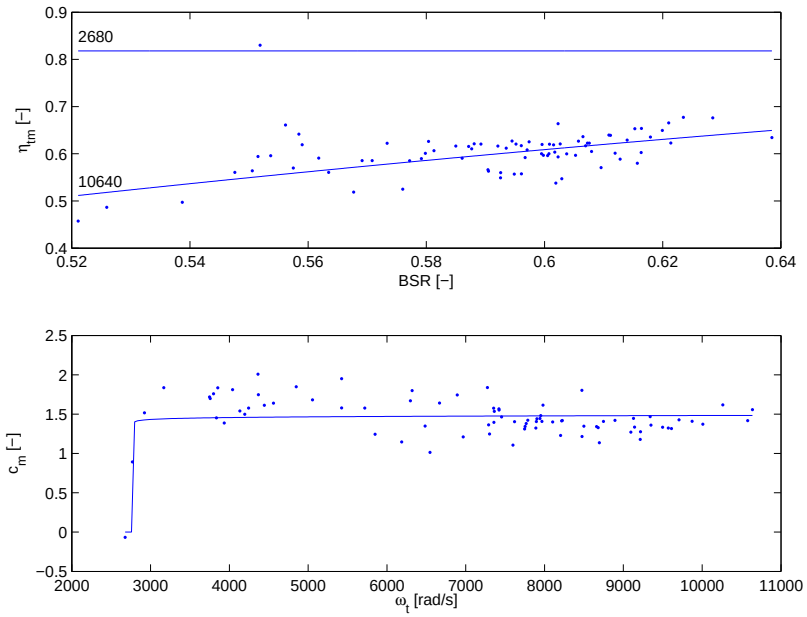

Figure 2.8 *Comparison of estimated points from measurements and the model for the turbine efficiency* η_{tm} *at steady state.* **Top:** η_{tm} *as function of blade speed ratio* BSR*. The estimated points are calculated by using Eq. (2.44) and (2.47). The model Eq. (2.46) is plotted at two different turbo speeds* ω_t*.* **Bottom:** *Parameter* c_m *as function of turbo speed* ω_t*. The estimated points are calculated by solving* c_m *from Eq. (2.46). The model is described by Eq. (2.48). Note that this plot is not a validation of* c_m *since the estimated points for* c_m *depend on the model tuning.*

where R_t is the turbine blade radius. The parameter c_m in the parabolic function varies due to mechanical losses and c_m is therefore modeled as a function of the turbo speed

$$c_m = c_{m1}(\omega_t - c_{m2})^{c_{m3}} \tag{2.48}$$

see Fig. 2.8 where c_m is plotted as function of ω_t.

Tuning parameters

- $\eta_{tm,max}$: maximum turbine efficiency
- BSR_{opt}: optimum BSR value for maximum turbine efficiency
- c_{m1}, c_{m2}, c_{m3}: parameters in the model for c_m

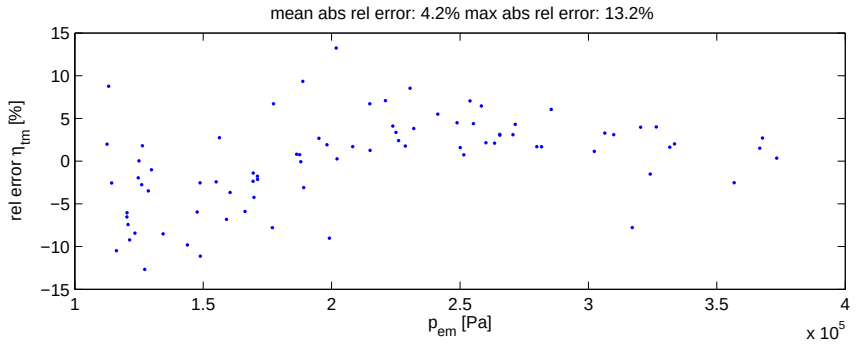

Figure 2.9 *Relative errors for the total turbine efficiency η_{tm} as function of exhaust manifold pressure p_{em} at steady state.*

Tuning method

The tuning parameters BSR_{opt}, c_{m2}, and c_{m3} are obtained by solving a non-linear least-squares problem that minimizes $(\eta_{tm} - \eta_{tm,meas})^2$ with BSR_{opt}, c_{m2}, and c_{m3} as the optimization variables. In each iteration in the non-linear least-squares solver, the values for $\eta_{tm,max}$ and c_{m1} are set to be the solution of a linear least-squares problem that minimizes $(\eta_{tm} - \eta_{tm,meas})^2$ for the current values of BSR_{opt}, c_{m2}, and c_{m3}. The efficiency η_{tm} is described by the model Eq. (2.46) and $\eta_{tm,meas}$ is estimated from measurements using Eq. (2.44). Stationary measurements are used as inputs to the model. The result of the tuning is shown in Fig. 2.8 and 2.9.

Turbine mass flow

The turbine mass flow W_t is modeled using the corrected mass flow (Heywood, 1988; Watson and Janota, 1982)

$$\frac{W_t \sqrt{T_{em}}}{p_{em}} = A_{vgtmax} f_{\Pi t}(\Pi_t) f_{vgt}(\tilde{u}_{vgt}) \tag{2.49}$$

where A_{vgtmax} is the maximum area in the turbine that the gas flows through. Measurements show that the corrected mass flow depends on the pressure ratio Π_t and the VGT actuator signal $\tilde{u}_{vgt}$. As the pressure ratio decreases, the corrected mass flow increases until the gas reaches the sonic condition and the flow is choked. This behavior can be described by a choking function

$$f_{\Pi t}(\Pi_t) = \sqrt{1 - \Pi_t^{K_t}} \tag{2.50}$$

which is not based on the physics of the turbine, but it gives good agreement with measurements using few parameters (Eriksson et al., 2002), see Fig. 2.10 where $f_{\Pi t}$ is plotted as function of Π_t.

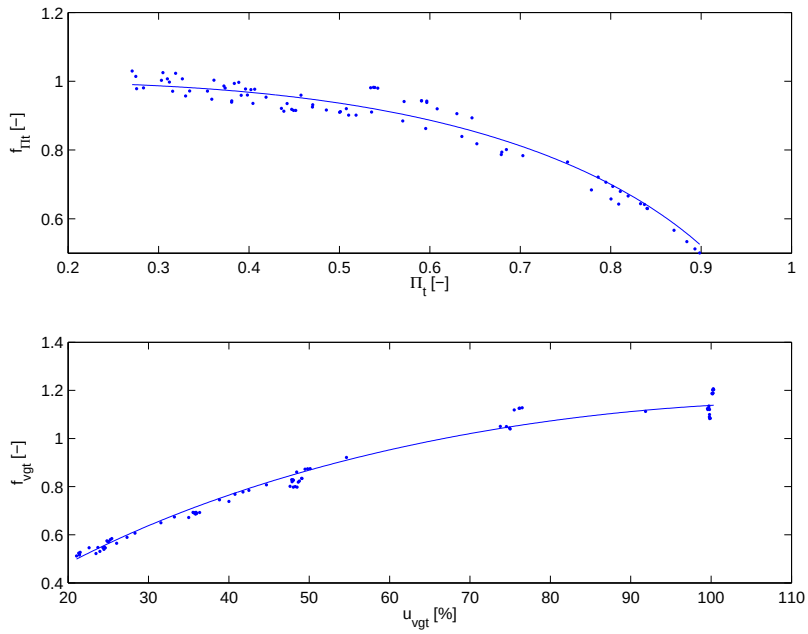

Figure 2.10 *Comparison of estimated points from measurements and two sub-models for the turbine mass flow at steady state showing how different variables in the sub-models depend on each other. Note that this is not a validation of the sub-models since the estimated points for the sub-models depend on the model tuning.* **Top:** *The choking function* $f_{\Pi t}$ *as function of the pressure ratio* Π_t*. The estimated points are calculated by solving* $f_{\Pi t}$ *from Eq. (2.49). The model is described by Eq. (2.50).* **Bottom:** *The effective area ratio function* f_{vgt} *as function of the control signal* u_{vgt}*. The estimated points are calculated by solving* f_{vgt} *from Eq. (2.49). The model is described by Eq. (2.54).*

When the VGT control signal u_{vgt} increases, the effective area increases and hence also the flow increases. Due to the geometry in the turbine, the change in effective area is large when the VGT control signal is large. This behavior can be described by a part of an ellipse (see Fig. 2.10 where f_{vgt} is plotted as function of u_{vgt})

$$\left(\frac{f_{vgt}(\tilde{u}_{vgt}) - c_{f2}}{c_{f1}}\right)^2 + \left(\frac{\tilde{u}_{vgt} - c_{vgt2}}{c_{vgt1}}\right)^2 = 1 \tag{2.51}$$

where f_{vgt} is the effective area ratio function and $\tilde{u}_{vgt}$ describes the VGT actuator

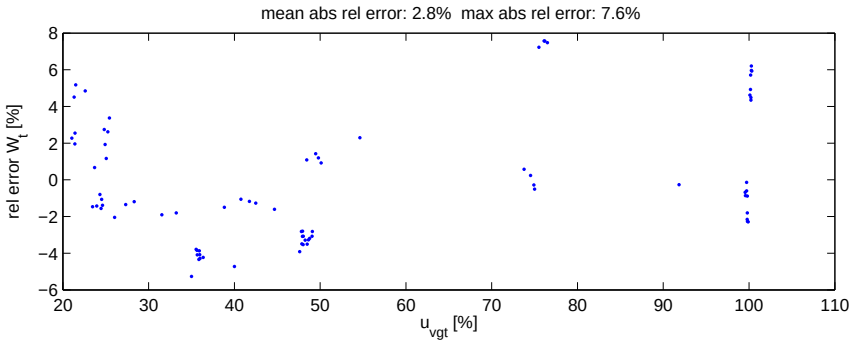

Figure 2.11 *Relative errors for turbine flow W_t as function of control signal u_{vgt} at steady state.*

dynamic

$$\frac{d}{dt}\tilde{u}_{vgt} = \frac{1}{\tau_{vgt}}(u_{vgt} - \tilde{u}_{vgt}) \tag{2.52}$$

The value of τ_{vgt} has been provided by industry. The flow can now be modeled by solving W_t from Eq. (2.49)

$$W_t = \frac{A_{vgtmax}\, p_{em}\, f_{\Pi t}(\Pi_t)\, f_{vgt}(\tilde{u}_{vgt})}{\sqrt{T_{em}}} \tag{2.53}$$

and solving f_{vgt} from Eq. (2.51)

$$f_{vgt}(\tilde{u}_{vgt}) = c_{f2} + c_{f1}\sqrt{1 - \left(\frac{\tilde{u}_{vgt} - c_{vgt2}}{c_{vgt1}}\right)^2} \tag{2.54}$$

Tuning parameters

- K_t: exponent in the choking function for the turbine flow
- c_{f1}, c_{f2}, c_{vgt1}, c_{vgt2}: parameters in the ellipse for the effective area ratio function

Tuning method

The tuning parameters above are obtained by solving a non-linear least-squares problem that minimizes $(W_t - W_{t,meas})^2$ with the tuning parameters as the optimization variables. The flow W_t is described by the model Eq. (2.53), (2.54), and (2.50), and $W_{t,meas}$ is estimated from measurements as $W_{t,meas} = W_c + W_f$, where W_f is estimated using Eq. (2.12). Stationary measurements are used as inputs to the model. The result of the tuning is shown in Fig. 2.11.

2.5.3 Compressor

The compressor models the compressor efficiency and the compressor mass flow.

Compressor efficiency

The compressor power P_c is modeled using the compressor efficiency η_c, which is defined as (Heywood, 1988)

$$\eta_c = \frac{P_{c,s}}{P_c} = \frac{T_{amb}\left(\Pi_c^{1-1/\gamma_a} - 1\right)}{T_c - T_{amb}} \tag{2.55}$$

where T_c is the temperature after the compressor, Π_c is the pressure ratio

$$\Pi_c = \frac{p_{im}}{p_{amb}} \tag{2.56}$$

and $P_{c,s}$ is the power from the isentropic process

$$P_{c,s} = W_c\, c_{pa}\, T_{amb}\left(\Pi_c^{1-1/\gamma_a} - 1\right) \tag{2.57}$$

where W_c is the compressor mass flow. The power P_c is modeled by solving P_c from Eq. (2.55) and using Eq. (2.57)

$$P_c = \frac{P_{c,s}}{\eta_c} = \frac{W_c\, c_{pa}\, T_{amb}}{\eta_c}\left(\Pi_c^{1-1/\gamma_a} - 1\right) \tag{2.58}$$

The efficiency is modeled using ellipses similar to Guzzella and Amstutz (1998), but with a non-linear transformation on the axis for the pressure ratio. The inputs to the efficiency model are Π_c and W_c (see Fig. 2.16). The flow W_c is not scaled by the inlet temperature and the inlet pressure since these two variables are constant. The ellipses can be described as

$$\eta_c = \eta_{cmax} - \chi^T\, Q_c\, \chi \tag{2.59}$$

χ is a vector which contains the inputs

$$\chi = \begin{bmatrix} W_c - W_{copt} \\ \pi_c - \pi_{copt} \end{bmatrix} \tag{2.60}$$

where the non-linear transformation for Π_c is

$$\pi_c = (\Pi_c - 1)^{pow_\pi} \tag{2.61}$$

and the symmetric matrix Q_c consists of three parameters

$$Q_c = \begin{bmatrix} a_1 & a_3 \\ a_3 & a_2 \end{bmatrix} \tag{2.62}$$

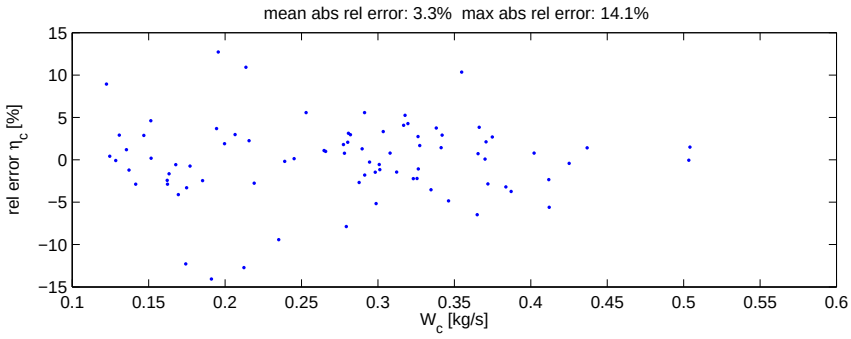

Figure 2.12 *Relative errors for* η_c *as function of* W_c *at steady state.*

Tuning model parameters

- η_{cmax}: maximum compressor efficiency
- W_{copt} and π_{copt}: optimum values of W_c and π_c for maximum compressor efficiency
- pow_π: exponent in the scale function, Eq. (2.61)
- a_1, a_2 and a_3: parameters in the matrix Q_c

Tuning method

The tuning parameters W_{copt}, π_{copt}, and pow_π are obtained by solving a non-linear least-squares problem that minimizes $(\eta_c - \eta_{c,meas})^2$ with W_{copt}, π_{copt}, and pow_π as the optimization variables. In each iteration in the non-linear least-squares solver, the values for η_{cmax}, a_1, a_2 and a_3 are set to be the solution of a linear least-squares problem that minimizes $(\eta_c - \eta_{c,meas})^2$ for the current values of W_{copt}, π_{copt}, and pow_π. The efficiency η_c is described by the model Eq. (2.59) to (2.62) and $\eta_{c,meas}$ is estimated from measurements using Eq. (2.55). Stationary measurements are used as inputs to the model. The result of the tuning is shown in Fig. 2.12.

Compressor mass flow

The mass flow W_c through the compressor is modeled using two dimensionless variables. The first variable is the energy transfer coefficient (Dixon, 1998)

$$\Psi_c = \frac{2\, c_{pa}\, T_{amb} \left(\Pi_c^{1-1/\gamma_a} - 1 \right)}{R_c^2\, \omega_t^2} \tag{2.63}$$

which is the quotient of the isentropic kinetic energy of the gas at the given pressure ratio Π_c and the kinetic energy of the compressor blade tip where R_c is compressor

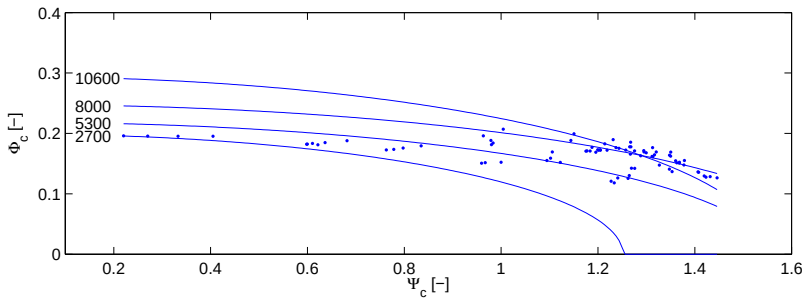

Figure 2.13 *Comparison of estimated points from measurements and model for the compressor mass flow W_c at steady state. Volumetric flow coefficient Φ_c as function of energy transfer coefficient Ψ_c. The estimated points are calculated using Eq. (2.63) and (2.64). The model (Eq. 2.68) is plotted at four different turbo speeds ω_t.*

blade radius. The second variable is the volumetric flow coefficient (Dixon, 1998)

$$\Phi_c = \frac{W_c/\rho_{amb}}{\pi R_c^3 \omega_t} = \frac{R_a T_{amb}}{p_{amb} \pi R_c^3 \omega_t} W_c \tag{2.64}$$

which is the quotient of volume flow rate of air into the compressor and the rate at which volume is displaced by the compressor blade where ρ_{amb} is the density of the ambient air. The relation between Ψ_c and Φ_c can be described by a part of an ellipse (Andersson, 2005), see Fig. 2.13 where Φ_c is plotted as function of Ψ_c.

$$c_{\Psi 1}(\omega_t)\,(\Psi_c - c_{\Psi 2})^2 + c_{\Phi 1}(\omega_t)\,(\Phi_c - c_{\Phi 2})^2 = 1 \tag{2.65}$$

where $c_{\Psi 1}$ and $c_{\Phi 1}$ varies with turbo speed ω_t and are modeled as polynomial functions.

$$c_{\Psi 1}(\omega_t) = c_{\omega\Psi 1}\,\omega_t^2 + c_{\omega\Psi 2}\,\omega_t + c_{\omega\Psi 3} \tag{2.66}$$

$$c_{\Phi 1}(\omega_t) = c_{\omega\Phi 1}\,\omega_t^2 + c_{\omega\Phi 2}\,\omega_t + c_{\omega\Phi 3} \tag{2.67}$$

In Fig. 2.14 the variables $c_{\Psi 1}$ and $c_{\Phi 1}$ are plotted as function of the turbo speed ω_t.

The mass flow is modeled by solving Φ_c from Eq. (2.65) and solving W_c from Eq. (2.64).

$$\Phi_c = \sqrt{\frac{1 - c_{\Psi 1}\,(\Psi_c - c_{\Psi 2})^2}{c_{\Phi 1}}} + c_{\Phi 2} \tag{2.68}$$

$$W_c = \frac{p_{amb} \pi R_c^3 \omega_t}{R_a T_{amb}} \Phi_c \tag{2.69}$$

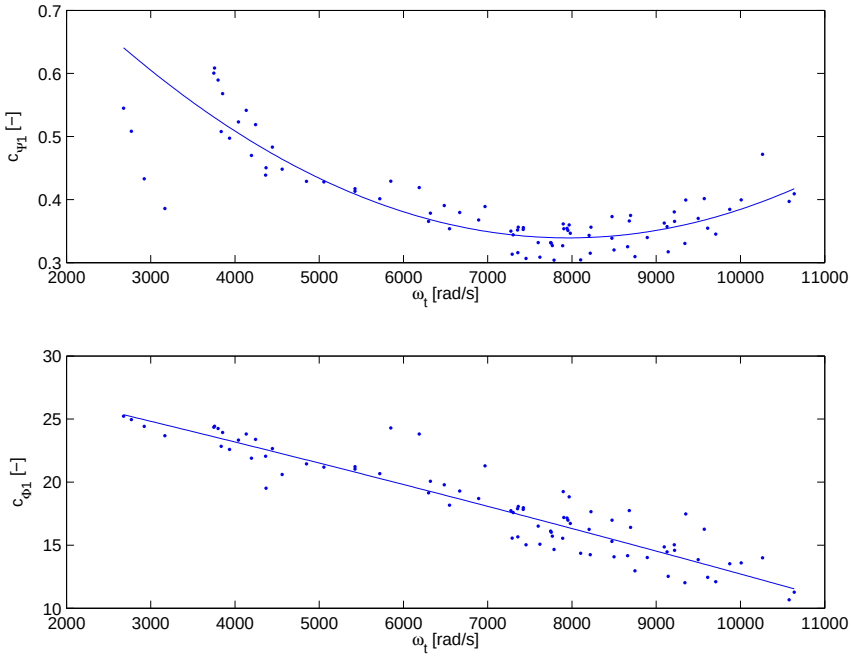

Figure 2.14 *Comparison of estimated points from measurements and two sub-models for the compressor mass flow at steady state showing how different variables in the sub-models depend on each other. Note that this is not a validation of the sub-models since the estimated points for the sub-models depend on the model tuning. The sub-models are the ellipse variables* $c_{\Psi 1}$ *and* $c_{\Phi 1}$ *as function of turbo speed* ω_t*. The estimated points are calculated by solving* $c_{\Psi 1}$ *and* $c_{\Phi 1}$ *from Eq. (2.65). The models are described by Eq. (2.66) and (2.67).*

Tuning model parameters

- $c_{\Psi 2}$, $c_{\Phi 2}$: parameters in the ellipse model for the compressor mass flow
- $c_{\omega\Psi 1}$, $c_{\omega\Psi 2}$, $c_{\omega\Psi 3}$: coefficients in the polynomial function Eq. (2.66)
- $c_{\omega\Phi 1}$, $c_{\omega\Phi 2}$, $c_{\omega\Phi 3}$: coefficients in the polynomial function Eq. (2.67)

Tuning method

The tuning parameters $c_{\Psi 2}$ and $c_{\Phi 2}$ are obtained by solving a non-linear least-squares problem that minimizes $(c_{\Psi 1}(\omega_t)\,(\Psi_c - c_{\Psi 2})^2 + c_{\Phi 1}(\omega_t)\,(\Phi_c - c_{\Phi 2})^2 - 1)^2$

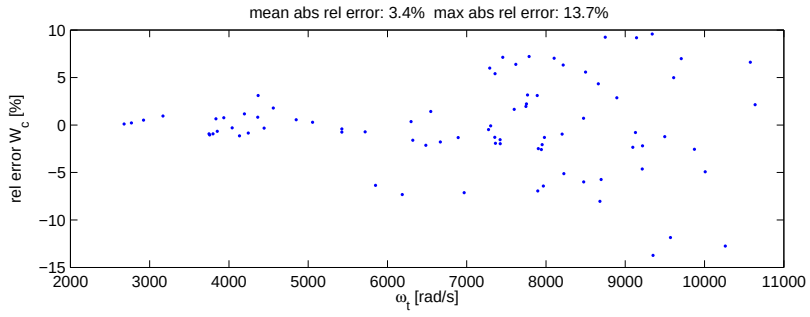

Figure 2.15 *Relative errors for compressor flow W_c as function of turbocharger speed ω_t at steady state.*

with $c_{\Psi 2}$ and $c_{\Phi 2}$ as the optimization variables. In each iteration in the nonlinear least-squares solver, the values for $c_{\omega\Psi 1}$, $c_{\omega\Psi 2}$, $c_{\omega\Psi 3}$, $c_{\omega\Phi 1}$, $c_{\omega\Phi 2}$, and $c_{\omega\Phi 3}$ are set to be the solution of a linear least-squares problem that minimizes $(c_{\Psi 1}(\omega_t)(\Psi_c - c_{\Psi 2})^2 + c_{\Phi 1}(\omega_t)(\Phi_c - c_{\Phi 2})^2 - 1)^2$ for the current values of $c_{\Psi 2}$ and $c_{\Phi 2}$. Stationary measurements are used as inputs to the model. The result of the tuning is shown in Fig. 2.15.

Compressor map

Compressor performance is usually presented by a map with constant efficiency lines and constant turbo speed lines and with Π_c and W_c on the axes. This is shown in Fig. 2.16 which has approximatively the same characteristics as Fig. 2.10 in Watson and Janota (1982). Consequently, the proposed compressor model has the expected behavior.

2.6 Intercooler and EGR-cooler

To construct a simple model, that captures the important system properties, the intercooler and the EGR-cooler are assumed to be ideal, i.e. the equations for the coolers are

$$\begin{aligned} p_{out} &= p_{in} \\ W_{out} &= W_{in} \\ T_{out} &= T_{cool} \end{aligned} \tag{2.70}$$

where T_{cool} is the cooling temperature. The model can be extended with non-ideal coolers, but these increase the complexity of the model since non-ideal coolers require that there are states for the pressures both before and after the coolers.

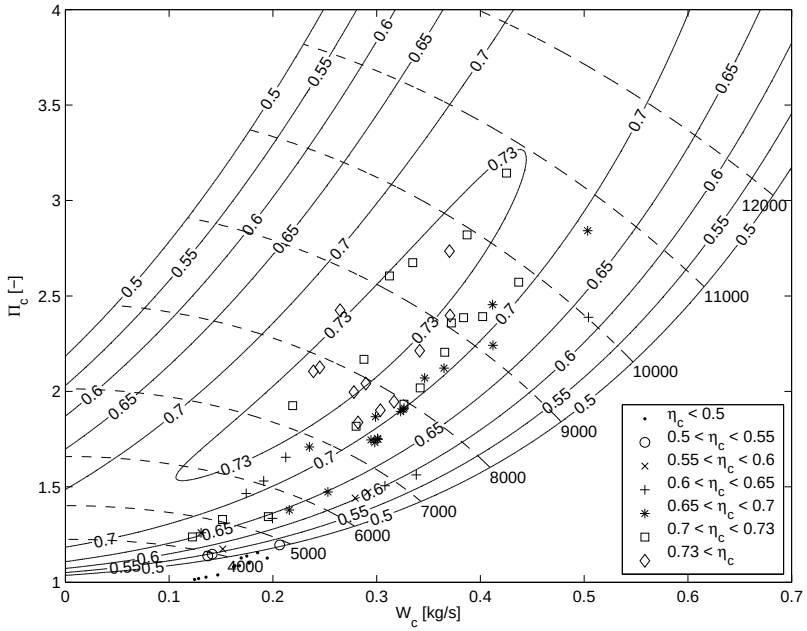

Figure 2.16 *Compressor map with modeled efficiency lines (solid line), modeled turbo speed lines (dashed line with turbo speed in rad/s), and estimated efficiency from measurements using Eq.* (2.55)*. The estimated points are divided into different groups. The turbo speed lines are described by the compressor flow model.*

2.7 Summary of assumptions and model equations

A summary of the model assumptions is given in Sec. 2.7.1 and the proposed model equations are given in Sec. 2.7.2 to 2.7.5.

2.7.1 Assumptions

To develop a simple model, that captures the dominating effects in the mass flows, the following assumptions are made:

- The intercooler and the EGR-cooler are ideal, i.e. the equations for the coolers are

$$\begin{aligned} p_{out} &= p_{in} \\ W_{out} &= W_{in} \\ T_{out} &= T_{cool} \end{aligned} \tag{2.71}$$

where T_{cool} is the cooling temperature.

- The manifolds are modeled as standard isothermal models.
- All gases are considered to be ideal and there are two sets of thermodynamic properties:
  1. Air has the gas constant R_a and the specific heat capacity ratio γ_a.
  2. Exhaust gas has the gas constant R_e and the specific heat capacity ratio γ_e.
- No heat transfer to or from the gas inside of the intake manifold.
- No backflow can occur.
- The intake manifold temperature is constant.
- The oxygen fuel ratio λ_O is always larger than one.

2.7.2 Manifolds

$$\begin{aligned} \frac{d}{dt} p_{im} &= \frac{R_a T_{im}}{V_{im}} (W_c + W_{egr} - W_{ei}) \\ \frac{d}{dt} p_{em} &= \frac{R_e T_{em}}{V_{em}} (W_{eo} - W_t - W_{egr}) \end{aligned} \tag{2.72}$$

$$x_{egr} = \frac{W_{egr}}{W_c + W_{egr}} \tag{2.73}$$

$$\begin{aligned} \frac{d}{dt} X_{Oim} &= \frac{R_a T_{im}}{p_{im} V_{im}} ((X_{Oem} - X_{Oim}) W_{egr} + (X_{Oc} - X_{Oim}) W_c) \\ \frac{d}{dt} X_{Oem} &= \frac{R_e T_{em}}{p_{em} V_{em}} (X_{Oe} - X_{Oem}) W_{eo} \end{aligned} \tag{2.74}$$

2.7.3 Cylinder

Cylinder flow

$$W_{ei} = \frac{\eta_{vol} p_{im} n_e V_d}{120 R_a T_{im}} \tag{2.75}$$

$$\eta_{vol} = c_{vol1} \sqrt{p_{im}} + c_{vol2} \sqrt{n_e} + c_{vol3} \tag{2.76}$$

$$W_f = \frac{10^{-6}}{120} u_\delta n_e n_{cyl} \tag{2.77}$$

$$W_{eo} = W_f + W_{ei} \tag{2.78}$$

$$\lambda_O = \frac{W_{ei} X_{Oim}}{W_f (O/F)_s} \tag{2.79}$$

$$X_{Oe} = \frac{W_{ei} X_{Oim} - W_f (O/F)_s}{W_{eo}} \tag{2.80}$$

Cylinder out temperature

$$
\begin{aligned}
q_{in,k+1} &= \frac{W_f\, q_{HV}}{W_{ei} + W_f}\,(1 - x_{r,k}) \\
x_{p,k+1} &= 1 + \frac{q_{in,k+1}\, x_{cv}}{c_{va}\, T_{1,k}\, r_c^{\gamma_a - 1}} \\
x_{v,k+1} &= 1 + \frac{q_{in,k+1}\,(1 - x_{cv})}{c_{pa}\left(\frac{q_{in,k+1}\, x_{cv}}{c_{va}} + T_{1,k}\, r_c^{\gamma_a - 1}\right)} \\
x_{r,k+1} &= \frac{\Pi_e^{1/\gamma_a}\, x_{p,k+1}^{-1/\gamma_a}}{r_c\, x_{v,k+1}} \\
T_{e,k+1} &= \eta_{sc}\, \Pi_e^{1-1/\gamma_a}\, r_c^{1-\gamma_a}\, x_{p,k+1}^{1/\gamma_a - 1}\left(q_{in,k+1}\left(\frac{1 - x_{cv}}{c_{pa}} + \frac{x_{cv}}{c_{va}}\right) + T_{1,k}\, r_c^{\gamma_a - 1}\right) \\
T_{1,k+1} &= x_{r,k+1}\, T_{e,k+1} + (1 - x_{r,k+1})\, T_{im}
\end{aligned}
\tag{2.81}
$$

$$
T_{em} = T_{amb} + (T_e - T_{amb})\, e^{-\frac{h_{tot}\,\pi\, d_{pipe}\, l_{pipe}\, n_{pipe}}{W_{eo}\, c_{pe}}} \tag{2.82}
$$

Cylinder torque

$$
M_e = M_{ig} - M_p - M_{fric} \tag{2.83}
$$

$$
M_p = \frac{V_d}{4\pi}\,(p_{em} - p_{im}) \tag{2.84}
$$

$$
M_{ig} = \frac{u_\delta\, 10^{-6}\, n_{cyl}\, q_{HV}\, \eta_{ig}}{4\pi} \tag{2.85}
$$

$$
\eta_{ig} = \eta_{igch}\left(1 - \frac{1}{r_c^{\gamma_{cyl} - 1}}\right) \tag{2.86}
$$

$$
M_{fric} = \frac{V_d}{4\pi} 10^5\,\left(c_{fric1}\, n_{eratio}^2 + c_{fric2}\, n_{eratio} + c_{fric3}\right) \tag{2.87}
$$

$$
n_{eratio} = \frac{n_e}{1000} \tag{2.88}
$$

2.7.4 EGR-valve

$$
W_{egr} = \frac{A_{egr}\, p_{em}\, \Psi_{egr}}{\sqrt{T_{em}\, R_e}} \tag{2.89}
$$

$$
\Psi_{egr} = 1 - \left(\frac{1 - \Pi_{egr}}{1 - \Pi_{egropt}} - 1\right)^2 \tag{2.90}
$$

$$\Pi_{egr} = \begin{cases} \Pi_{egropt} & \text{if } \frac{p_{im}}{p_{em}} < \Pi_{egropt} \\ \frac{p_{im}}{p_{em}} & \text{if } \Pi_{egropt} \leq \frac{p_{im}}{p_{em}} \leq 1 \\ 1 & \text{if } 1 < \frac{p_{im}}{p_{em}} \end{cases} \tag{2.91}$$

$$A_{egr} = A_{egrmax}\, f_{egr}(\tilde{u}_{egr}) \tag{2.92}$$

$$f_{egr}(\tilde{u}_{egr}) = \begin{cases} c_{egr1}\, \tilde{u}_{egr}^2 + c_{egr2}\, \tilde{u}_{egr} + c_{egr3} & \text{if } \tilde{u}_{egr} \leq -\frac{c_{egr2}}{2\, c_{egr1}} \\ c_{egr3} - \frac{c_{egr2}^2}{4\, c_{egr1}} & \text{if } \tilde{u}_{egr} > -\frac{c_{egr2}}{2\, c_{egr1}} \end{cases} \tag{2.93}$$

$$\frac{d}{dt}\tilde{u}_{egr} = \frac{1}{\tau_{egr}}(u_{egr}(t - \tau_{degr}) - \tilde{u}_{egr}) \tag{2.94}$$

2.7.5 Turbo

Turbo inertia

$$\frac{d}{dt}\omega_t = \frac{P_t\, \eta_m - P_c}{J_t\, \omega_t} \tag{2.95}$$

Turbine efficiency

$$P_t\, \eta_m = \eta_{tm}\, W_t\, c_{pe}\, T_{em} \left(1 - \Pi_t^{1-1/\gamma_e}\right) \tag{2.96}$$

$$\Pi_t = \frac{p_{amb}}{p_{em}} \tag{2.97}$$

$$\eta_{tm} = \eta_{tm,max} - c_m (BSR - BSR_{opt})^2 \tag{2.98}$$

$$BSR = \frac{R_t\, \omega_t}{\sqrt{2\, c_{pe}\, T_{em} \left(1 - \Pi_t^{1-1/\gamma_e}\right)}} \tag{2.99}$$

$$c_m = c_{m1} (\omega_t - c_{m2})^{c_{m3}} \tag{2.100}$$

Turbine mass flow

$$W_t = \frac{A_{vgtmax}\, p_{em}\, f_{\Pi t}(\Pi_t)\, f_{vgt}(\tilde{u}_{vgt})}{\sqrt{T_{em}}} \tag{2.101}$$

$$f_{\Pi t}(\Pi_t) = \sqrt{1 - \Pi_t^{K_t}} \tag{2.102}$$

$$f_{vgt}(\tilde{u}_{vgt}) = c_{f2} + c_{f1} \sqrt{1 - \left(\frac{\tilde{u}_{vgt} - c_{vgt2}}{c_{vgt1}}\right)^2} \tag{2.103}$$

$$\frac{d}{dt}\tilde{u}_{vgt} = \frac{1}{\tau_{vgt}}(u_{vgt} - \tilde{u}_{vgt}) \tag{2.104}$$

Compressor efficiency

$$P_c = \frac{W_c\, c_{pa}\, T_{amb}}{\eta_c}\left(\Pi_c^{1-1/\gamma_a} - 1\right) \tag{2.105}$$

$$\Pi_c = \frac{p_{im}}{p_{amb}} \tag{2.106}$$

$$\eta_c = \eta_{cmax} - \chi^T\, Q_c\, \chi \tag{2.107}$$

$$\chi = \begin{bmatrix} W_c - W_{copt} \\ \pi_c - \pi_{copt} \end{bmatrix} \tag{2.108}$$

$$\pi_c = (\Pi_c - 1)^{pow_\pi} \tag{2.109}$$

$$Q_c = \begin{bmatrix} a_1 & a_3 \\ a_3 & a_2 \end{bmatrix} \tag{2.110}$$

Compressor mass flow

$$W_c = \frac{p_{amb}\, \pi\, R_c^3\, \omega_t}{R_a\, T_{amb}}\Phi_c \tag{2.111}$$

$$\Phi_c = \sqrt{\frac{1 - c_{\psi 1}\,(\Psi_c - c_{\psi 2})^2}{c_{\Phi 1}}} + c_{\Phi 2} \tag{2.112}$$

$$\Psi_c = \frac{2\, c_{pa}\, T_{amb}\left(\Pi_c^{1-1/\gamma_a} - 1\right)}{R_c^2\, \omega_t^2} \tag{2.113}$$

$$c_{\psi 1} = c_{\omega\psi 1}\, \omega_t^2 + c_{\omega\psi 2}\, \omega_t + c_{\omega\psi 3} \tag{2.114}$$

$$c_{\Phi 1} = c_{\omega\Phi 1}\, \omega_t^2 + c_{\omega\Phi 2}\, \omega_t + c_{\omega\Phi 3} \tag{2.115}$$

2.8 Model tuning and validation

To develop a model that describes the system dynamics and the nonlinear effects, the model have to be tuned and validated. In Sec. 2.8.1 static and dynamic models are tuned and in Sec. 2.8.2 a validation of the complete model is performed using dynamic data. In the validation, it is important to investigate if the model captures the essential dynamic behaviors and nonlinear effects.

2.8.1 Tuning

The tuning of static and dynamic models are described in the following sections.

Static models

In Tab. 2.3 there is a summary of the absolute relative model errors from Sec. 2.3 to 2.5 between static models and stationary measurements for each subsystem. The stationary measurements consist of 82 operating points, that are scattered over a large operating region with different loads, speeds, VGT- and EGR-positions. These 82 operating points also include the European Stationary Cycle (ESC). The mean absolute relative errors are equal to or lower than 6.1 %. The EGR mass flow model has the largest mean relative error and the cylinder mass flow model has the smallest mean relative error.

Table 2.3 *The mean and maximum absolute relative errors between static models and steady state measurements for each subsystem in the diesel engine model, i.e. a summary of the mean and maximum absolute relative errors in Sec. 2.3 to 2.5.*

Subsystem	Mean absolute relative error [%]	Maximum absolute relative error [%]
Cylinder mass flow	0.9	2.5
Exhaust gas temperature	1.7	5.4
Engine torque	1.9	7.1
EGR mass flow	6.1	22.2
Turbine efficiency	4.2	13.2
Turbine mass flow	2.8	7.6
Compressor efficiency	3.3	14.1
Compressor mass flow	3.4	13.7

Dynamic models

The tuning parameters for the dynamic models are the manifold volumes V_{im} and V_{em} in Sec. 2.2 and the turbo inertia J_t in Sec. 2.5.1. These parameters are adjusted manually until simulations of the complete model follow dynamic responses in dynamic measurements by considering time constants. The tuning is performed using a dynamic tuning data, the data C in Tab. 2.4, that consists of 77 different steps in VGT control signal and EGR control signal in an operating point with 50 % load and n_e=1500 rpm. All the data in Tab. 2.4 are used for validation in Sec. 2.8.2. Note that the dynamic measurements are limited in sample rate with a sample frequency of 1 Hz for data A-E and with a sample frequency of 10 Hz for data F. This leads to that the data does not captures the fastest dynamics in the system.

A dynamometer is fitted to the engine via an axle in order to brake or supply torque to the engine. This dynamometer and axle lead to that the measured engine torque has a time constant that is not modeled due to that the torque will not be used as a feedback in the controller. However, in order to validate the engine torque

Table 2.4 *The mean absolute relative errors between diesel engine model simulation and dynamic tuning or validation data that consist of steps in VGT-position, EGR-valve, and fuel injection. The data C and F are used for tuning of dynamic models, the data A, B, D, E, and F are used for validation of time constants, and all the data are used for validation of static models and essential system properties.*

	VGT-EGR steps					u_δ steps
Data name	A	B	C	D	E	F
Speed [rpm]	1200		1500	1900		1500
Load [%]	25	75	50	25	75	-
Number of steps	77	77	77	77	55	7
p_{im}	2.0	10.6	6.3	5.0	4.5	2.9
p_{em}	2.4	6.8	5.5	4.5	4.6	4.7
W_c	3.2	10.6	8.0	6.7	6.7	3.8
n_t	4.4	11.9	7.0	6.0	4.1	3.0
M_e	-	-	-	-	-	7.3

model during dynamic responses, this dynamic is modeled in the validation as a first order system

$$\frac{d}{dt} M_{e,meas} = \frac{1}{\tau_{Me}} (M_e - M_{e,meas}) \tag{2.116}$$

where $M_{e,meas}$ is the measured torque and M_e is the output torque from the engine. The time constant τ_{Me} is tuned by adjusting it manually until simulations of the complete model follow the measured torque during steps in fuel injection at 1500 rpm, i.e. the data F in Tab. 2.4.

2.8.2 Validation

Due to that the stationary measurements are few, both the static and the dynamic models are validated by simulating the total model and comparing it with dynamic validation data that consists of several different steps in VGT-position, EGR-valve, and fuel injection. The steps in VGT-position and EGR-valve are performed in 5 different operating points and the steps in fuel injection are performed in one operating point. The result of this validation can be seen in Tab. 2.4 that shows that the mean absolute relative errors are less than 12 %. Note that the engine torque is not measured during VGT and EGR steps. The relative errors are due to mostly steady state errors, but since the engine model will be used in a controller the steady state accuracy is less important since a controller will take care of steady state errors. However, in order to design a successful controller, it is important that the model captures the essential dynamic behaviors and nonlinear effects. Therefore, time constants and essential system properties are validated in the following

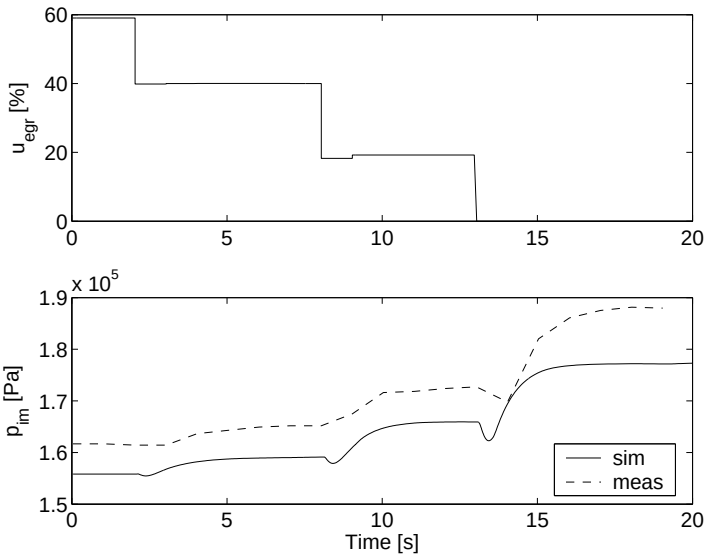

Figure 2.17 *Comparison between diesel engine model simulation and dynamic validation data during steps in EGR-valve position showing that the model captures the non-minimum phase behavior in* p_{im}*. Operating point: 25 % load,* n_e*=1900 rpm and* u_{vgt}*=50 %.*

sections.

Validation of time constants

In Sec. 2.8.1, the dynamic models are tuned by considering the time constants in the data C in Tab. 2.4. These time constants are validated using the dynamic validation data A, B, D, and E in Tab. 2.4. Some parts of this validation are plotted in Fig. 2.17 and 2.18. The non-minimum phase behavior in p_{im} in Fig. 2.17 shows that the model captures the fast dynamic in the beginning of the response and that the model captures the slow dynamic in the end of the response. The overshoot in the third response in Fig. 2.18 also shows that model captures both fast and slow dynamics.

Validation of essential system properties

Kolmanovsky et al. (1997) and Jung (2003) show the essential system properties for the pressures and the flows in a diesel engine with VGT and EGR. Some of these properties are a non-minimum phase behavior in the intake manifold pressure and a non-minimum phase behavior, an overshoot, and a sign reversal in the compressor

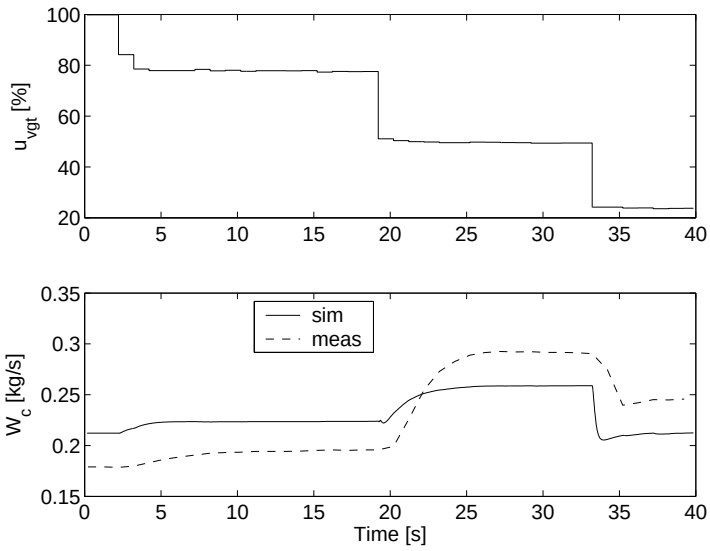

Figure 2.18 *Comparison between diesel engine model simulation and dynamic validation data during steps in VGT position showing that the model captures the overshoot and the sign reversal in* W_c. *Operating point: 75 % load,* n_e*=1200 rpm and* u_{egr}*=40 %.*

mass flow. These system properties are validated using the dynamic data A-E in Tab. 2.4. Some parts of this validation are shown in Fig. 2.17 to 2.19. Fig. 2.17 shows that the model captures the non-minimum phase behavior in the transfer function u_{egr} to p_{im} and the second step in Fig. 2.19 shows that the model captures the non-minimum phase behavior in the transfer function u_{vgt} to W_c. Note that the non-minimum phase behaviors in the measurements are not obvious due to a low sample frequency. Further, the third step in Fig. 2.18 and the third step in Fig. 2.19 show that the model captures the overshoot and the sign reversal in the transfer function u_{vgt} to W_c. These properties are discussed more in detail in Chap. 3.

2.9 Results

A mean value model of a diesel engine with VGT and EGR including oxygen mass fraction was developed and validated. The intended applications of the model are system analysis, simulation, and development of model-based control systems. To be able to implement a model-based controller, the model must be small. Therefore the model has only seven states: intake and exhaust manifold pressures, oxygen

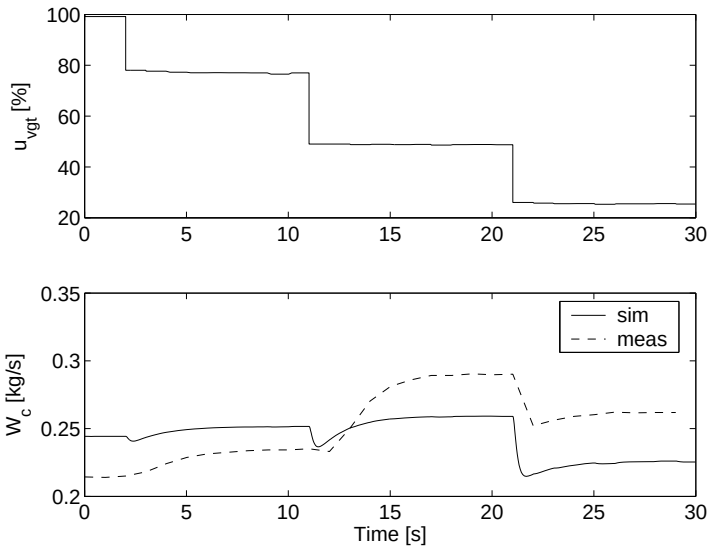

Figure 2.19 *Comparison between diesel engine model simulation and dynamic tuning data during steps in VGT position showing that the model captures the non-minimum phase behavior, the overshoot, and the sign reversal in* W_c. *Operating point: 50 % load,* n_e*=1500 rpm and* u_{egr}*=81.5 %.*

mass fraction in the intake and exhaust manifold, turbocharger speed, and two states describing the actuator dynamics for the EGR-valve and the VGT-position.

Model equations and tuning methods for the model parameters was described for each subsystem in the model. Parameters in the static models are tuned automatically using least square optimization and stationary measurements in 82 different operating points. The tuning shows that the mean relative errors are equal to or lower than 6.1 %. Parameters in dynamic models are tuned by adjusting these parameters manually until simulations of the complete model follow the dynamic responses in the dynamic measurements. In order to decrease the amount of tuning parameters, flows and efficiencies are modeled using physical relationships and parametric models instead of look-up tables.

Static and dynamic validations of the entire model were performed using dynamic measurements, which consist of steps in fuel injection, EGR control signal, and VGT control signal. The validations show mean relative errors which are less than 12 %. The validations also show that the proposed model captures the essential system properties, i.e. a non-minimum phase behavior in the transfer function u_{egr} to p_{im} and a non-minimum phase behavior, an overshoot, and a sign reversal in the transfer function u_{vgt} to W_c.

3

System analysis

An analysis of the characteristics and the behavior of a system aims at obtaining insight into the control problem. This is known to be important for a successful design of a EGR and VGT controller due to non-trivial intrinsic properties, see for example Kolmanovsky et al. (1997). Therefore, the essential system properties for the model in Chap. 2 are physically explained in Sec. 3.1 by looking at step responses in a set of selected operating points that cover the principle behaviors. In Sec. 3.2 a mapping of these system properties are performed by simulating step responses over the entire operating region. This is done for the main performance variables oxygen/fuel ratio, λ_O, and EGR-fraction, x_{egr}. Further, λ_O and x_{egr} are mapped in Sec. 3.3 in order to investigate the interactions in the system. Also, the pumping work is mapped in Sec. 3.3 since control objective 6 in Sec. 1.2 is to minimize this variable.

3.1 Physical intuition for system properties

As described in Sec. 2.8.2, the system in Chap. 2 has non-minimum phase behaviors, overshoots, and sign reversals. The fundamental physical explanation of these system properties is that the system consists of two dynamic effects that interact: a fast pressure dynamic in the manifolds and a slow turbocharger dynamic. These two dynamic effects often work against each other which results in the system properties above. For example, if the fast dynamic effect is small and the slow dynamic effect is large, the result will be a non-minimum phase behavior, see λ_O in Fig. 3.1. However, if the fast dynamic effect is large and the slow dynamic effect is small, the result will be an overshoot and a sign reversal, see λ_O in Fig. 3.2. The

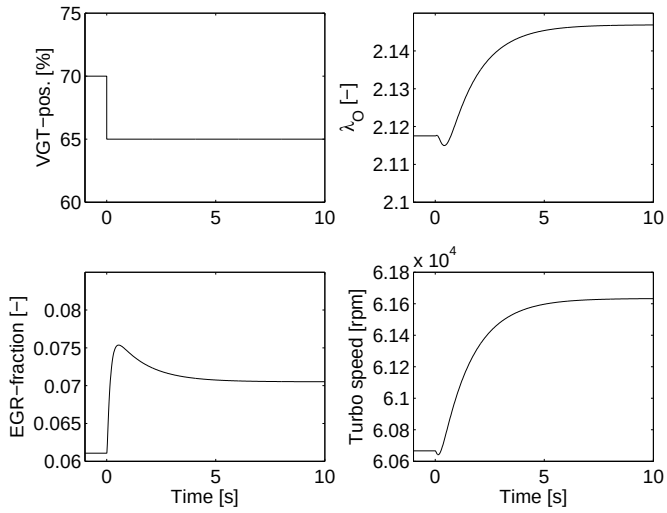

Figure 3.1 *Responses to a step in VGT position showing non-minimum phase behaviors in* λ_O *and in the turbo speed. Operating point:* u_δ*=110 mg/cycle,* n_e*=1500 rpm and* u_{egr}*=80 %. Initial* u_{vgt}*=70 %.*

precise conditions for this sign reversal is due to a complex interaction between flows, temperatures, and pressures in the entire engine. More physical explanations of the system properties for VGT position and EGR-valve responses are found in the following sections.

3.1.1 Physical intuition for VGT position response

Model responses to steps in VGT position are shown in Fig. 3.1 and 3.2. In Fig. 3.1 a closing of the VGT leads to an increase in exhaust manifold pressure and therefore an increase in EGR-fraction which leads to a decrease in intake manifold oxygen mass fraction and a decrease in λ_O in the beginning of the step. However, an increase in exhaust manifold pressure thereafter leads to an increase in turbocharger speed and thus compressor mass flow. The result is a larger increase in λ_O than the initial decrease. The increase in λ_O is slower due to the slower dynamics of the turbocharger speed, which means that VGT position to λ_O has a non-minimum phase behavior. There is also a non-minimum phase behavior in the turbocharger speed response. The non-minimum phase behavior in λ_O increases with increasing EGR-valve opening and decreasing VGT opening until the sign of the DC-gain is reversed and the non-minimum phase behavior becomes an overshoot instead. This sign reversal can be seen in Fig. 3.2, where the size of the step is equal but the initial VGT position is more closed compared to Fig. 3.1. Contrary to Fig. 3.1,

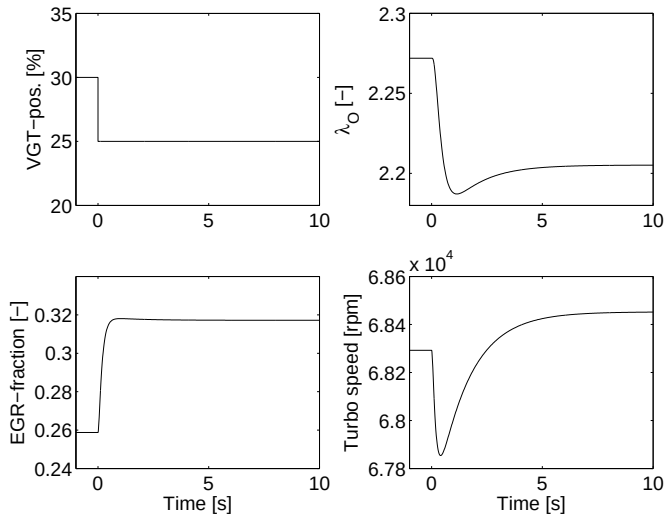

Figure 3.2 *Responses to a step in VGT position showing a sign reversal in* λ_O *compared to Fig. 3.1. Operating point:* u_δ*=110 mg/cycle,* n_e*=1500 rpm and* u_{egr}*=80 %. Initial* u_{vgt}*=30 %.*

Fig. 3.2 shows that a closing of the VGT position leads to a total decrease in λ_O. Further, the non-minimum phase behavior in the turbocharger speed response in Fig. 3.2 is larger compared to Fig. 3.1.

3.1.2 Physical intuition for EGR-valve response

Model responses to steps in EGR-valve are shown in Fig. 3.3 and 3.4. In Fig. 3.3, λ_O has a non-minimum phase behavior which has the following physical explanation. The closing of the EGR-valve leads to an immediate decrease in EGR-fraction, yielding an immediate decrease in p_{im}. However, closing the EGR-valve also means that less exhaust gases are recirculated and there are thus more exhaust gases to drive the turbine. This causes the turbocharger to speed up and produce more compressor flow which results in a larger increase in p_{im} than the initial decrease. This effect is slower though due to the slower dynamics of the turbocharger speed, which gives that EGR-valve to p_{im} has a non-minimum phase behavior. Since p_{im} affects the total flow into the engine and thereby λ_O, there is also a non-minimum phase behavior in λ_O. This non-minimum phase behavior increases with decreasing EGR-valve opening and increasing engine speed until the sign of the DC-gain is reversed. This sign reversal can be seen in Fig. 3.4, where the step in EGR-valve is performed in an operating point with higher torque and higher engine speed compared to Fig. 3.3. Contrary to Fig. 3.3, Fig. 3.4 shows that a closing of the EGR-valve leads to a total decrease in λ_O and in n_t.

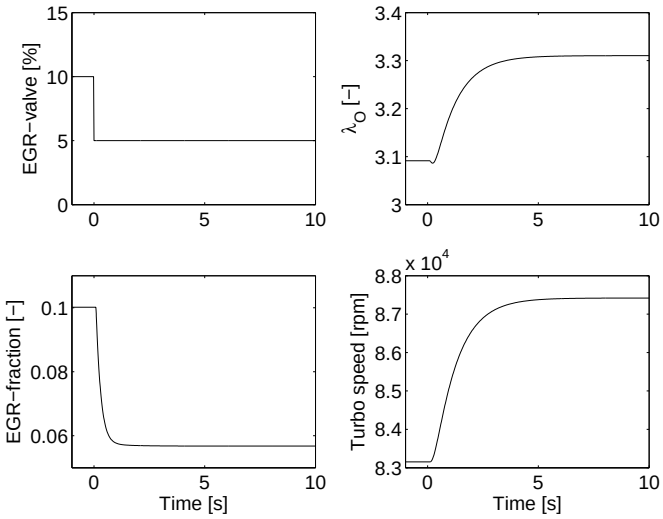

Figure 3.3 *Responses to a step in EGR-valve showing a non-minimum phase behavior in* λ_O*. Operating point:* u_δ*=110 mg/cycle,* n_e*=1500 rpm and* u_{vgt}*=30 %.*

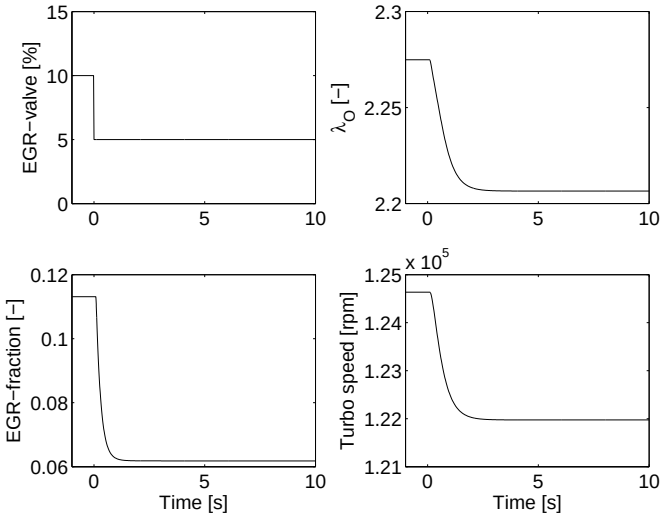

Figure 3.4 *Responses to a step in EGR-valve showing sign reversals in* λ_O *and in the turbo speed compared to Fig. 3.3. Operating point:* u_δ*=230 mg/cycle,* n_e*=2000 rpm and* u_{vgt}*=30 %.*

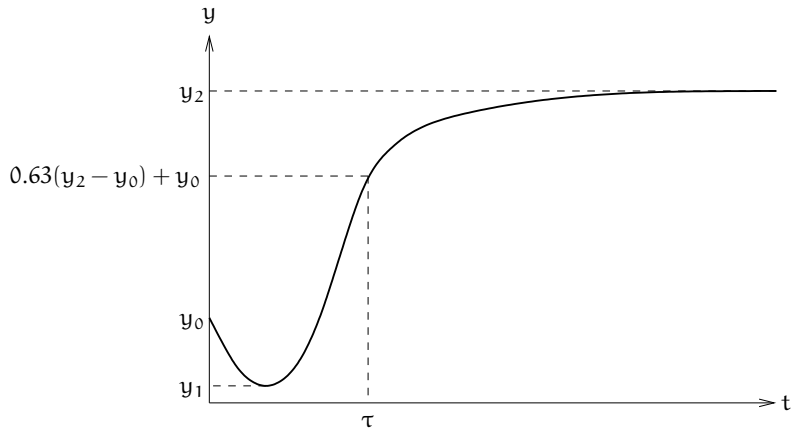

Figure 3.5 *A step response with an initial value y_0, a final value y_2, a non-minimum phase behavior with an undershoot y_1, and a time constant τ.*

3.2 Mapping of system properties

The step responses in Sec. 3.1 show that there are non-minimum phase behaviors and sign reversals in the main performance variables λ_O and x_{egr}. Knowledge about these system properties and time constants in the entire operating region is important when developing a control structure. Therefore, the DC-gain K, the non-minimum phase behavior with an relative undershoot x_N, and the time constant τ are mapped by simulating step responses in the entire operating region. The DC-gain K is defined as

$$K = \frac{y_2 - y_0}{\Delta u} \tag{3.1}$$

where y_0 is the initial value and y_2 is the final value of a step response according to Fig. 3.5 where the input has a step size Δu. The relative undershoot x_N is defined as

$$x_N = \frac{y_0 - y_1}{y_2 - y_1} \tag{3.2}$$

where y_1 is the minimum value of the step response in Fig. 3.5. The time constant τ is defined in Fig. 3.5. The step responses are simulated at 20 different u_{vgt} points, 20 different u_{egr} points, 3 different n_e points, and 3 different u_δ points. The size of the steps in u_{vgt} and u_{egr} are 5% of the difference between two adjoining operating points. The figures in the sections below show the most interesting and important part of the operating region.

In addition to a mapping of the system properties over the operating region for the engine, it is interesting to see where the engine frequently operates. Therefore, simulation of the European Transient Cycle is performed in Sec. 3.2.3, and the relative frequency for different sub-regions are presented.

3.2.1 DC-gains

The contour plots of the DC-gain, K, for the transfer functions $u_{vgt} \rightarrow \lambda_O$ and $u_{egr} \rightarrow \lambda_O$ in Fig. 3.6 and 3.7 show the operating points where the sign reversals occur. It is important to investigate where a sign reversal occurs since a sign reversal in a transfer function cause problems when controlling the corresponding feedback loop (this will be discussed in Sec. 4.1.1). The DC-gain for the transfer function $u_{vgt} \rightarrow \lambda_O$ (see Fig. 3.6) has reversed sign (positive sign) in operating points with closed to half open VGT, half to fully open EGR-valve, low to medium n_e, and medium to large u_δ or in operating points with half to fully open VGT, low n_e, and small u_δ. Further, the DC-gain for the transfer function $u_{egr} \rightarrow \lambda_O$ (see Fig. 3.7) has reversed sign (positive sign) in a smaller operating region, compared to $u_{vgt} \rightarrow \lambda_O$, which is in operating points with closed to half open EGR-valve, high n_e, and medium to large u_δ.

The DC-gains for all four transfer functions (Fig. 3.6 to 3.9) are also equal to zero in some other operating points where no sign reversal occurs. The DC-gains for the transfer functions $u_{egr} \rightarrow \lambda_O$, $u_{vgt} \rightarrow x_{egr}$, and $u_{egr} \rightarrow x_{egr}$ are equal to zero in operating points with half to fully open VGT, low to medium n_e and medium to large u_δ. In these operating points $p_{em} < p_{im}$ (see Fig. 3.14) which leads to that $x_{egr} = 0$ since no backflow is modeled in the EGR-flow model. As a consequence, the control signal u_{egr} cannot influence the system and the control signal u_{vgt} cannot influence the EGR-fraction. The DC-gain for the transfer function $u_{vgt} \rightarrow x_{egr}$ is also equal to zero when $u_{egr} = 0$.

The mapping of the DC-gains also shows that the DC-gains vary much between different operating points in all four transfer functions. A common trend is that the DC-gains for the transfer functions $u_{vgt} \rightarrow \lambda_O$ and $u_{vgt} \rightarrow x_{egr}$ are large when the VGT is closed and small when the VGT is open. Similarly, the DC-gains for the transfer functions $u_{egr} \rightarrow \lambda_O$ and $u_{egr} \rightarrow x_{egr}$ are large when the EGR-valve is closed and small when the EGR-valve is open.

The contour plots of the DC-gain in Fig. 3.6 to 3.9 show the most interesting and important part of the operating region. No interesting properties occurs outside this operating region, except for the left bottom plot in Fig. 3.6. Looking at the entire operating region in Fig. 3.12, the left bottom plot shows that for almost all EGR-valve positions the sign is reversed twice when the VGT goes from closed to fully open.

Finally, it is worth to note that the transfer function $u_{egr} \rightarrow x_{egr}$ has positive DC-gain, while $u_{vgt} \rightarrow x_{egr}$ and $u_{egr} \rightarrow \lambda_O$ have negative DC-gain in almost the entire operating region.

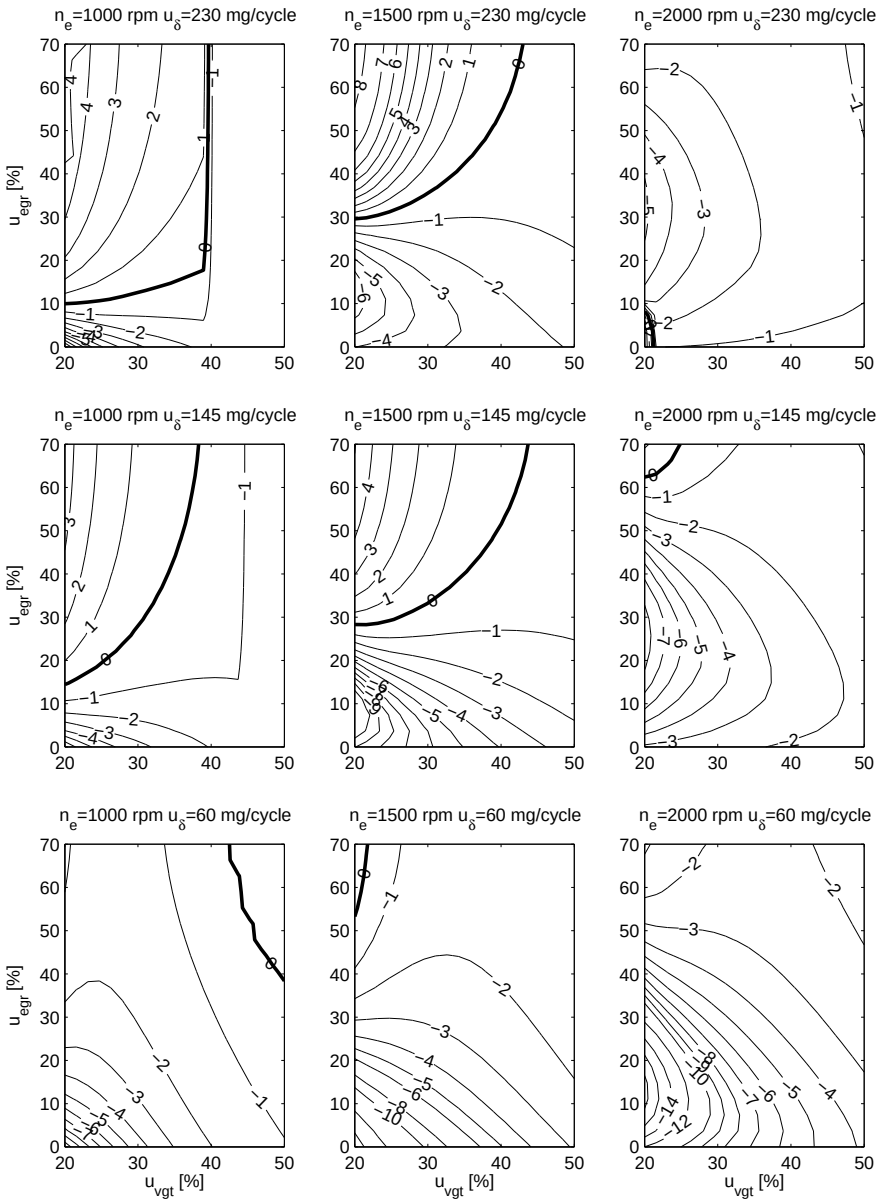

Figure 3.6 *Contour plots of the DC-gain, $100 \cdot K$, for the transfer function $u_{vgt} \rightarrow \lambda_O$ at 3 different n_e and 3 different u_δ. The DC-gain has a sign reversal that occurs at the thick line. Looking at the entire operating region in Fig. 3.12, the left bottom plot shows that for almost all EGR-valve positions the sign is reversed twice when the VGT goes from closed to fully open.*

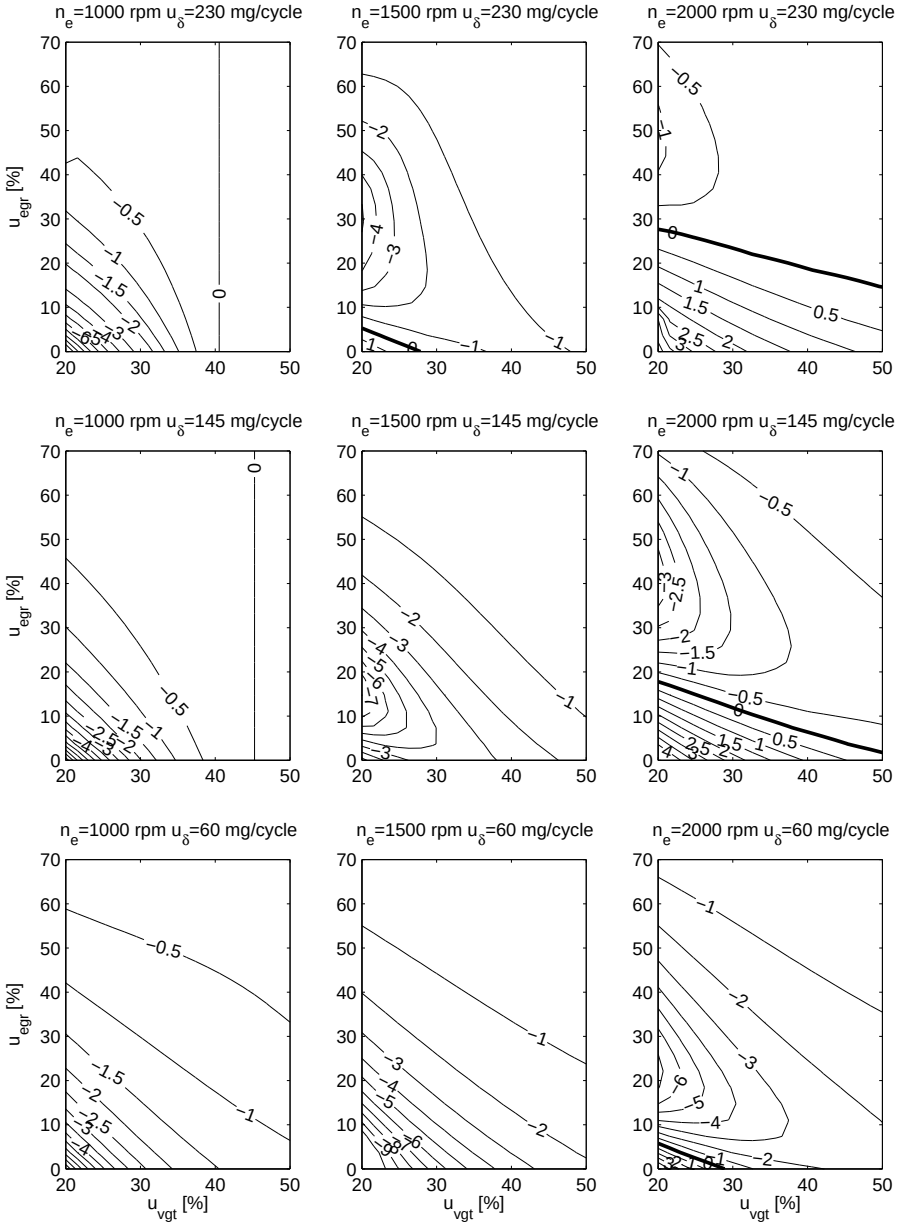

Figure 3.7 *Contour plots of the DC-gain, $100 \cdot K$, for the transfer function $u_{egr} \rightarrow \lambda_O$ at 3 different n_e and 3 different u_δ. The DC-gain has a sign reversal that occurs at the thick line.*

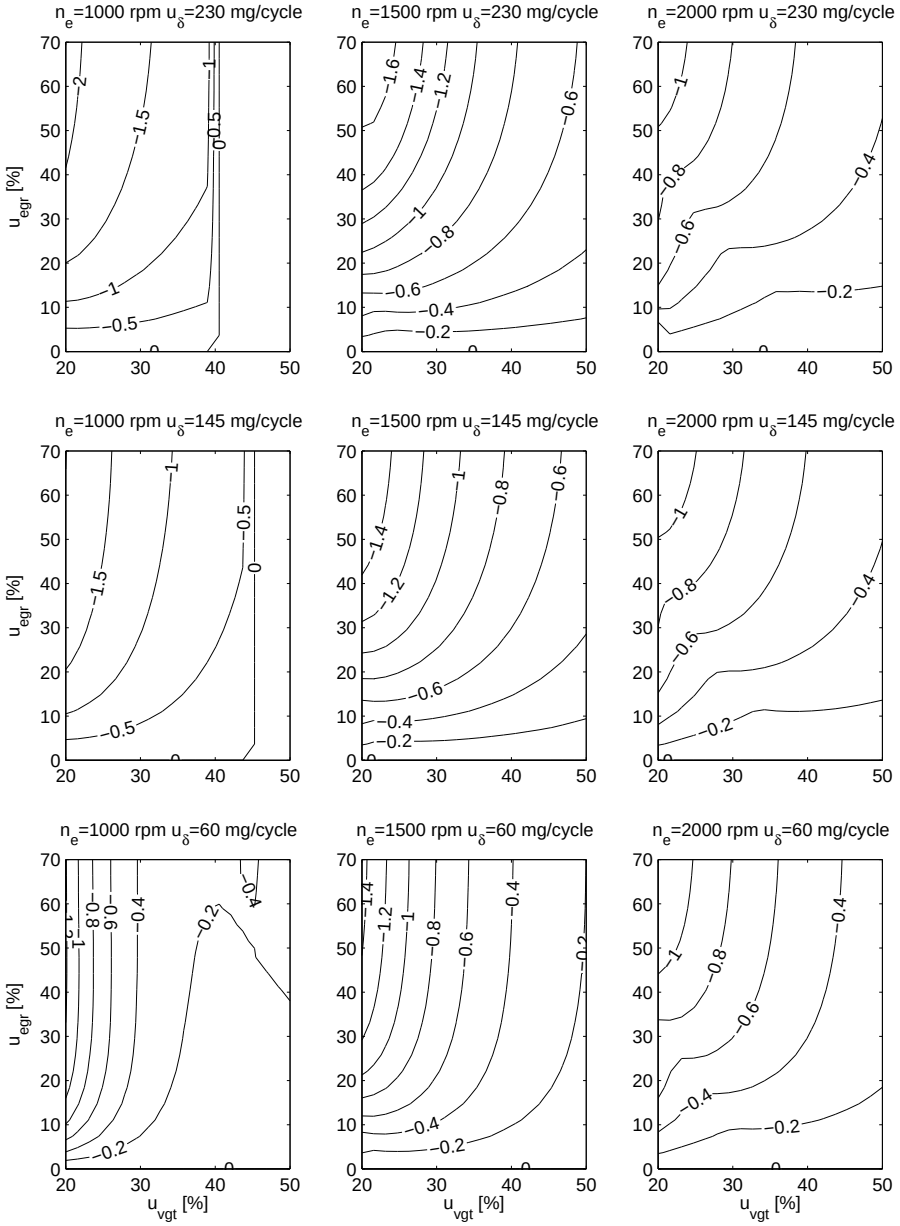

Figure 3.8 *Contour plots of the DC-gain,* $100 \cdot \mathsf{K}$*, for the transfer function* $\mathrm{u_{vgt}} \rightarrow \mathrm{x_{egr}}$ *at 3 different* $\mathrm{n_e}$ *and 3 different* $\mathrm{u_\delta}$*. The DC-gain is negative and also equal to zero in some operating points.*

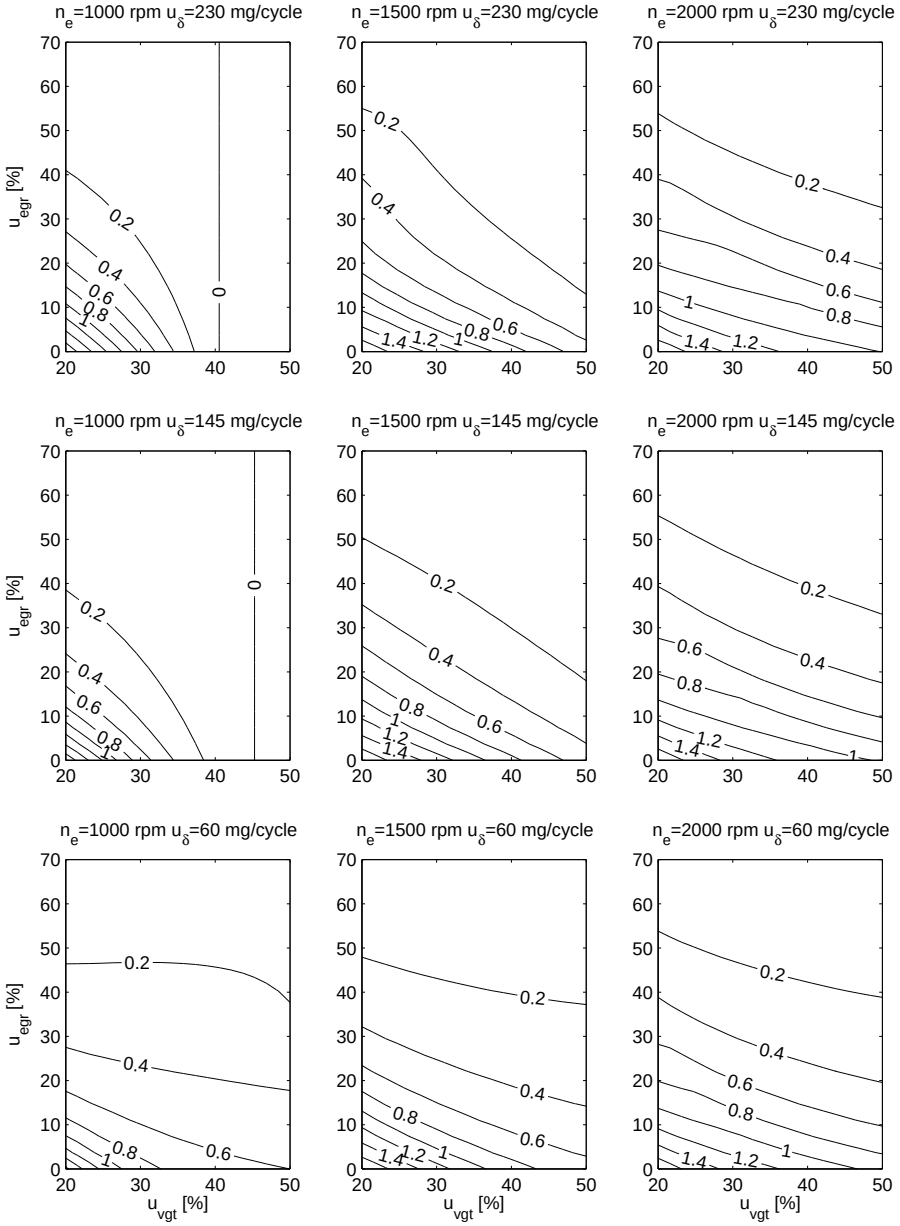

Figure 3.9 *Contour plots of the DC-gain,* $100 \cdot K$*, for the transfer function* $u_{egr} \rightarrow x_{egr}$ *at 3 different* n_e *and 3 different* u_δ*. The DC-gain is positive and also equal to zero in some operating points.*

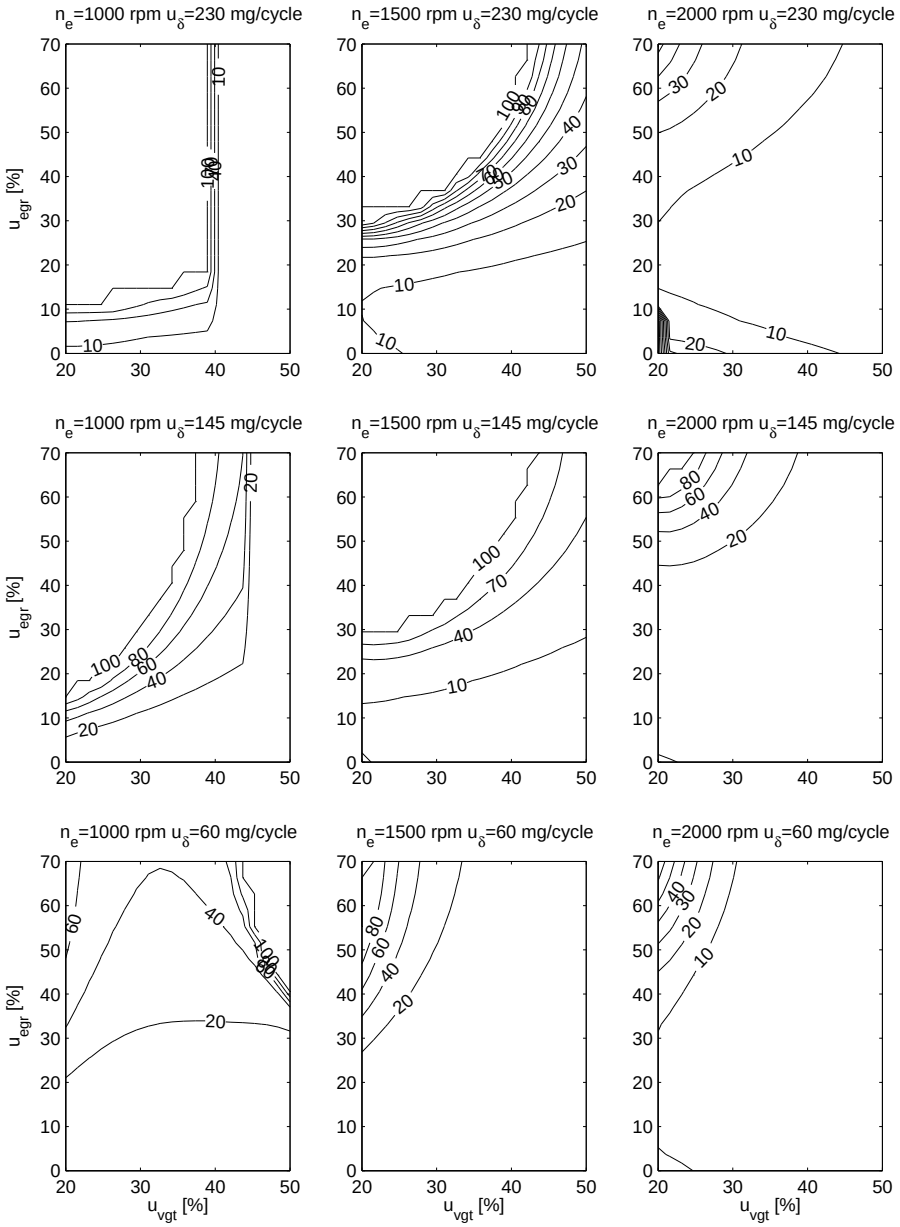

Figure 3.10 *Contour plots of the relative undershoot,* $\mathfrak{x}_{\mathrm{N}}\,[\%]$*, (see Eq. (3.2)) in a non-minimum phase behavior for the transfer function* $\mathfrak{u}_{\mathrm{vgt}} \rightarrow \lambda_{\mathrm{O}}$ *at 3 different* $\mathfrak{n}_{\mathrm{e}}$ *and 3 different* $\mathfrak{u}_{\delta}$*.*

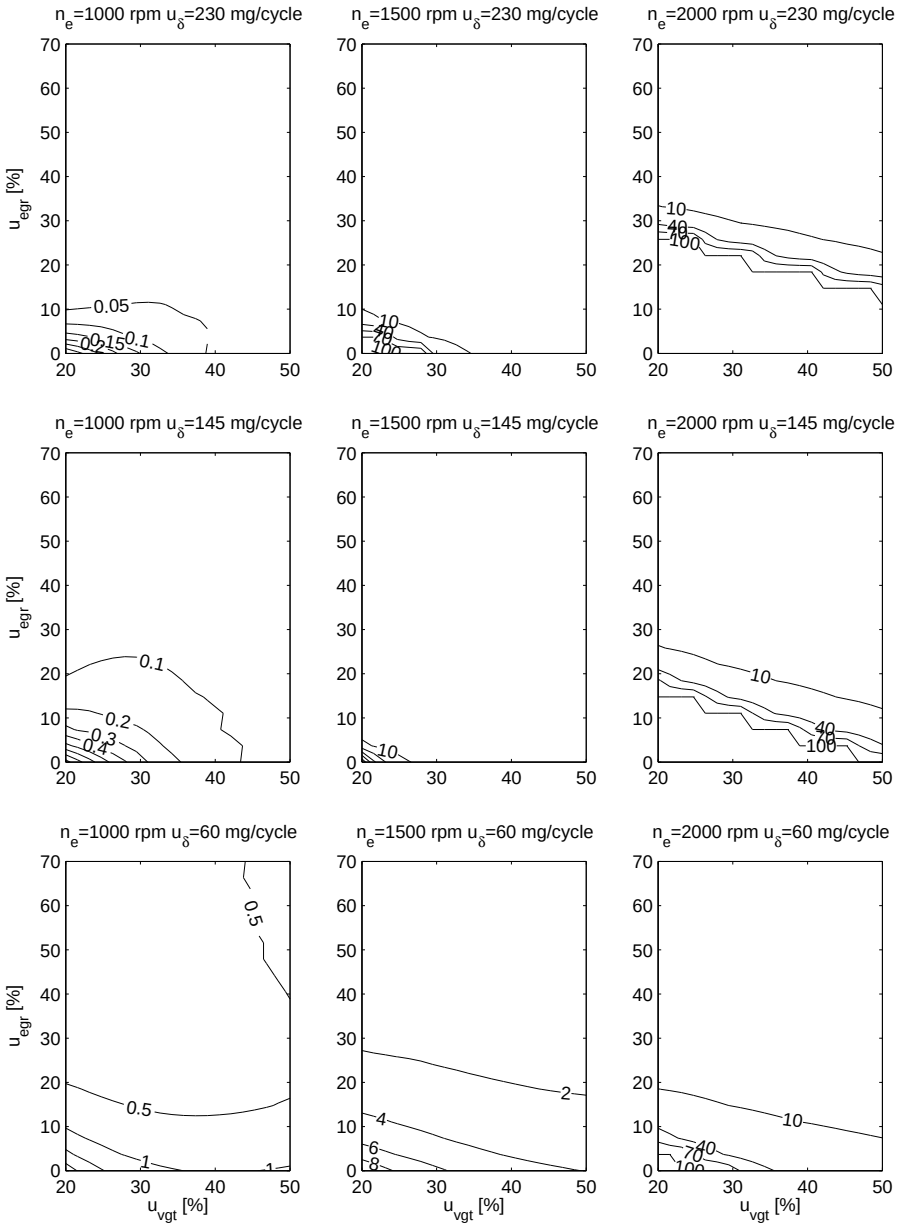

Figure 3.11 *Contour plots of the relative undershoot,* $\mathfrak{x}_{\mathrm{N}}$ [%], *(see Eq. (3.2)) in a non-minimum phase behavior for the transfer function* $\mathfrak{u}_{\mathrm{egr}} \rightarrow \lambda_{\mathrm{O}}$ *at 3 different* $\mathfrak{n}_{\mathrm{e}}$ *and 3 different* $\mathfrak{u}_{\delta}$.

3.2.2 Non-minimum phase

A mapping of the non-minimum phase behaviors is performed by calculating the relative undershoot x_N (see Eq. (3.2)) over the entire operating region. This is performed for the transfer functions $u_{vgt} \rightarrow \lambda_O$ and $u_{egr} \rightarrow \lambda_O$ in Fig. 3.10 and 3.11. The transfer functions $u_{vgt} \rightarrow x_{egr}$ and $u_{egr} \rightarrow x_{egr}$ have no non-minimum phase behaviors.

The relative undershoot for the transfer function $u_{vgt} \rightarrow \lambda_O$ is larger than 20 % in operating points with half to fully open EGR-valve and closed to half open VGT for all n_e and u_δ. However, the relative undershoot for the transfer function $u_{egr} \rightarrow \lambda_O$ is larger than 20 % in a smaller operating region, where the EGR-valve is closed to half open and the n_e is high. Both these non-minimum phase behaviors in $u_{vgt} \rightarrow \lambda_O$ and $u_{egr} \rightarrow \lambda_O$ occur only in operating points with negative DC-gain near the sign reversal. In the operating points with reversed sign (positive sign) the non-minimum phase behavior becomes an overshoot instead (see also Fig. 3.1 and Fig. 3.2 where the non-minimum phase behavior in λ_O becomes an overshoot).

3.2.3 Operation pattern for the European Transient Cycle

A mapping of the operating points where the engine frequently operates is important in order to understand what system properties in the sections above that should be considered in the control design. This mapping is performed by simulating the complete control system in Sec. 4.2 during the European Transient Cycle. The control parameters are tuned using the method in Sec. 4.3 and the weighting factors $\gamma_{Me} = 1$ and $\gamma_{egr} = 1$. This simulation is described further in Sec. 4.4. In Fig. 3.12, this simulation is plotted by first sampling the signals n_e, u_δ, u_{vgt}, and u_{egr} with a frequency of 10 Hz, and then dividing these simulated points into 9 different operating regions by selecting the nearest operating region to each simulated point. These operating regions corresponds to the 9 different plots in Fig. 3.12 where each plot has u_{egr} on the y-axis and u_{vgt} on the x-axis, i.e. exactly as the contour plots in the previous sections. The percentage of simulated points in each operating region is also shown in the plots.

Comparing Fig. 3.12 with Fig. 3.10 and 3.11, the conclusion is that the engine frequently operates in operating points where the sign reversal and the non-minimum phase occur for the transfer function $u_{vgt} \rightarrow \lambda_O$ and that the engine does not frequently operate in operating points where the sign reversal and the non-minimum phase occur for $u_{egr} \rightarrow \lambda_O$. Consequently, it is important to consider the sign reversal and the non-minimum phase for $u_{vgt} \rightarrow \lambda_O$ in the control design. The engine does not operate at $n_e > 1750$ rpm due to that the European Transient Cycle only consists of n_e that are lower than 1750 rpm.

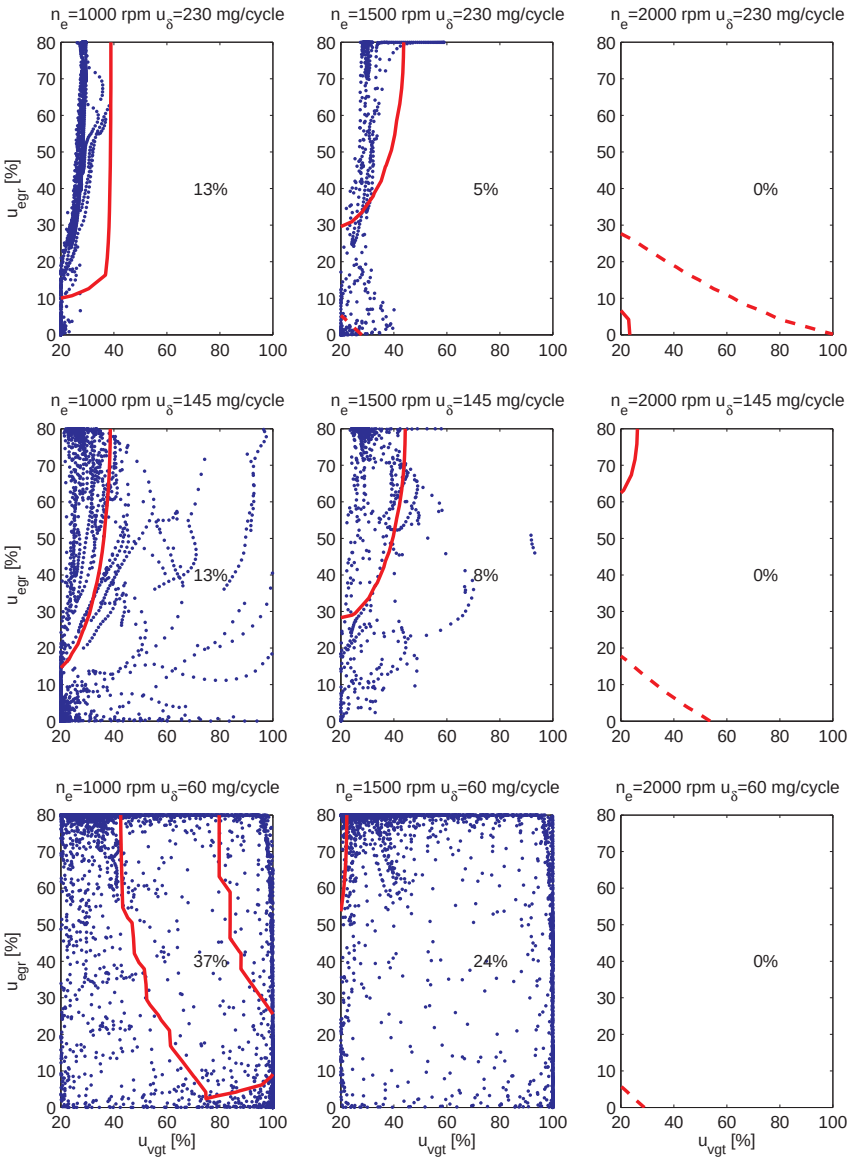

Figure 3.12 *Operating points during European Transient Cycle simulations of the control system showing that the engine frequently operates in operating points where the sign reversal occurs for the transfer function* $\mathrm{u_{vgt}} \rightarrow \lambda_O$ *(solid line) and that the engine does not frequently operate in operating points where the sign reversal occurs for the transfer function* $\mathrm{u_{egr}} \rightarrow \lambda_O$ *(dashed line).*

Table 3.1 *The minimum, mean, and maximum value of the time constants in the entire operating region for the transfer functions* $u_{vgt} \rightarrow \lambda_O$, $u_{egr} \rightarrow \lambda_O$, $u_{vgt} \rightarrow x_{egr}$, *and* $u_{egr} \rightarrow x_{egr}$.

Transfer function	$u_{vgt} \rightarrow \lambda_O$	$u_{egr} \rightarrow \lambda_O$	$u_{vgt} \rightarrow x_{egr}$	$u_{egr} \rightarrow x_{egr}$
Minimum τ	0.02	0.03	0.05	0.18
Mean τ	1.20	1.25	0.16	0.31
Maximum τ	5.70	3.02	0.30	1.06

3.2.4 Time constants

The time constants, τ, for the transfer functions $u_{vgt} \rightarrow \lambda_O$, $u_{egr} \rightarrow \lambda_O$, $u_{vgt} \rightarrow x_{egr}$, and $u_{egr} \rightarrow x_{egr}$, respectively, are mapped over the entire operating region using the definition in Fig. 3.5. The result is presented in Appendix B, while the minimum, mean, and maximum value for each time constant are shown in Tab. 3.1.

The variations of the time constants for the transfer functions $u_{vgt} \rightarrow \lambda_O$ and $u_{egr} \rightarrow \lambda_O$ are larger compared to the time constants for the transfer functions $u_{vgt} \rightarrow x_{egr}$ and $u_{egr} \rightarrow x_{egr}$. This is because the transfer functions $u_{vgt} \rightarrow \lambda_O$ and $u_{egr} \rightarrow \lambda_O$ have sign reversals. These two transfer functions have small time constants when the overshoot is large, which is in operating points with positive DC-gains near the sign reversals. The transfer functions $u_{vgt} \rightarrow \lambda_O$, $u_{egr} \rightarrow \lambda_O$, and $u_{egr} \rightarrow x_{egr}$ have large time constants in operating points with fully open EGR-valve, almost closed VGT, low n_e, and small u_δ. The transfer function $u_{vgt} \rightarrow x_{egr}$ has a small time constant in the entire operating region due to overshoots in almost the entire operating region.

3.3 Mapping of performance variables

Besides looking at dynamic responses of different loops, it is valuable to study the interaction. This is done in Sec. 3.3.1 for λ_O and x_{egr}. Further, in Sec. 3.3.2 the pumping losses are mapped to give insight into how to handle objective 6 in Sec. 1.2.

3.3.1 System coupling in steady state

A mapping of the main performance variables λ_O and x_{egr} as function of u_{egr} and u_{vgt} in steady state are given in Fig. 3.13. The system is decoupled, in steady state, in one point if and only if one of the contour lines is horizontal at the same time as the other line is vertical. This is almost the case in operating points where the sign reversals occur, i.e. at the thick solid and dashed lines. In all other operating points, the system is strongly coupled.

In operating points where the sign reversal occurs for the transfer function $u_{vgt} \rightarrow \lambda_O$ (thick solid line), u_{vgt} only affects x_{egr} and u_{egr} almost only affects

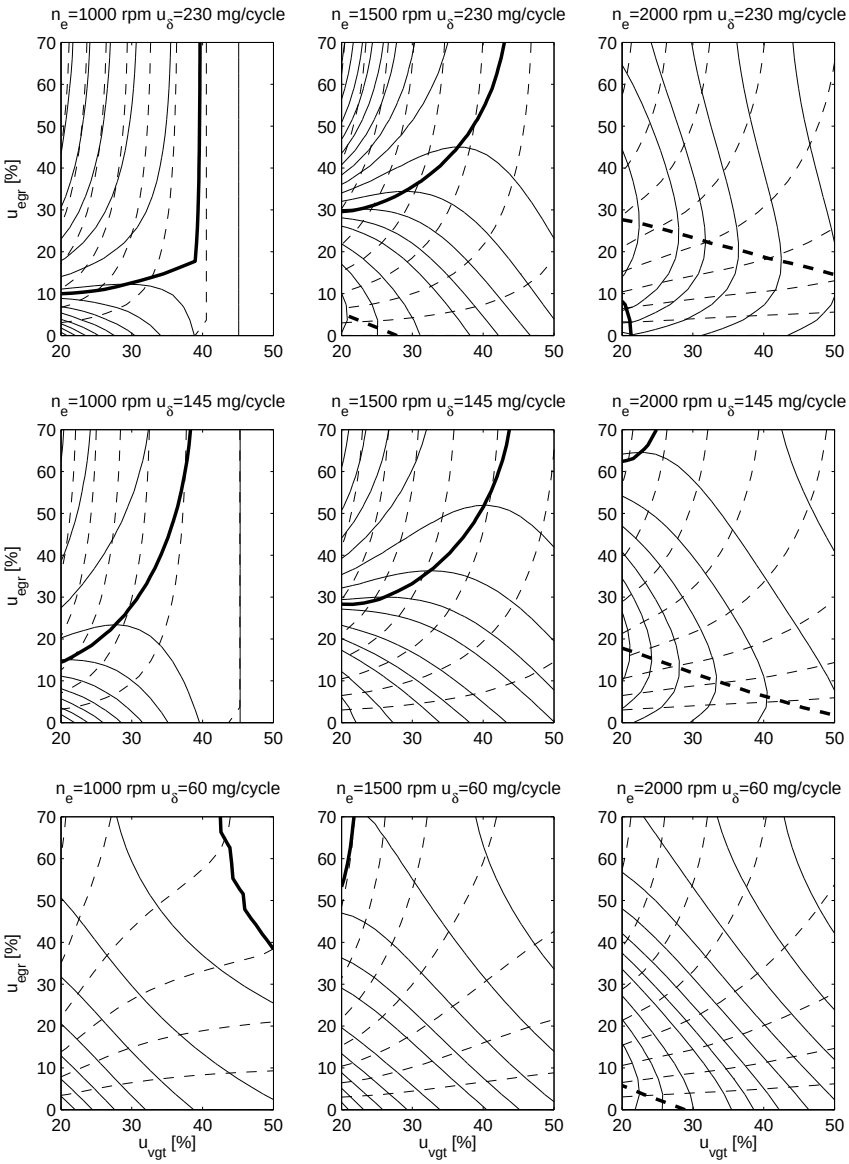

Figure 3.13 *Contour plots of λ_O (thin solid line) and x_{egr} (thin dashed line) in steady-state at 3 different n_e and 3 different u_δ. The system from u_{egr} and u_{vgt} to λ_O and x_{egr} is strongly coupled in steady state in almost the entire operating region except for operating points where the sign reversals occur for the transfer functions $u_{vgt} \rightarrow \lambda_O$ (thick solid line) and $u_{egr} \rightarrow \lambda_O$ (thick dashed line).*

λ_O except for operating points with closed VGT and closed to half open EGR-valve where u_{egr} also affects x_{egr}. In operating points where the sign reversal occurs for the transfer function $u_{egr} \rightarrow \lambda_O$ (thick dashed line), u_{egr} only affects x_{egr} and u_{vgt} almost only affects λ_O.

3.3.2 Pumping losses in steady state

A mapping of the pumping losses in steady state over the entire operating region gives insight how to develop the pumping work minimization in the control structure. Fig. 3.14 shows that the pumping losses $p_{em} - p_{im}$ decrease with increasing EGR-valve and VGT opening. Further, the pumping losses are negative in operating points with half to fully open VGT, low to medium n_e, and medium to large u_δ, and the pumping losses are high in operating points with closed VGT and high n_e.

3.4 Results

A system analysis shows that the transfer functions $u_{vgt} \rightarrow \lambda_O$ and $u_{egr} \rightarrow \lambda_O$ have non-minimum phase behaviors and sign reversals, and it was shown that the engine frequently operates in operating points where these properties occur for the transfer function $u_{vgt} \rightarrow \lambda_O$. Consequently, it is important to consider the sign reversal and the non-minimum phase behavior for $u_{vgt} \rightarrow \lambda_O$ in the control design. Further, it was demonstrated that the four transfer functions $(u_{vgt}, u_{egr}) \rightarrow (\lambda_O, x_{egr})$ have varying DC-gains and time constants. A mapping of the performance variables λ_O and x_{egr} shows that the system from u_{egr} and u_{vgt} to λ_O and x_{egr} is strongly coupled. It was also illustrated that the pumping losses $p_{em} - p_{im}$ decrease with increasing EGR-valve and VGT opening over the entire operating region.

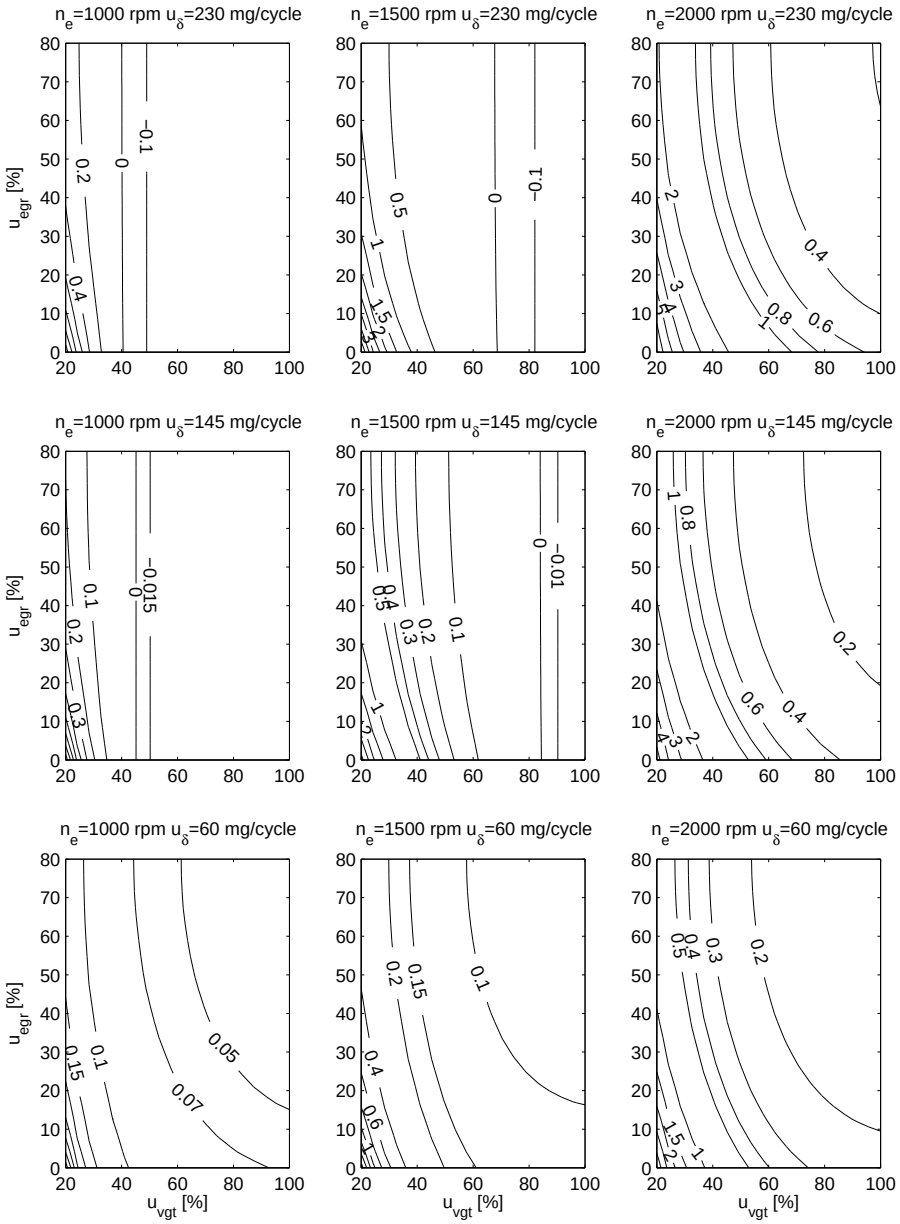

Figure 3.14 *Contour plots of* $\mathrm{p_{em}} - \mathrm{p_{im}}$ *[bar] in steady-state at 3 different* $\mathrm{n_e}$ *and 3 different* $\mathrm{u_\delta}$*, showing that* $\mathrm{p_{em}} - \mathrm{p_{im}}$ *decreases with increasing EGR-valve and VGT opening.*

4

Control design

The goal of the control design is to coordinate the EGR-valve (u_{egr}), the VGT position (u_{vgt}), and the fuel injection (u_{δ}) in order to achieve the control objectives stated in Sec. 1.2. As seen in the previous chapter there are variations in DC-gains, variations in time constants, and interactions between performance variables that influence the control design. Variations in DC-gains and variations in time constants could be considered using gain scheduling of controller parameters, and interactions between performance variables could be considered using linear multivariable controllers, e.g. Linear Quadric Control (Anderson and Moore, 1989; Glad and Ljung, 2000) or Model Predictive Control (Maciejowski, 2002; Bemporad and Morari, 1999), and all the properties above could be considered using non-linear controllers, see e.g. Isidori (1989) and Khalil (2002). However, all these possibilities are left for future work. Instead, here the approach is to build a controller structure using min/max-selectors and SISO controllers for EGR and VGT control, and to use feedforward for fuel control. The idea is to develop a structure that captures the essential requirements on a controller handling all the control objectives.

Based on the system properties in Sec. 3.2 a choice of main feedback loops for the EGR and VGT controller is proposed in Sec. 4.1. Based on this choice and the control objectives in Sec. 1.2 a complete control structure is proposed in Sec. 4.2. In particular Sec. 4.2.4 discusses the pumping minimizing mechanisms in the proposed structure. For successful application of a control structure, it is advantageous that it besides good behavior and good interfaces is straightforward to calibrate and re-calibrate. Therefore, an automatic tuning method for the controller parameters is developed in Sec. 4.3. The tuning method is based on optimization of a cost function, that reflects the control objectives, over a set of automatically

selected different transients that exhibit different challenges for the controller. Such a method is valuable for example to save time when adapting to new hardware changes. In Sec. 4.4 simulations on an European Transient Cycle (ETC) are used to illustrate the transient selection method, and controller tuning and performance. Different performance trade-offs are illustrated and discussed.

4.1 Main feedback loops

The control approach for the EGR and VGT controllers depicted in Fig. 1.1 is to use SISO controllers. Many different SISO controllers are available, but throughout the presentation PID controllers will be used. Based on the structure in Sec. 1.1 and the system properties in Sec. 3.2, the following main feedback loops are proposed

$$\begin{aligned} u_{egr} &= -\text{PID}_a\left(e_{\lambda_O}\right) \\ u_{vgt} &= -\text{PID}_b\left(e_{xegr}\right) \end{aligned} \tag{4.1}$$

where $e_{\lambda_O} = \lambda_{OSetp} - \lambda_O$ and $e_{xegr} = x_{egrSetp} - x_{egr}$. These two main feedback loops are selected to handle items 1 and 3 of the control objectives stated in Sec. 1.2. In the first loop λ_O is controlled to a set-point λ_{OSetp} with the control signal u_{egr} and in the second loop intake manifold EGR-fraction, x_{egr}, is controlled to its set-point, $x_{egrSetp}$, with the control signal u_{vgt}. The PID controllers have a minus sign since the corresponding transfer functions have negative DC-gain in almost the entire operating region (see Sec. 3.2.1).

The rationale behind the choice of the two main feedback loops are as follows. Relating to the system properties in Sec. 3.2, both actuators could straightforwardly be chosen for control of the EGR-fraction. However, for both actuators the λ_O performance variable requires care and the proposed choice of main control loops has the advantages that are described in the following three subsections.

4.1.1 System properties for $u_{vgt} \rightarrow \lambda_O$

According to the system analysis in Sec. 3.2, the transfer function $u_{vgt} \rightarrow \lambda_O$ has a non-minimum phase behavior and a sign reversal which can cause problems when controlling the corresponding feedback loop. These two properties occur in operating points where the engine frequently operates (see Sec. 3.2.3) and these properties are avoided in the proposed control structure Eq. (4.1) by controlling λ_O with u_{egr}. The following example illustrates the problem with the opposite selection of input and output pairs when passing the sign reversal in $u_{vgt} \rightarrow \lambda_O$.

Example 4.1 Illustration of different input output pairings when passing the sign reversal in $u_{vgt} \rightarrow \lambda_O$.

Compared to Eq. (4.1) the other possible pairing of inputs and outputs would be

$$\begin{aligned} u_{egr} &= \text{PID}_c\left(e_{xegr}\right) \\ u_{vgt} &= -\text{PID}_d\left(e_{\lambda_O}\right) \end{aligned} \tag{4.2}$$

Note that there is no minus sign for $\text{PID}_\text{c}(e_{\text{xegr}})$ since the corresponding transfer function has a positive DC-gain and that $-\text{PID}_\text{d}(e_{\lambda_\text{O}})$ has a minus sign since the corresponding transfer function has a negative DC-gain in almost the entire operating region (see Sec. 3.2.1).

In Fig. 4.1 a closed loop system is simulated using the model in Chap. 2 and two different controllers: the proposed main feedback loops Eq. (4.1) and the alternative main feedback loops Eq. (4.2). Two steps in $\text{x}_{\text{egrSetp}}$ are performed with constant values for n_e, u_δ, and λ_{OSetp} in order to move the operating point from a point A with negative DC-gain in $\text{u}_{\text{vgt}} \rightarrow \lambda_\text{O}$ to a point B with positive DC-gain in $\text{u}_{\text{vgt}} \rightarrow \lambda_\text{O}$ and back again, i.e. the operating point passes the sign reversal, as seen in the bottom plot in Fig. 4.1 which is a contour plot corresponding to the middle plot in Fig. 3.13. In this illustration the PID parameters are tuned manually and the tuning objective is to get a fast control without overshoots and without oscillations for these steps. No derivative parts are used for the PID controllers. Note also that the EGR-valve position is saturated at 80% due to that the EGR-valve does not affect the system if the EGR-valve position is larger than 80%, see Fig. 2.6.

Not surprisingly, the alternative choice of main control loops Eq. (4.2) give oscillations in the operating point with positive DC-gain due to that the controller $-\text{PID}_\text{d}(e_{\lambda_\text{O}})$ in Eq. (4.2) has a negative sign that is designed for operating points with negative DC-gain. Further, the proposed main feedback loops Eq. (4.1) give a step response that follows the set-points. For both selections of main loops, λ_O reacts to a step in EGR-fraction set-point which leads to transients in λ_O. This is a consequence of that the system from u_{vgt} and u_{egr} to λ_O and x_{egr} is coupled which is not accounted for in the control structures.

4.1.2 System properties for $\text{u}_{\text{egr}} \rightarrow \lambda_\text{O}$

The transfer function $\text{u}_{\text{egr}} \rightarrow \lambda_\text{O}$ has also a non-minimum phase behavior and a sign reversal (see Sec. 3.2) that could cause problems. However, these two properties only occur in operating points where λ_O, pumping loss M_p, and turbocharger speed n_t are high. There are significant drawbacks when operating in these operating points. Therefore, any reasonable control structure should be designed so that these operating points are avoided. In all these operating points the EGR-valve is closed to half open and λ_O is much larger than its set-point λ_{OSetp}. Therefore, the proposed structure Eq. (4.1) (more specifically the first row) will open up the EGR-valve, and consequently force the system to leave these operating points. Thus, the non-minimum phase behavior and the sign reversal only have effects in transients passing these operating points.

4.1.3 Performances during a load transient

Another reason for the choice of the main control loops are that more overshoots in EGR-fraction may appear during a load transient if the alternative main control

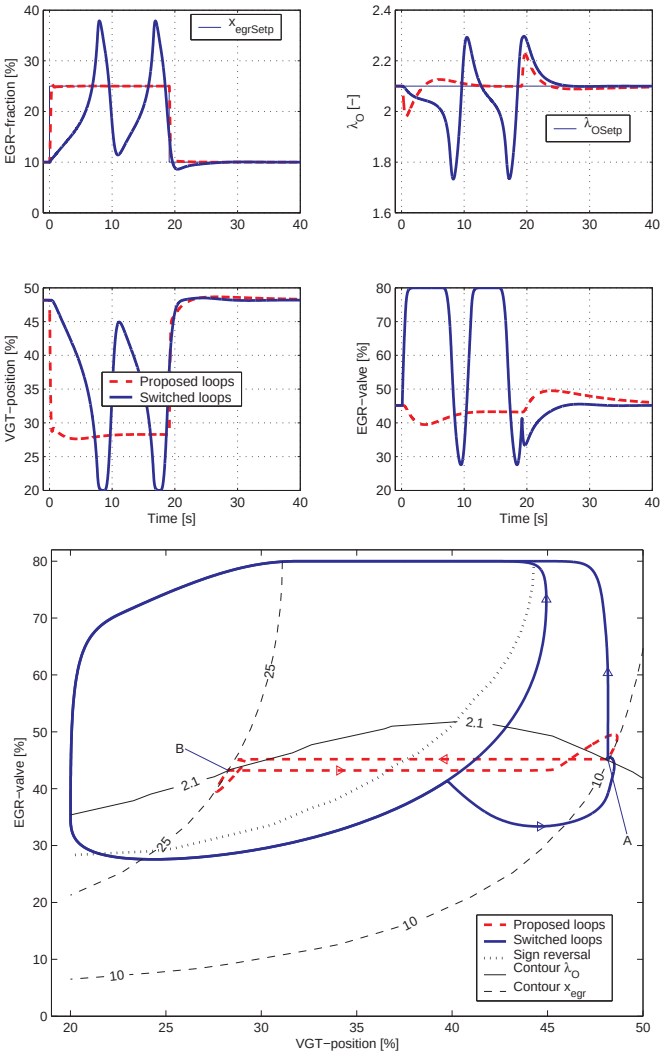

Figure 4.1 *Illustrative example simulating the closed loop system using the proposed main feedback loops Eq.* (4.1) *and the alternative choice of main feedback loops Eq.* (4.2) *showing that the alternative choice of the loops give oscillations due to the sign reversal in* $u_{vgt} \rightarrow \lambda_O$. *Two steps in* $x_{egrSetp}$ *are performed in order to move the operating point from a point A with negative DC-gain in* $u_{vgt} \rightarrow \lambda_O$ *to a point B with positive DC-gain in* $u_{vgt} \rightarrow \lambda_O$ *and back again. The simulations are plotted as function of time and in a contour plot using the middle plot in Fig. 3.13. Operating point:* $n_e = 1500$ *rpm and* $u_\delta = 145$ *mg/cycle.*

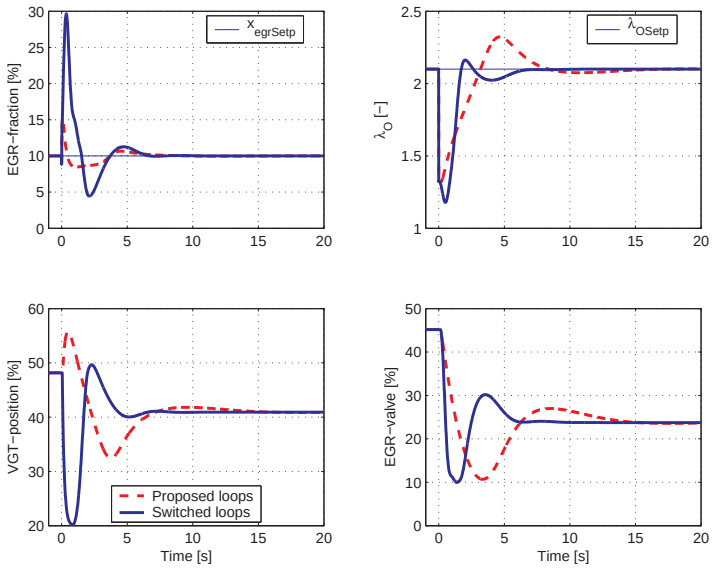

Figure 4.2 *Illustrative simulation of the closed loop system using the proposed main feedback loops Eq.* (4.1) *and the alternative choice of main feedback loops Eq.* (4.2) *during a load transient showing that the latter gives more overshoots in EGR-fraction and more undershoots in* λ_O *compared to the proposed choice. Step in* u_δ*: 145 → 230 mg/cycle. Speed:* n_e*=1500 rpm.*

loops are used. This is illustrated in the following example.

Example 4.2 Illustration of different input output pairings during a load transient.

In Fig. 4.2 a closed loop system is simulated using the model in Chap. 2 and the two different controllers: the proposed Eq. (4.1) and the alternative Eq. (4.2). A step in fuel injection u_δ is performed with constant values for n_e, $x_{egrSetp}$, and λ_{OSetp}. In this illustration the PID parameters are tuned manually and the objective is to balance fast response with small overshoots and small oscillations for this transient. No derivative parts are used for the PID controllers.

Fig. 4.2 shows that a decrease in λ_O coupled to a load increase leads to that the switched loops Eq. (4.2) give a direct closing of the VGT, yielding a pressure build up in the exhaust manifold and therefore a large increase in EGR fraction and then a closing of the EGR-valve. However, the proposed loops give a closing of the EGR-valve before the VGT which results in that the EGR-valve will be closed before the pressure build up in the exhaust manifold, yielding a much smaller overshoot in EGR-fraction compared to the switched loops.

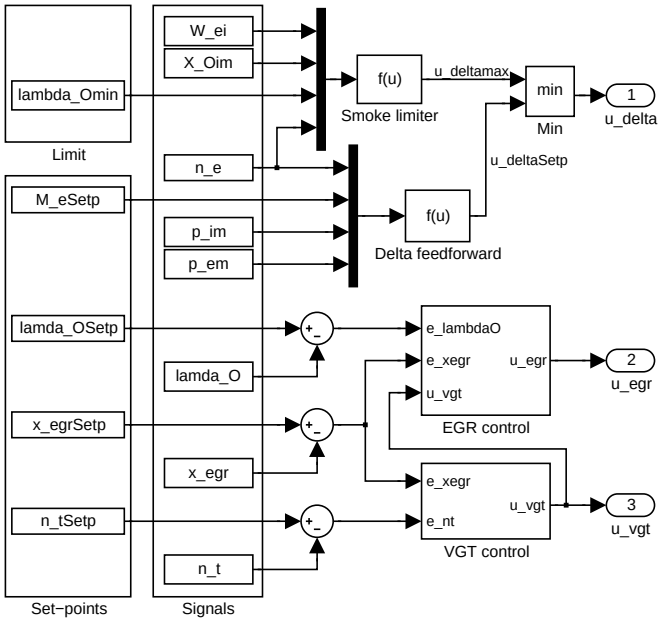

Figure 4.3 *The proposed control structure, as* MATLAB/SIMULINK *block diagram, showing; a limit, set-points, measured and observed signals, fuel control with smoke limiter, together with the main controllers for EGR and VGT.*

4.2 Control structure

The discussion above has motivated the selection of the main feedback loops, and now the attention is turned to the proposed structure and how it handles the control objectives given in Sec. 1.2. The proposed control structure will be presented step by step in the following sections, and a MATLAB/SIMULINK schematic of the full control structure is shown in Fig. 4.3, where all signals and the fuel controller are included together with the EGR and VGT controller depicted in Fig. 1.1.

4.2.1 Signals, set-points and a limit

The signals needed for the controller are assumed to be either measured or estimated using observers. The measured signals are engine speed (n_e), intake and exhaust manifold pressure (p_{im}, p_{em}) and turbocharger speed (n_t). The observed signals are the mass flow into the engine W_{ei}, oxygen mass fraction X_{Oim}, λ_O and x_{egr}. All these signals can be seen in the block "Signals" in Fig. 4.3.

The set-points and the limit needed for the controller (see Fig. 4.3) vary with operation conditions during driving. These signals are provided by an engine and

emission management system as depicted in Fig. 1.1. The limit and the set-points are obtained from measurements and tuned to achieve the legislated emissions requirements. They are then represented as look-up tables being functions of operating conditions.

4.2.2 Main feedback loops

Based on the discussion in Sec. 4.1, the following main feedback loops are used

$$u_{egr} = -\text{PID}\,(e_{\lambda_O}) \tag{4.3}$$

$$u_{vgt} = -\text{PID}\,(e_{xegr}) \tag{4.4}$$

4.2.3 Additional feedback loops

In order to achieve all the control objectives stated in Sec. 1.2, a set of additional control modes are added to the main control loops in Eq. (4.3) to (4.4) according to

$$u_{egr}(t_i) = \begin{cases} \min\left(-\text{PID}_1(e_{\lambda_O}), \text{PID}_2(e_{xegr})\right) & \text{, if } u_{vgt}(t_{i-1}) = 100 \\ -\text{PID}_1(e_{\lambda_O}) & \text{, else} \end{cases} \tag{4.5}$$

$$u_{vgt}(t_i) = \begin{cases} 100 & \text{, if } (u_{vgt}(t_{i-1}) = 100) \\ & \quad \& (e_{xegr} < 0.01) \\ \max\left(-\text{PID}_3(e_{xegr}), -\text{PID}_4(e_{nt})\right) & \text{, else} \end{cases} \tag{4.6}$$

where $e_{nt} = n_{tSetp} - n_t$. Note that there is no minus sign for PID_2 since the corresponding transfer function has positive DC-gain. All other transfer functions have negative DC-gain (see Sec. 3.2). All the PID controllers have integral action, and their derivative part will be discussed in Sec. 4.2.6.

The additional modes in the structure, Eq. (4.5) and (4.6), are motivated as follows. In operating points with low engine torque there is too much EGR, although the VGT is fully open. To achieve control objective 3 also for these operating points, a lower EGR-fraction x_{egr} is obtainable by closing the EGR-valve u_{egr} when the VGT is fully open (case 1 in Eq. (4.5)). The appropriate value for u_{egr} is then the smallest value of the outputs from the two different PID controllers i.e. the more closed EGR setting is used when the VGT is fully open. To achieve control objective 5 and avoid over-speeding of the turbo, the VGT is also influenced by the turbine speed n_t (case 2 in Eq. (4.6)). In this case n_t is controlled with u_{vgt} to a set-point n_{tSetp} which has a value slightly lower than the maximum limit n_{tmax}. The appropriate value for u_{vgt} is then the largest value of the outputs from the two different controllers, which means that the VGT is opened up, thereby decreasing the input torque to the turbocharger, and thereby keeping its speed within limits. In case 1 in Eq. (4.6) the VGT is locked to fully open (the value 100) until $e_{xegr} > 0.01$ in order to avoid oscillations between case 1 and 2 in Eq. (4.5).

4.2.4 Minimizing pumping work

The proposed structure, i.e. Eq. (4.5) and (4.6), minimizes the pumping work in stationary points by striving to open the actuators as much as possible. Looking at the pumping work minimization in more detail the important controller action is coupled to λ_O, and in particular the operating conditions where there is a degree of freedom i.e. when $\lambda_O > \lambda_{OSetp}$. For these conditions there are now two cases. In the first case the proposed controller strives to reduce λ_O by opening the EGR-valve, through the second row in Eq. (4.5). To maintain $x_{egrSetp}$, this action also forces the VGT to be opened as much as possible. Either λ_{OSetp} is reached or $\text{PID}_1(e_{\lambda_O})$ saturates at fully open, due to the integral action. In the other case, coupled to the first rows in Eq. (4.5) and (4.6), the VGT is fully open and it is necessary to reduce x_{egr} by closing the EGR-valve to reach $x_{egrSetp}$. In both cases the actuators are thus opened as much as possible while achieving control objectives 1 and 3.

From the physics we know that opening a valve reduces the pressure differences over the corresponding restriction, in particular Eq. (2.31) results in a lower pressure loss and minimized pumping work Eq. (2.26). Therefore control objective 6 is achieved through the mechanism that was explained above and that opens the EGR-valve and VGT. These properties are also proved in Fig. 3.14, which shows that the lowest pumping work is achieved when the EGR-valve and VGT are opened as much as possible while keeping the control objectives.

Comparing pumping work with another controller

Another structure is used to illustrate that the proposed control structure in Eq. (4.5) and (4.6) has low pumping work. That other control structure, from Wahlström et al. (2005), also achieves control objective 1 and 3 through the following equations for the EGR-valve and the VGT

$$\begin{aligned} u_{egr} &= \min(-\text{PID}_1(e_{\lambda_O}), \text{PID}_2(e_{xegr})) \\ u_{vgt} &= \max(-\text{PID}_3(e_{xegr}), -\text{PID}_4(e_{nt})) \end{aligned} \tag{4.7}$$

In this structure u_{egr} is always calculated using a minimum selector compared to Eq. (4.5) which has a minimum selector only when $u_{vgt} = 100$. This subtle difference results in an increased pumping work that can be understood from the model equations. It is clear from Eq. (2.31) that a given flow W_{egr} can be achieved for different combinations of flow area $A_{egr}(\tilde{u}_{egr})$ and $\frac{p_{em}\Psi_{egr}\left(\frac{p_{im}}{p_{em}}\right)}{\sqrt{T_{em}}}$. The key observation is that there are many combinations of the flow area and pressure loss that can give the same flow, and consequently there are many u_{egr} and u_{vgt} that can give the same x_{egr} in cases when $\lambda_O > \lambda_{OSetp}$. Thus in some cases when $\lambda_O > \lambda_{OSetp}$ both u_{egr} and u_{vgt} are governed by e_{xegr}. In stationary conditions, when $\text{PID}_2(e_{xegr})$ and $\text{PID}_3(e_{xegr})$ in Eq. (4.7) have converged, the controller fulfills the control objectives but the EGR-valve and VGT are not guaranteed to be open as much as possible.

Simulations have been performed under the same conditions as in Wahlström et al. (2005). They show that the control structure proposed in Eq. (4.5) and (4.6) reduces the pumping work with 66% compared to the control structure in Eq. (4.7).

4.2.5 PID parameterization and implementation

Each PID controller has the following parameterization

$$\text{PID}_j(e) = K_j \left(e + \frac{1}{T_{ij}} \int e \, dt + T_{dj} \frac{de}{dt} \right) \tag{4.8}$$

where the index j is the number of the different PID controllers in Eq. (4.5) and (4.6). The PID controllers are implemented in incremental form which leads to anti-windup and bump-less transfer between the different control modes (Åström and Hägglund, 1995).

4.2.6 Derivative parts

It is worth to point out that the loop from VGT-position to turbocharger speed ($\text{PID}_4(e_{nt})$ in Eq. (4.6)) does benefit from a derivative part in order to predict high turbocharger speeds. This is due to the large time constant in the corresponding open-loop transfer function. The transfer function $u_{egr} \rightarrow \lambda_O$ also has a large time constant, but there is a lower demand on the band width for $\text{PID}_1(e_{\lambda_O})$ compared to $\text{PID}_4(e_{nt})$, and consequently $\text{PID}_1(e_{\lambda_O})$ does not need a derivative part. None of the other PID controllers need a derivative part due to smaller time constants in the corresponding transfer functions.

4.2.7 Feedforward fuel control

Engine torque control, control objective 4, is achieved by feedforward from the set-point M_{eSetp} by utilizing the torque model and calculating the set-point value for u_δ according to

$$u_{\delta Setp} = c_1 M_{eSetp} + c_2(p_{em} - p_{im}) + c_3 n_e^2 + c_4 n_e + c_5$$

which is obtained by solving u_δ from Eq. (2.25)–(2.29). This feedforward control is implemented in the block "Delta feedforward" in Fig. 4.3.

Aggressive transients can cause λ_O to go below its hard limit λ_{Omin} resulting in exhaust smoke. The PID controller in the main loop (Eq. (4.3)) is not designed to handle this problem. To handle control objective 2, a smoke limiter is used which calculates the maximum value of u_δ. The calculation is based on engine speed n_e, mass flow into the engine W_{ei}, oxygen mass fraction X_{Oim} and lower limit of oxygen/fuel ratio λ_{Omin}

$$u_{\delta max} = \frac{W_{ei} X_{Oim} 120}{\lambda_{Omin} (O/F)_s 10^{-6} n_{cyl} n_e}$$

which is implemented in the block "Smoke limiter" in the top of Fig. 4.3.

Combining these two the final fuel control command is given by

$$u_\delta = \min(u_{\delta max}, u_{\delta Setp}) \tag{4.9}$$

which concludes the description and the motivation of the control structure in Fig. 4.3.

4.3 Automatic Controller Tuning

In the proposed structure there are four PID controllers that need tuning. This can be a cumbersome work and therefore the next step is to develop an efficient method for automatically finding the tuning parameters K_j, T_{ij}, and T_{dj} in Eq. (4.8), based upon the control objectives in Sec. 1.2.

4.3.1 Cost function

The automatic tuning method is obtained by formulating the control objectives in Sec. 1.2 as a non-linear least squares problem

$$\begin{aligned} &\min V(\theta) \\ &\theta > 0 \end{aligned} \tag{4.10}$$

where θ is the PID parameters

$$\theta = [K_1,\, T_{i1},\, K_2,\, T_{i2},\, K_3,\, T_{i3},\, K_4,\, T_{i4},\, T_{d4}]^T$$

The cost function $V(\theta)$, where each term reflects a control objective or actuator stress, is calculated as

$$\begin{aligned} V(\theta) = \sum_{i=1}^{N} &\gamma_{Me} \left(\frac{e_{Me}(t_i,\theta)}{M_{eNorm}} \right)^2 + \gamma_{egr} \left(\frac{e_{xegr}(t_i,\theta)}{x_{egrNorm}} \right)^2 \\ &+ \left(\frac{u_{egr}(t_i,\theta) - u_{egr}(t_{i-1},\theta)}{u_{egrNorm}} \right)^2 + \left(\frac{u_{vgt}(t_i,\theta) - u_{vgt}(t_{i-1},\theta)}{u_{vgtNorm}} \right)^2 \\ &+ \gamma_{nt} \left(\frac{\max(n_t(t_i,\theta) - n_{tmax}, 0)}{n_{tNorm}} \right)^2 \end{aligned} \tag{4.11}$$

where t_i is the time at sample number i.

The motives for the different terms in the cost function are:

Term 1: Minimizes engine torque deficiency ($e_{Me} = M_{eSetp} - M_e$) in order to follow the engine torque set-point from the driver's demand. Torque deficiency appears when the smoke limiter in Sec. 4.2.7 restricts the amount of fuel injected, i.e. when $u_{\delta Setp} > u_{\delta max}$.

Term 2: Minimizes EGR error ($e_{xegr} = x_{egrSetp} - x_{egr}$).

Term 3 and 4: Avoid oscillations in the EGR valve and in the VGT control signals. The terms have equal weight.

Term 5: Avoids the turbocharger speed to exceed its maximum limit using a high penalty, $\gamma_{nt} = 10^3$.

A remark is that the error e_{λ_O} is not punished since a negative e_{λ_O} is allowed. As seen in Eq. (4.11) all the terms are normalized in order to get the same order of magnitude for the five terms, and this means that the weighting factors have an order of magnitude as $\gamma_{Me} \approx 1$ and $\gamma_{egr} \approx 1$,

4.3.2 Optimization

A solver is proposed for the optimization problem stated in the previous section, and it consists of three phases: an initialization method, a globalization heuristic, and a local solver.

The tuning parameters are initialized using the Åström-Hägglund step-response method for pole-placement (Åström and Hägglund, 1995). The values of the parameters are calculated in several different operating points since the system is non-linear, and then the mean value of the parameters over the entire operating range is used.

The non-linear least squares problem in Eq. (4.10) has several local minima, wherefore precautions must be taken to avoid ending up in a bad local minimum. A global optimization method could be used, but these have the drawback of requiring long computational times. Instead a heuristic method is used to scan a large region around the initial values from Åström-Hägglund. This is done in Phase 2 below, by taking large steps in all directions narrowing in on a good local minimum with relatively short computational times. Then in Phase 3 a standard non-linear least squares solver is used.

Phase 1: Find an initial guess.

1. Initialization: Åström-Hägglund step-response method.

Phase 2: Find a solution near a good local minimum.

1. For all n =1 to 9:
   - Multiply $\theta(n)$ with 3, compute $V(\theta)$ and save its value together with the corresponding θ.
   - Divide $\theta(n)$ with 3, compute $V(\theta)$ and save its value together with the corresponding θ.
2. Choose the set of parameters θ which corresponds to the smallest value of the computed $V(\theta)$ in step 1.
3. Go to step 1 until the calculations don't find any smaller $V(\theta)$.

Phase 3: Finds the solution for the good local minimum.

1. Initial guess: Solution from phase 2.
2. Use a standard Matlab non-linear least squares problem solver.

This algorithm results in a better local minimum compared to if only phases 1 and 3 are used, so the heuristic in phase 2 is valuable.

4.3.3 Transient selection

If a complete driving cycle is used in the automatic tuning when calculating the cost function in Eq. (4.11) it gives a long computational time. This computational time can be decreased if only some few transients are used. For example the European Transient Cycle (ETC) gives a computational time of 30 hours, but if only three transients from the ETC cycle are used the computational time is reduced to 3 hours. When selecting transients it is important that they are representative and aggressive, and therefore the following criteria are formulated.

Criterion 1: Below the EGR error measure E_{xegr} and the torque deficiency measure E_{Me} are introduced. The selected transients should be such that both these measures and the turbocharger speed n_t are high. This is achieved by selecting transients that consist of say at least one of the ten highest values of each of these three.

The EGR error measure, E_{xegr}, increases linearly as function of time when $|e_{xegr}| > 1.5\%$ according to

$$E_{xegr}(t_i) = \begin{cases} E_{xegr}(t_{i-1}) + T_s(t_i) & \text{, if } (|e_{xegr}(t_i)| > 1.5\%) \,\&\, (i \geq 1) \\ 0 & \text{, else} \end{cases}$$

where T_s is the sample time and $e_{xegr} = x_{egrSetp} - x_{egr}$. The torque deficiency measure, E_{Me}, increases when $e_{Me} > 0$ according to

$$E_{Me}(t_i) = \begin{cases} E_{Me}(t_{i-1}) + T_s(t_i)\, e_{Me}(t_i) & \text{, if } (e_{Me}(t_i) > 0) \,\&\, (i \geq 1) \\ 0 & \text{, else} \end{cases}$$

where $e_{Me} = M_{eSetp} - M_e$.

Criterion 2: To capture the entire operating region the transients should include operating points with low flows and high flows respectively, i.e. low speed and torque and high speed and torque.

Criterion 3: It is important to find transients which excite all control modes in Eq. (4.5) and (4.6). Therefore the third criterion is to find transients which excite all control modes in the following control mode signals. The activation times for the different control modes shall be of approximately similar length.

Control modes for the EGR valve:

$$\mathtt{mode}_{egr} = \begin{cases} 1 & \text{, if } \mathrm{PID}_1(e_{\lambda_O}) \text{ active} \\ 2 & \text{, if } \mathrm{PID}_2(e_{xegr}) \text{ active} \end{cases} \tag{4.12}$$

Control modes for the VGT position:

$$\mathtt{mode}_{vgt} = \begin{cases} 1 & \text{, if } u_{vgt} = 100 \\ 2 & \text{, if } \mathrm{PID}_3(e_{xegr}) \text{ active} \\ 3 & \text{, if } \mathrm{PID}_4(e_{nt}) \text{ active} \end{cases} \tag{4.13}$$

Criterion 4: If the driving cycle consists of several driving conditions, at least one transient from each driving condition should be included in order to get representative transients for the complete driving cycle.

4.4 Results from European Transient Cycle simulations

The transient selection method and the control tuning method are illustrated and applied, and a simulation study is performed on the European Transient Cycle (ETC). The cycle consists of three parts representing different driving conditions: urban (0-600 s), rural (600-1200 s), and high-way (1200-1800 s) driving.

The closed loop system, consisting of the model in Chap. 2 and the proposed control structure in Sec. 4.2 (depicted in Fig. 4.3), is simulated in Matlab/Simulink. The set points for λ_O and x_{egr} are authentic recordings that have been provided by industry. A remark is that an observer is not used in the simulations. Instead a low pass filter is used on all variables assumed to come from an observer in order to model its time constant. This is done in the block "Signals" in Fig. 4.3. The different signals in the cost function (Eq. (4.11)) are calculated by simulating the complete system and sampling the signals with a frequency of 100 Hz. Note also that the EGR-valve position is saturated at 80% due to that the EGR-valve does not affect the system if the EGR-valve position is larger than 80%, see Fig. 2.6.

4.4.1 Transient selection results for the European Transient Cycle

The four criteria in the transient selection method (see Sec. 4.3.3) are fulfilled for the ETC cycle by selecting the transients according to Tab. 4.1, where the characteristics of each transient are summarized in the right column. More details about the selection are as follows. To apply the selection criteria, the control system is simulated during the complete ETC cycle using the initialized PID parameters according to Sec. 4.3.2, see Fig. 4.4. High values for the performance measures, as

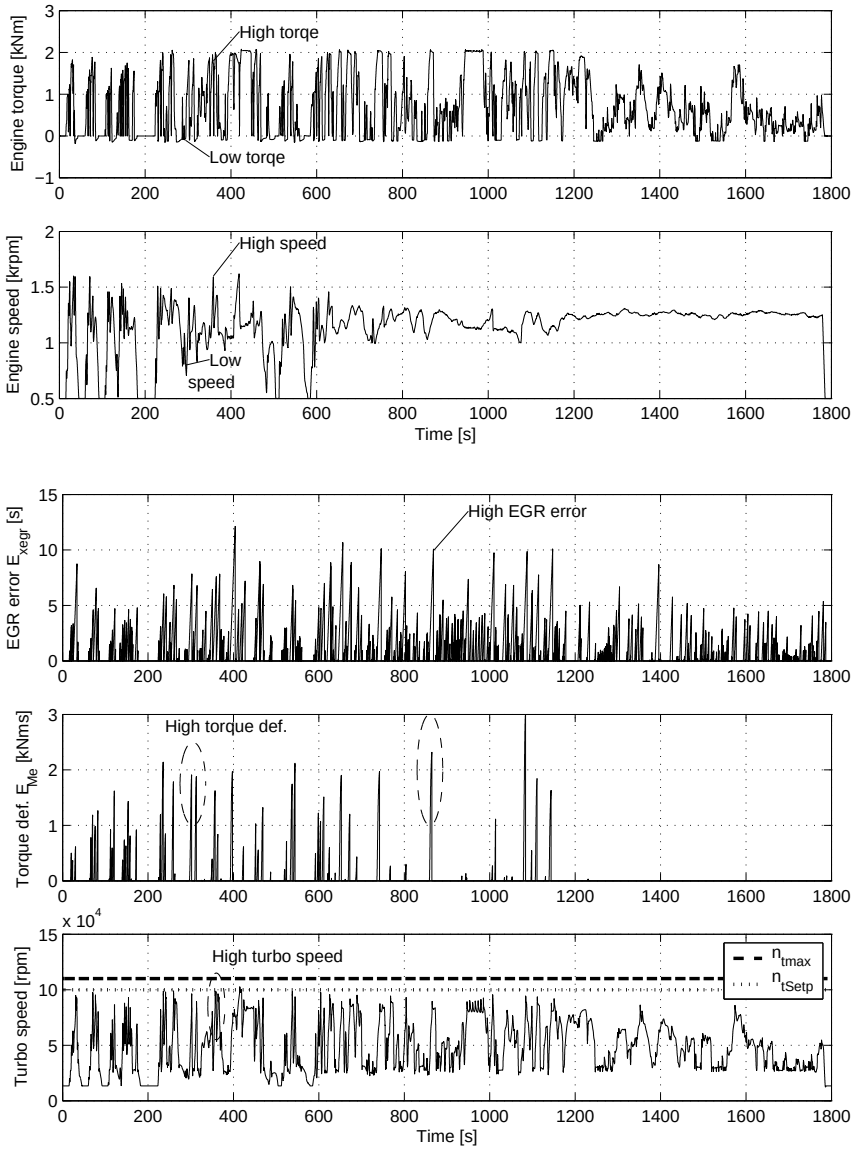

Figure 4.4 *Simulation of the control system during the complete ETC cycle using the initialized PID parameters according to Sec. 4.3.2. The goal is to find transients where the EGR error measures* $\mathsf{E}_{\mathtt{xegr}}$*, the torque deficiency measures* $\mathsf{E}_{\mathcal{M}e}$*, and the turbo speed are high and where the torque and speed are low and high, see Sec. 4.3.3. The result is the first two transients in Tab. 4.1, i.e. 285-360 s and 850-870 s.*

Table 4.1 *Selected transients from the ETC cycle that meet the criteria in Sec. 4.3.3. These transients are used when calculating the cost function* $V(\theta)$ *in Eq.* (4.11).

Transient time interval	Characteristics
285-360 s	Urban driving, high torque deficiency, high turbocharger speed, low and high flow.
850-870 s	Rural driving, high EGR error and high torque deficiency.
1680-1720 s	High-way driving, $\mathtt{mode}_{egr} = 2$ and $\mathtt{mode}_{vgt} = 1$ have long activation times.

Table 4.2 *Activation times for the different control modes in* $\mathtt{mode}_{egr}$ *(Eq.* (4.12)*) and in* $\mathtt{mode}_{vgt}$ *(Eq.* (4.13)*) expressed in percentages of the total transient time for each selected transient in Tab. 4.1.*

	$\mathtt{mode}_{egr}$		$\mathtt{mode}_{vgt}$		
Transient	1	2	1	2	3
285-360 s	83	17	22	48	30
850-870 s	81	19	23	51	27
1680-1720 s	36	64	66	34	0

well as low and high values for both torque and engine speed that are close to each other are found in the first two transients in Tab. 4.1. Consequently, criteria 1 and 2 are fulfilled. Tab. 4.2 shows the activation times for the different control modes in $\mathtt{mode}_{egr}$ and $\mathtt{mode}_{vgt}$ (see Eq. (4.12) and (4.13)). In the first two transients, $\mathtt{mode}_{egr} = 2$ and $\mathtt{mode}_{vgt} = 1$ have short activation times. In order to get longer activation times for these two modes, the third transient is also used and thereby criterion 3 is fulfilled. Criterion 4 is fulfilled since the three transients in Tab. 4.1 are selected from the three driving conditions: urban, rural, and high-way driving.

4.4.2 Actuator oscillations

The importance of term 3 and 4 (actuator oscillations) in the cost function is illustrated in Fig. 4.5, where the control system is simulated with two sets of PID parameters. The first set of PID parameters is optimized using the cost function in Eq. (4.11) and the second is optimized without term 3 and 4. The second set of PID parameters gives oscillations in the control signals. Consequently term 3 and 4 in the cost function are important in order to decrease the actuator oscillations. This is also shown in Tab. 4.3, where the values of term 3 and 4 are lower at the optimized PID parameters than the values at the initialized PID parameters.

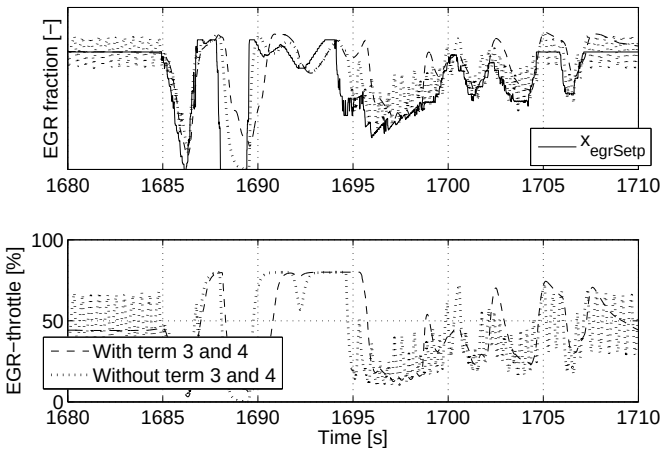

Figure 4.5 *Comparison between two simulations of the control system using two sets of PID parameters. The first set of PID parameters is optimized using the cost function in Eq.* (4.11) *and the second is optimized without term 3 and 4. The second set of PID parameters gives oscillations in the control signals. Consequently term 3 and 4 in the cost function are important in order to avoid oscillations.*

Further, a tuning rule for avoiding oscillations in the control signals u_{egr} and u_{vgt} is to decrease the sum $\gamma_{Me} + \gamma_{egr}$ until the oscillations in the control signals disappear.

4.4.3 Balancing control objectives

The weighting factors γ_{Me}, γ_{egr}, and γ_{nt} in the cost function (Eq. (4.11)) are tuning parameters. When tuning these, trade-offs are made between torque deficiency, EGR error, pumping losses, and turbo over-speed.

A tuning strategy for the relation between γ_{Me} and γ_{egr} is to increase γ_{Me} when a controller tuner wants to decrease the torque deficiency and increase γ_{egr} when a controller tuner wants to decrease the EGR error and the pumping losses. It is important that the sum $\gamma_{Me} + \gamma_{egr}$ is constant in order to avoid influence of the third and fourth term in the cost function when tuning the first and the second term. In the following sections $\gamma_{Me} + \gamma_{egr} = 2$. A tuning strategy for avoiding turbo over-speeding is to increase γ_{nt} until the fifth term becomes equal to zero.

The effects of the automatic tuning on the dynamic behavior, on the complete cycle, and on the controller parameters are described in the following sections.

Effect of tuning on dynamic behavior

The effect of the automatic tuning on the dynamic behavior is shown in Fig. 4.6, where the control system is simulated with two sets of PID parameters. The first set of PID parameters are optimized using the weighting factors $\gamma_{Me} = 1$ and $\gamma_{egr} = 1$. The second set of PID parameters are optimized using the weighting factors $\gamma_{Me} = 3/2$ and $\gamma_{egr} = 1/2$. The latter set of weighting factors punishes the torque deficiency more than the first one.

Fig. 4.6 shows that $\gamma_{Me} = 3/2$ and $\gamma_{egr} = 1/2$ give less torque deficiency but more EGR error and more pumping losses compared to $\gamma_{Me} = 1$ and $\gamma_{egr} = 1$. Between 305 and 308 s the engine torque is low which leads to a high λ_O, an open EGR-valve, and that the VGT position controls the EGR-fraction so that the EGR error is low. Thereafter, an increase in engine torque at 308 s leads to a decrease in λ_O and therefore a closing of the EGR-valve. This closing is faster if γ_{Me}/γ_{egr} is increased from 1 to 3 which leads to a lower EGR-fraction (i.e. more EGR error), a more closed VGT position, a faster increase in turbocharger speed, and consequently a lower torque deficiency. Note also that there are more pumping losses at $\gamma_{Me} = 3/2$ and $\gamma_{egr} = 1/2$ due to that the EGR-valve and the VGT position are more closed. Recall that the actuators are still more open than the other control structure in Sec. 4.2.4.

Effect of tuning on complete cycle

The effect of the automatic tuning on the complete cycle is shown in Tab. 4.3, where the cost function (Eq. (4.11)) and its 5 terms together with the mean value of the pumping loss are calculated from simulations of the complete ETC cycle. Exactly as Fig. 4.6, Tab. 4.3 shows that $\gamma_{Me} = 3/2$ and $\gamma_{egr} = 1/2$ give less torque deficiency but more EGR error and more pumping losses compared to $\gamma_{Me} = 1$ and $\gamma_{egr} = 1$. Consequently, the selected transients in Sec. 4.4.1 are representative for the complete ETC cycle. Tab. 4.3 also shows that the turbocharger speed never exceeds its maximum limit during the ETC cycle except for $\gamma_{Me} = 1/2$ and $\gamma_{egr} = 3/2$ where the term 5 has a small positive value.

It is important to note that the pumping loss is minimized in stationary points by the proposed control structure in all 4 cases in Tab. 4.3 compared to the other control structure in Sec. 4.2.4 that gives higher pumping losses. However, in dynamic conditions trade-offs are made between torque deficiency and pumping loss according to Fig. 4.6. These trade-offs can also be seen in Tab. 4.3, where a decrease in pumping loss leads to a increase in torque deficiency.

Using the cost function in Sec. 4.3.1 for tuning has significant effect in order to improve the control performance compared to if only the initialization method in Sec. 4.3.2 is used. This is seen in Tab. 4.3, where the optimal values of the cost function V are lower than the initial values of V for all cases. It can also be seen that the values of the 5 terms in the cost function decrease for the optimized PID parameters compared to the values of the terms for the initialized PID parameters, except for the torque deficiency and turbo over-speed at $\gamma_{Me} = 1/2$ and $\gamma_{egr} = 3/2$.

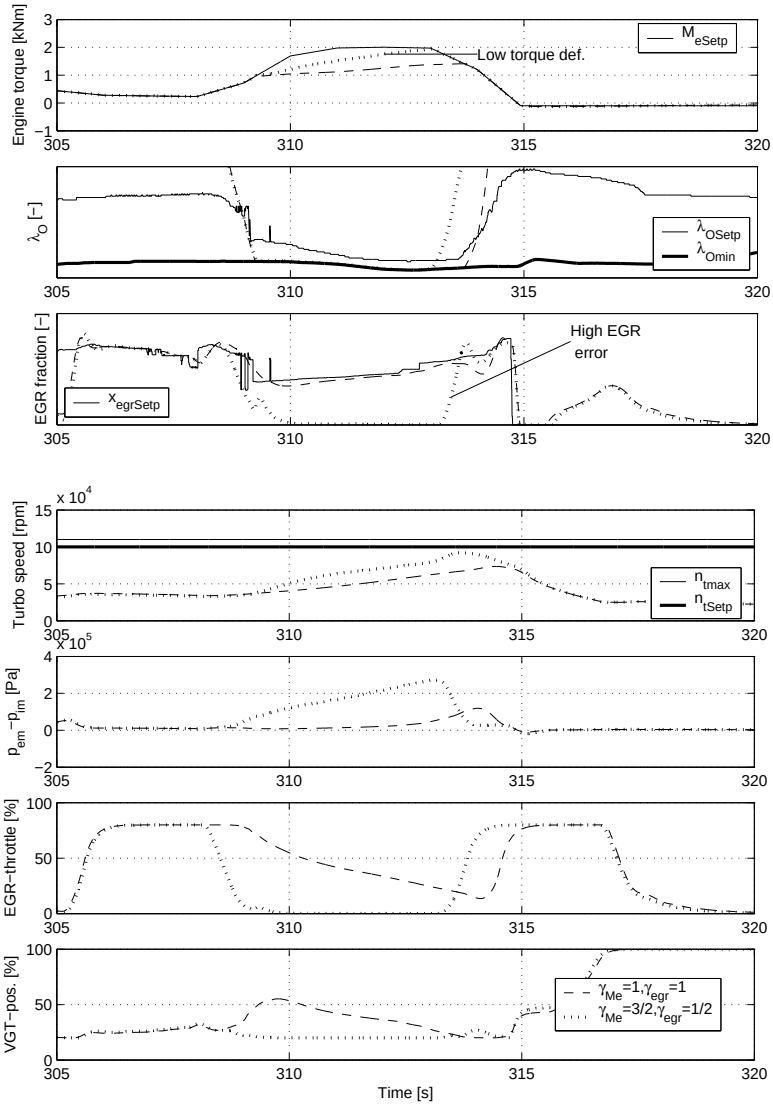

Figure 4.6 *Comparison between two simulations of the control system using two sets of PID parameters. The first set of PID parameters are optimized using the weighting factors* $\gamma_{\mathrm{Me}} = 1$ *and* $\gamma_{\mathrm{egr}} = 1$*. The second set of PID parameters are optimized using the weighting factors* $\gamma_{\mathrm{Me}} = 3/2$ *and* $\gamma_{\mathrm{egr}} = 1/2$*. The latter set of PID parameters gives less torque deficiency but more EGR error and more pumping losses compared to the first set of PID parameters.*

Table 4.3 *Values of different variables computed from simulations of the complete ETC cycle using initialized and optimized PID parameters for three different sets of weighting factors. The variables are the 5 terms in the cost function (Eq. (4.11)), the cost function V, and the time mean value of the pumping loss. These variables show that the automatic tuning has a significant effect and improves the control performance. Note that the weighting factors are not included in the 5 terms.*

	Initial θ	Optimized θ		
Weighting factors		$\gamma_{Me} = 3/2$ $\gamma_{egr} = 1/2$	$\gamma_{Me} = 1$ $\gamma_{egr} = 1$	$\gamma_{Me} = 1/2$ $\gamma_{egr} = 3/2$
Term 1, torque deficiency	0.36	0.25	0.29	0.75
Term 2, EGR error	1.74	1.34	1.10	0.57
Term 3, u_{egr} diff.	0.32	0.17	0.14	0.07
Term 4, u_{vgt} diff.	0.17	0.05	0.04	0.07
Term 5, turbo over-speed	0	0	0	5e-05
V(Optimal θ)		1.27	1.57	1.41
V(Initial θ)		1.90	2.59	3.29
$\frac{1}{T}\int_0^T (p_{em} - p_{im})\,dt$ [bar]	0.27	0.35	0.31	0.22

Effect of tuning on controller parameters

The optimization steps in the automatic tuning method in Sec. 4.3.2 have a significant effect on the controller parameters. This is shown in Fig. 4.7 where the initialized and optimized PID parameters are calculated. The difference between the initialized and optimized K_4 is about 10^2 and for K_1 and K_3 the differences are about 10^1. Consequently, the initialization is far away from the optimal solution. It can also be seen in Fig. 4.7 that the optimized gains K_j are decreased compared to the initialized gains (except for K_2 at $\gamma_{Me} = 1$, $\gamma_{egr} = 1$), which means that the optimized PID parameters give a more cautious control compared to the initialized parameters.

4.5 Results

A control structure with PID controllers and selectors has been proposed and investigated for coordinated control of oxygen/fuel ratio λ_O and intake manifold EGR-fraction. Based on a system analysis, a key characteristic behind the structure is that λ_O is controlled by the EGR-valve and EGR-fraction by the VGT-position, in order to handle the sign reversal in the system from VGT to λ_O.

Besides controlling the two main performance variables, oxygen/fuel ratio λ_O and intake manifold EGR-fraction, the control structure also successfully handles torque control including torque limitation due to smoke control, and supervisory

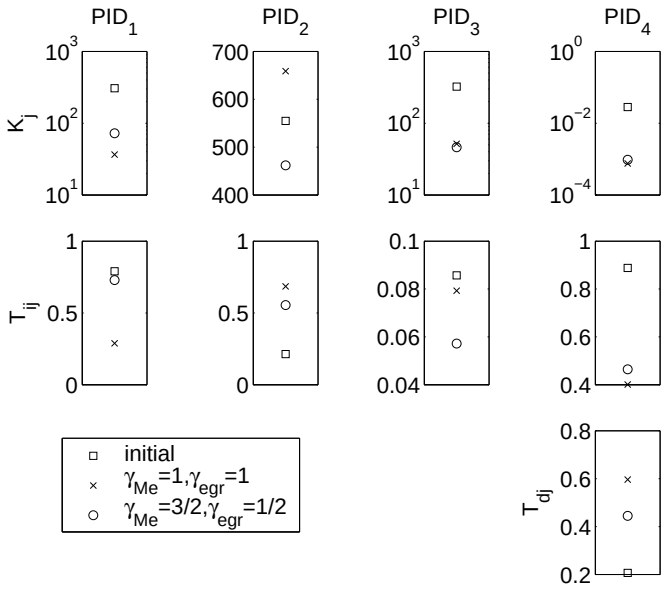

Figure 4.7 *Comparison between initialized and optimized PID parameters showing that there is a significant difference between them. The optimized PID parameters are calculated for two different sets of weighting factors.*

control of turbo charger speed for avoiding over-speeding. Furthermore, in situations where λ_O is greater than its set-point, it takes advantage of the extra degree of freedom and minimizes the pumping work. Compared to another control structure which closes the EGR-valve and the VGT more, the pumping work is substantially reduced.

For efficient calibration an automatic controller tuning method was developed. The objective of minimizing pumping work is handled by the structure, but the other control objectives are captured in a cost function, and the tuning is formulated as a non-linear least squares problem. Important steps in obtaining the solution are: precautions to local minima in a separate phase and the knowledge that went into the method for selecting transients to evaluate the cost function on.

The performance was evaluated on the European Transient Cycle. It was demonstrated how the weights in the cost function influence behavior, and that the tuning method is important in order to improve the control performance compared to if only the initialization method is used. It was also demonstrated that the controller structure performs well regarding all control objectives.

5

Conclusions

Legislators steadily increase the demands on lowered emissions from heavy duty vehicles. To meet these demands it is necessary to integrate technologies like EGR and VGT together with advanced control systems. A control structure with PID controllers and selectors has been proposed for coordinated control of oxygen/fuel ratio λ_O and intake manifold EGR-fraction. These are introduced and chosen as performance variables since they are strongly coupled to the emissions. Therefore they also give advantages in an industrial perspective where the inner loop is combined with an outer loop in an engine management system in a way well suited for efficient calibration.

To design a successful control structure, a physically based model of the engine is desirable. Therefore, a mean value model of a diesel engine with VGT and EGR, and that includes oxygen mass fraction, has been developed and validated. The intended applications of the model are system analysis, simulation, and development of model-based control systems. Model equations and tuning methods for the model parameters were described for each subsystem in the model. In order to decrease the amount of tuning parameters, flows and efficiencies are modeled using physical relationships and parametric models instead of look-up tables. Tuning of parameters in static models shows mean relative errors which are equal to or lower than 6.1 %. Static and dynamic validations of the entire model show mean relative errors which are less than 12 %.

To get insight into the control problem, a system analysis of the model was performed which shows that the transfer function $u_{vgt} \rightarrow \lambda_O$ has a non-minimum phase behavior and a reversed sign in operating points where the engine frequently operates, and that $u_{egr} \rightarrow \lambda_O$ has a non-minimum phase behavior and a reversed

sign in operating points that should be avoided due to high turbo speeds. Further, it is demonstrated that the pumping losses $p_{em} - p_{im}$ decrease with increasing EGR-valve and VGT opening.

Based on this system analysis, a complete control structure has been proposed. A key characteristic behind the structure is that λ_O is controlled by the EGR-valve and EGR-fraction by the VGT-position, in order to handle the sign reversal in the system from VGT to λ_O. Besides controlling the two main performance variables, oxygen/fuel ratio λ_O and intake manifold EGR-fraction, the control structure also successfully handles torque control including torque limitation due to smoke control, and supervisory control of turbo charger speed for avoiding over-speeding. Furthermore, in situations where λ_O is greater than its set-point, it takes advantage of the extra degree of freedom and minimizes the pumping work.

For efficient calibration an automatic controller tuning method was developed. The objective of minimizing pumping work is handled by the structure, but the other control objectives are captured in a cost function, and it is evaluated using a method developed to choose representative transients. The performance was evaluated on the European Transient Cycle. It was demonstrated how the weights in the cost function influence behavior, and that the tuning method is important in order to improve the control performance compared to if only an initialization method is used. It was also demonstrated that the controller structure performs well regarding all control objectives. In combination with its efficient tuning, the controller structure thus fulfills all requirements for successful application.

References

Amman, M., Fekete, N., Guzzella, L., and Glattfelder, A. (2003). Model-based Control of the VGT and EGR in a Turbocharged Common-Rail Diesel Engine: Theory and Passenger Car Implementation. *SAE Technical paper 2003-01-0357*.

Amstutz, A. and Re, L. D. (1995). EGO sensor based robust output control of EGR in diesel engines. *IEEE Transactions on Control System Technology*, pages 37–48.

Anderson, B. D. and Moore, J. B. (1989). *Optimal Control: Linear-Quadratic Methods*. Prentice-Hall, Englewood Cliffs, NJ.

Andersson, P. (2005). *Air Charge Estimation in Turbocharged Spark Ignition Engines*. PhD thesis, Linköpings Universitet.

Andersson, P. and Eriksson, L. (2004). Mean-value observer for a turbocharged SI-engine. In *IFAC Symposium on Advances in Automotive Control, Universty of Salerno, Italy, April 19–23, 2004*, pages 146–151.

Bemporad, A. and Morari, M. (1999). Control of systems integrating logic, dynamics, and constraints. *Automatica*, 35(3):407–427.

Dixon, S. (1998). *Fluid Mechanics and Thermodynamics of Turbomachinery*. Butterworth Heinemann, Woburn, 4:th edition.

Eriksson, L. (2002). Mean value models for exhaust system temperatures. *SAE 2002 Transactions, Journal of Engines, 2002-01-0374*, 111(3).

Eriksson, L., Nielsen, L., Brugård, J., Bergström, J., Pettersson, F., and Andersson, P. (2002). Modeling and simulation of a turbo charged SI engine. *Annual Reviews in Control*, 26(1):129–137.

Glad, T. and Ljung, L. (2000). *Control Theory: Multivariable and Nonlinear Methods*. Taylor and Francis, London.

Guzzella, L. and Amstutz, A. (1998). Control of diesel engines. *IEEE Control Systems Magazine*, 18:53–71.

Heywood, J. (1988). *Internal Combustion Engine Fundamentals*. McGraw-Hill Book Co.

Isidori, A. (1989). *Nonlinear control systems*. Springer-Verlag New York, Inc., New York, NY, USA.

Jankovic, M., Jankovic, M., and Kolmanovsky, I. (1998). Robust nonlinear controller for turbocharged diesel engines. In *Proceedings of the American Control Conference*, pages 1389–1394, Philadelphia, Pennsylvania.

Jerhammar, A. and Höckerdal, E. (2006). Gas flow observer for a Scania diesel engine with VGT and EGR. Master's thesis, Linköpings Universitet, SE-581 83 Linköping.

Jung, M. (2003). *Mean-Value Modelling and Robust Control of the Airpath of a Turbocharged Diesel Engine*. PhD thesis, University of Cambridge.

Khalil, H. K. (2002). *Nonlinear Systems*. Prentice Hall, third edition.

Kolmanovsky, I., Stefanopoulou, A., Moraal, P., and van Nieuwstadt, M. (1997). Issues in modeling and control of intake flow in variable geometry turbocharged engines. In *Proceedings of* 18^{th} *IFIP Conference on System Modeling and Optimization*, Detroit.

Kolmanovsky, I., Sun, J., and Druzhinina, M. (2000). Charge control for direct injection spark ignition engines with EGR. In *Proceedings of the American Control Conference*, Chicago.

Maciejowski, J. (2002). *Predictive Control with Constraints*. Prentice-Hall.

Nieuwstadt, M., Kolmanovsky, I., Moraal, P., Stefanopoulou, A., and Jankovic, M. (2000). EGR–VGT control schemes: Experimental comparison for a high-speed diesel engine. *IEEE Control Systems Magazine*, pages 63–79.

Nieuwstadt, M., Moraal, P., Kolmanovsky, I., Stefanopoulou, A., Wood, P., and Widdle, M. (1998). Decentralized and multivariable designs for EGR–VGT control of a diesel engine. In *IFAC Workshop, Advances in Automotive Control*, Ohio, USA.

Rajamani, R. (2005). Control of a variable-geometry turbocharged and wastegated diesel engine. *Proceedings of the I MECH E Part D Journal of Automobile Engineering*, pages 1361–1368.

Rückert, J., Richert, F., Schloßer, A., Abel, D., Herrmann, O., Pischinger, S., and Pfeifer, A. (2004). A model based predictive attempt to control boost pressure and EGR–rate in a heavy duty diesel engine. In *Preprints of IFAC Symposium on Advances in Automotive Control*, pages 127–133, Salerno, Italy.

Skogtjärn, P. (2002). Modelling of the exhaust gas temperature for diesel engines. Master's thesis LiTH-ISY-EX-3379, Department of Electrical Engineering, Linköping University, Linköping, Sweden.

Stefanopoulou, A., Kolmanovsky, I., and Freudenberg, J. (2000). Control of variable geometry turbocharged diesel engines for reduced emissions. *IEEE Transactions on Control Systems Technology*, 8(4).

Swartling, F. (2005). Gas flow observer for diesel engines with EGR. Master's thesis, Linköpings Universitet, SE-581 83 Linköping.

Vigild, C. (2001). *The Internal Combustion Engine Modelling, Estimation and Control Issues*. PhD thesis, Technical University of Denmark, Lyngby.

Wahlström, J., Eriksson, L., Nielsen, L., and Pettersson, M. (2005). PID controllers and their tuning for EGR and VGT control in diesel engines. In *Preprints of the 16th IFAC World Congress*, Prague, Czech Republic.

Watson, N. and Janota, M. (1982). *Turbocharging the Internal Combustion Engine*. The Mechanical Press Ltd, Hong Kong.

Åström, K. J. and Hägglund, T. (1995). *PID Controllers: Theory, Design and Tuning*. Research Triangle Park, Instrument Society of America, 2nd edition.

A

Notation

Table A.1 *Symbols used in the thesis.*

Symbol	Description	Unit
A	Area	m^2
BSR	Blade speed ratio	–
c_p	Spec. heat capacity, constant pressure	$J/(kg \cdot K)$
c_v	Spec. heat capacity, constant volume	$J/(kg \cdot K)$
e	Control error	–
E	Performance measure	–
J	Inertia	$kg \cdot m^2$
K	DC-gain	–
K_j	Gain in a PID	–
M	Torque	Nm
M_e	Engine torque	Nm
M_p	Pumping torque	Nm
n_{cyl}	Number of cylinders	–
n_e	Rotational engine speed	rpm
n_t	Rotational turbine speed	rpm
$(O/F)_s$	Stoichiometric oxygen-fuel ratio	–
p	Pressure	Pa
P	Power	W
q_{HV}	Heating value of fuel	J/kg
r_c	Compression ratio	–

Symbol	Description	Unit
R	Gas constant	$J/(kg \cdot K)$
R	Radius	m
t	Time	s
T	Temperature	K
T_{dj}	Derivative time in a PID	s
T_{ij}	Integral time in a PID	s
T_s	Sample time	s
u_{egr}	EGR control signal. 100:open 0:closed	%
u_{vgt}	VGT control signal. 100:open 0:closed	%
u_δ	Injected amount of fuel	$mg/cycle$
V	Volume	m^3
V	Cost function	–
W	Mass flow	kg/s
x_{egr}	EGR fraction	–
x_N	Relative undershoot in a non-minimum phase behavior	–
X_O	Oxygen mass fraction	–
γ	Specific heat capacity ratio	–
γ	Weighting factor	–
η	Efficiency	–
θ	PID parameters	–
λ_O	Oxygen-fuel ratio	–
Π	Pressure quotient	–
ρ	Density	kg/m^3
τ	Time constant	s
Φ_c	Volumetric flow coefficient	–
Ψ_c	Energy transfer coefficient	–
ω	Rotational speed	rad/s

Table A.2 *Indices used in the thesis.*

Index	Description
$_{a}$	air
$_{amb}$	ambient
$_{c}$	compressor
$_{d}$	displaced
$_{e}$	exhaust
$_{egr}$	EGR
$_{ei}$	engine cylinder in
$_{em}$	exhaust manifold
$_{eo}$	engine cylinder out
$_{f}$	fuel
$_{fric}$	friction
$_{ig}$	indicated gross
$_{im}$	intake manifold
$_{m}$	mechanical
$_{Norm}$	normalized
$_{Setp}$	set-point
$_{t}$	turbine
$_{vgt}$	VGT
$_{vol}$	volumetric
$_{\delta}$	fuel injection

B

Time constants

The time constants, τ, (see Fig. 3.5) for the transfer functions $u_{vgt} \rightarrow \lambda_O$, $u_{egr} \rightarrow \lambda_O$, $u_{vgt} \rightarrow x_{egr}$, and $u_{egr} \rightarrow x_{egr}$ are shown in Fig. B.1 to B.4 over the most interesting and important part of the operating region, i.e. the same operating region as Fig. 3.6 to 3.11 and 3.13.

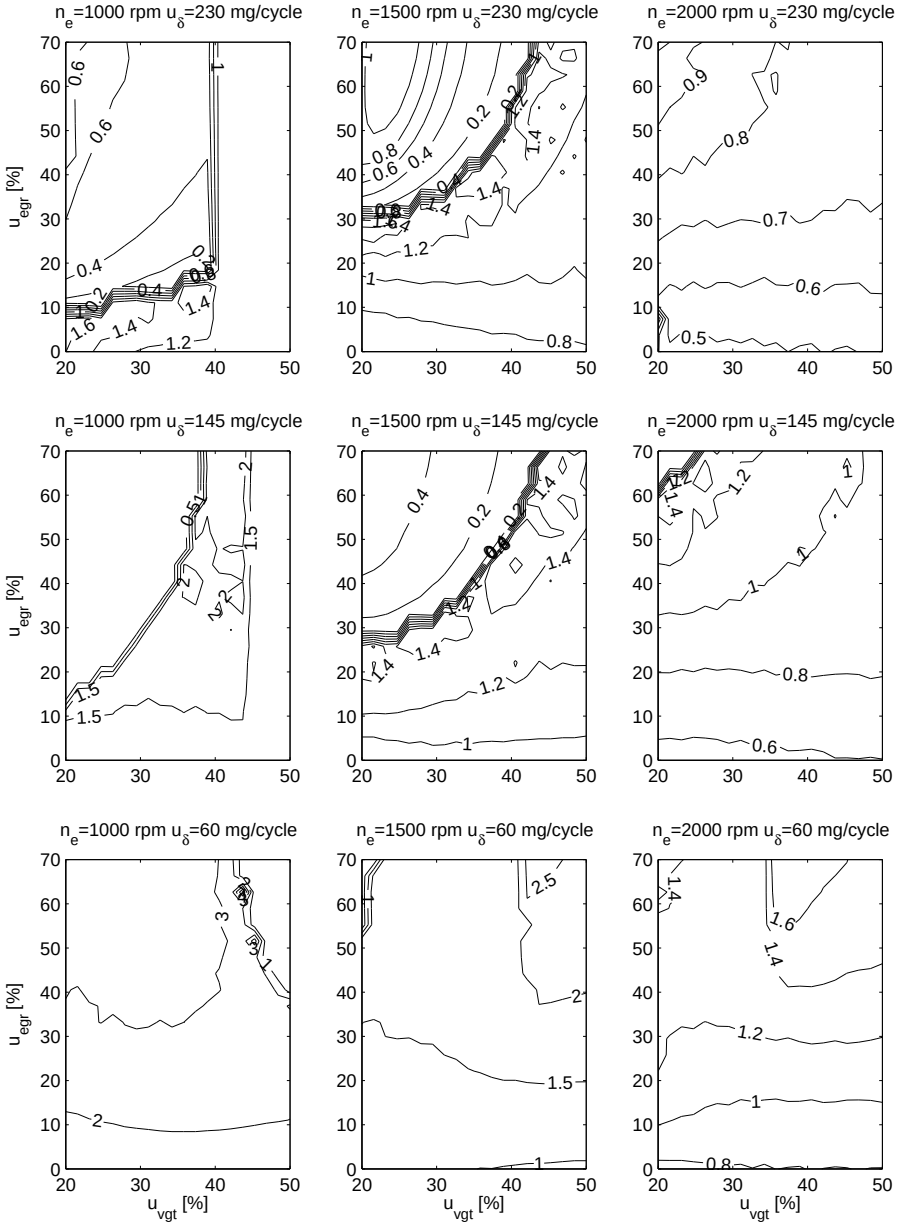

Figure B.1 *Contour plots of the time constant, τ [s], for the transfer function $u_{vgt} \rightarrow \lambda_O$ at 3 different n_e and 3 different u_δ, i.e. 3*3=9 different n_e and u_δ points.*

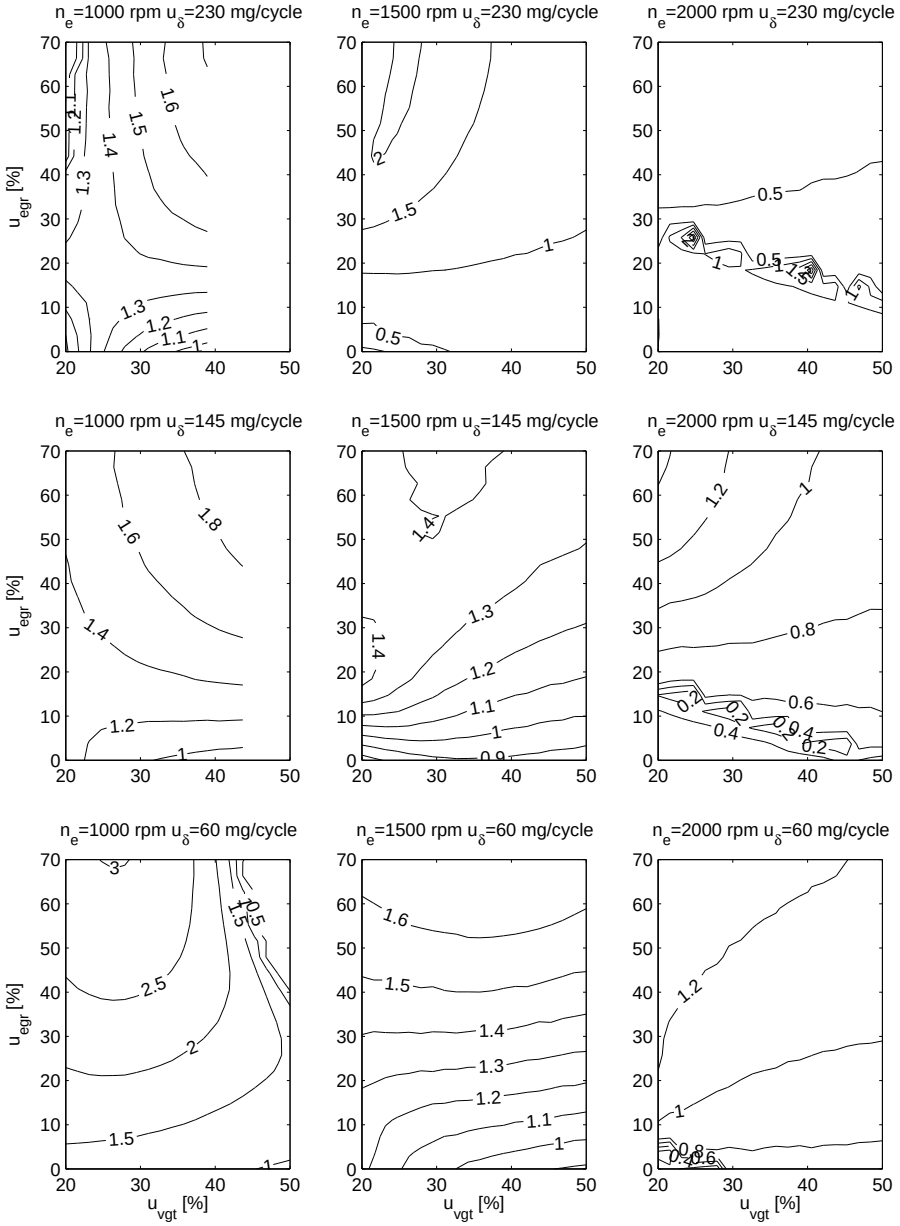

Figure B.2 *Contour plots of the time constant, τ [s], for the transfer function $u_{egr} \rightarrow \lambda_O$ at 3 different n_e and 3 different u_δ, i.e. 3*3=9 different n_e and u_δ points.*

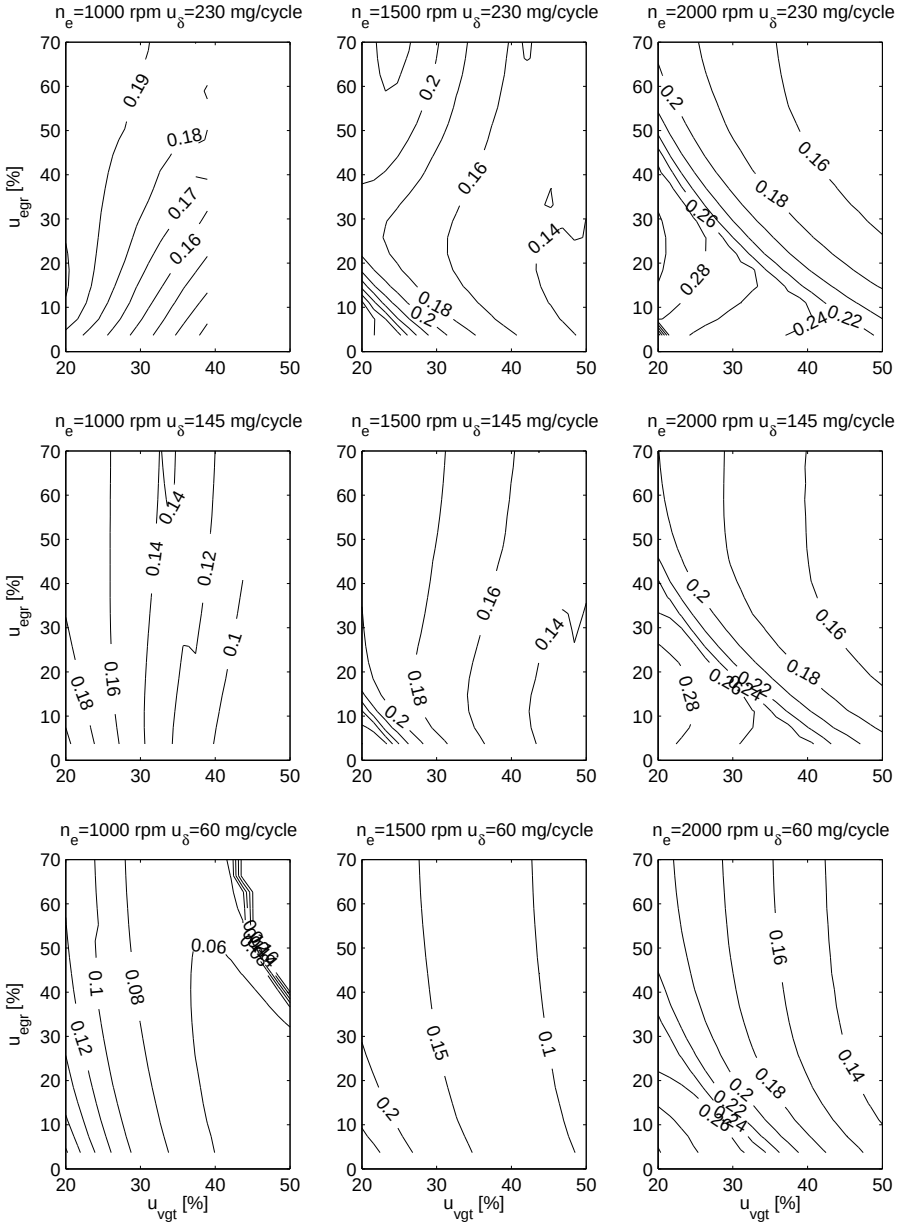

Figure B.3 *Contour plots of the time constant, τ [s], for the transfer function $u_{vgt} \rightarrow x_{egr}$ at 3 different n_e and 3 different u_δ, i.e. 3*3=9 different n_e and u_δ points.*

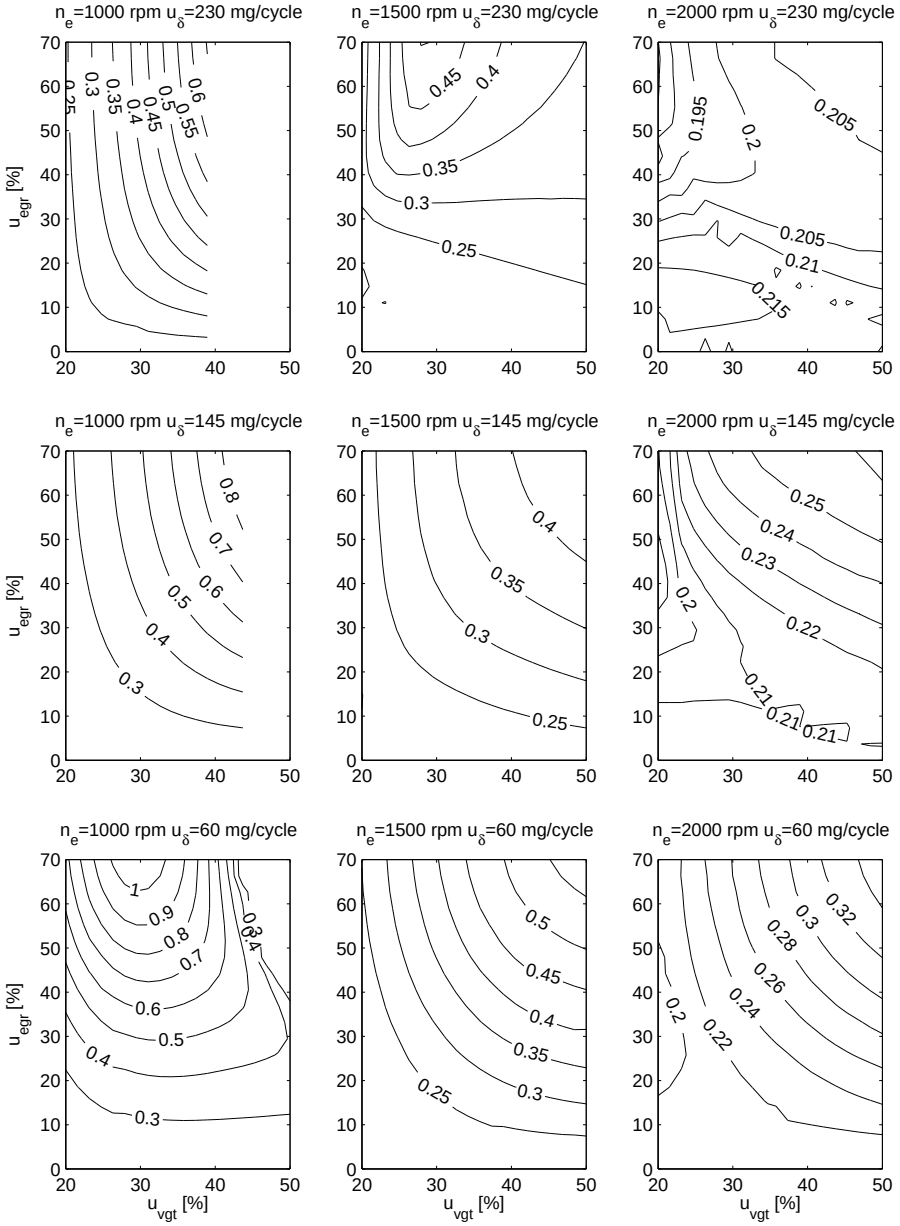

Figure B.4 *Contour plots of the time constant, τ [s], for the transfer function $u_{egr} \rightarrow x_{egr}$ at 3 different n_e and 3 different u_δ, i.e. 3*3=9 different n_e and u_δ points.*